

Fall 1996

# Synthesis and characterization of LPCVD SiC films using novel precursors

Mahalingam Bhaskaran

*New Jersey Institute of Technology*

Follow this and additional works at: <https://digitalcommons.njit.edu/dissertations>



Part of the [Electrical and Electronics Commons](#)

---

## Recommended Citation

Bhaskaran, Mahalingam, "Synthesis and characterization of LPCVD SiC films using novel precursors" (1996). *Dissertations*. 1052.  
<https://digitalcommons.njit.edu/dissertations/1052>

This Dissertation is brought to you for free and open access by the Theses and Dissertations at Digital Commons @ NJIT. It has been accepted for inclusion in Dissertations by an authorized administrator of Digital Commons @ NJIT. For more information, please contact [digitalcommons@njit.edu](mailto:digitalcommons@njit.edu).

## **Copyright Warning & Restrictions**

The copyright law of the United States (Title 17, United States Code) governs the making of photocopies or other reproductions of copyrighted material.

Under certain conditions specified in the law, libraries and archives are authorized to furnish a photocopy or other reproduction. One of these specified conditions is that the photocopy or reproduction is not to be “used for any purpose other than private study, scholarship, or research.” If a user makes a request for, or later uses, a photocopy or reproduction for purposes in excess of “fair use” that user may be liable for copyright infringement,

This institution reserves the right to refuse to accept a copying order if, in its judgment, fulfillment of the order would involve violation of copyright law.

**Please Note: The author retains the copyright while the New Jersey Institute of Technology reserves the right to distribute this thesis or dissertation**

Printing note: If you do not wish to print this page, then select “Pages from: first page # to: last page #” on the print dialog screen

The Van Houten library has removed some of the personal information and all signatures from the approval page and biographical sketches of theses and dissertations in order to protect the identity of NJIT graduates and faculty.

## ABSTRACT

### SYNTHESIS AND CHARACTERIZATION OF LPCVD SiC FILMS USING NOVEL PRECURSORS

by  
**Mahalingam Bhaskaran**

A unique low pressure chemical vapor deposition (LPCVD) process has been developed to synthesize amorphous and crystalline SiC films using *environmentally benign chemicals*. The interrelationships governing the process variables, compositions and select properties of the resulting films were established. Such films can be used to produce high quality mask membrane for x-ray lithography. These films can also be used in fabricating high power electrical devices, and heterojunction devices in conjunction with silicon.

Amorphous SiC films were synthesized using a single precursor, ditertiarybutylsilane, at temperatures below 850°C. Compositional analysis performed on these deposits revealed that, in the deposition temperature range of 625 to 750°C, the composition of the deposits changed progressively from slightly silicon rich (55% Si) to slightly carbon rich (51%C). Above 750°C, there was a rapid increase in the carbon content from the near stoichiometric value to about 75%-C at 850°C. The stoichiometric films exhibited high stress values of  $700 \pm 50$  MPa. Attempts to reduce the stress values resulted in films with excess carbon content of about 60%-C. From the high frequency C-V characterization, the dielectric constant for these films was estimated to be  $10.1 \pm 0.5$ . Temperature bias stressing studies revealed a trapped charge density of  $0.869 \times 10^7 \text{ cm}^{-2}$  within the bulk.

Crystalline silicon carbide films were grown on silicon substrates using dichlorosilane and acetylene as precursors, in the temperature range of 950°C to 1050°C. The carbon content in the film was found to be increasing with the deposition temperature, when the flow ratio of precursors was one. The carbon composition was also found to be sharply dependent on acetylene flow, for constant deposition temperature and pressure. Stoichiometric films were achieved for dichlorosilane to acetylene flow ratio of 4:1. X-ray diffraction studies confirmed the growth of  $\beta$ -SiC with  $\langle 111 \rangle$  orientation in all the cases. The voltage-current relationship for Si-film-metal structure showed a diode behavior with an ideality factor of 4.03 in the diffusion current dominating regime.

**SYNTHESIS AND CHARACTERIZATION OF LPCVD SiC FILMS USING  
NOVEL PRECURSORS**

by  
**Mahalingam Bhaskaran**

**A Dissertation  
Submitted to the Faculty of  
New Jersey Institute of Technology  
in Partial Fulfillment of the Requirements for the Degree of  
Doctor of Philosophy**

**Department of Electrical and Computer Engineering**

**January 1997**

Copyright © 1996 by Mahalingam Bhaskaran

ALL RIGHTS RESERVED

**APPROVAL PAGE**

**SYNTHESIS AND CHARACTERIZATION OF LPCVD SiC FILMS USING  
NOVAL PRECURSORS**

**Mahalingam Bhaskaran**

Dr. Roland Levy  
Distinguished Professor of Physics, NJIT

Date

Dr. Roy H. Cornely  
Professor of Electrical Engineering, NJIT

Date

Dr. Kenneth Sohn  
Professor of Electrical Engineering, NJIT

Date

Dr. Durga Misra  
Associate Professor of Electrical Engineering, NJIT

Date

Dr. James Grow  
Associate Professor of Chemistry, NJIT

Date



## BIOGRAPHICAL SKETCH

**Author:** Mahalingam Bhaskaran  
**Degree:** Doctor of Philosophy  
**Date:** January, 1997

### **Undergraduate and Graduate Education:**

- Master of Science in Electrical Engineering,  
New Jersey Institute of Technology, Newark, New Jersey, May 1996
- Bachelor of Science in Electronics and Communication Engineering,  
P.S.G College of Technology, Coimbatore, Tamil Nadu, India, February 1985

**Major: Electrical Engineering**

### **Presentations and Publications**

- Synthesis and characterization of LPCVD silicon carbide films, presented at the 179th ECS meeting in Washington D.C., May 1991 and published in Extended Abstracts of the Electrochemical Society.
- Synthesis and characterization of silicon carbide masks for x-ray lithography presented at ATC-SEM symposium, Rutgers University, Piscataway, New Jersey, May 1991 and published in Abstracts of Advanced Technological Center for Surface Engineered Materials.
- Low pressure chemical vapor deposition of silicon carbide from ditertiarybutylsilane, J.M. Grow, R.A. Levy, and M. Bhaskaran, NJIT, H.J. Boeglin and R. Shlvoy, Olin Chemicals Research, Cheshire, J. Electrochem. Soc., Vol. 140, No. 10, October 1993, 3001-3007.
- Growth kinetics and characterization of low pressure chemically vapor deposited  $\text{Si}_3\text{N}_4$  films from  $(\text{C}_4\text{H}_9)_2\text{SiH}_2$  and  $\text{NH}_3$ , J.M. Grow, R.A. Levy, X.Fan, M.Bhaskaran, NJIT, Materials Letters 23 (1995), 187-193.
- Thermal stability of dry etch damage in SiC, S.J. Pearton and J.W. Lee, University of Florida, Gainesville, Florida 32611, J.M. Grow and M. Bhaskaran, New Jersey Institute of Technology, Newark, New Jersey 07102, F. Ren, AT&T Bell Laboratories, Murray Hill, New Jersey 07974, Applied Physics Letters 68 (21), 20 May 1996, 2987-2989.

This dissertation is dedicated to  
my parents

## ACKNOWLEDGMENT

The author expresses his sincere gratitude to his advisor, Distinguished Professor Roland A. Levy, and to his co-advisor, Associate Professor James Grow, for their guidance, inspiration, and support throughout this research. Special thanks to Professor Roy H. Cornely, Professor Kenneth Sohn, and Associate Professor Durga Misra for serving as members of the dissertation review committee. Acknowledgments are due to Dr. Wahib Mohammed for providing X-ray diffraction analysis data for amorphous SiC films, Dr. Robert Pfeffer, and Dr. Herman J. Boeglin for providing compositional analysis results. The author appreciates the timely help provided by Dr. P. K. Swain in doing CV and IV analysis of SiC films. Finally, the author wishes to express his thanks to the members of CVD laboratory of New Jersey Institute of Technology including Vitaly Sigal, Romiana Petrova, Venkat Paturi, John Opyrchal, Elizabeth A. McKay, Manish Narayan, Chenna Ravindranath, and Kiran V. Chatty for their support in performing experiments at various stages.

## TABLE OF CONTENTS

Chapter	Page
1 INTRODUCTION.....	1
1.1 Review of Lithography.....	1
1.1.1 Comparison of Lithographic Techniques.....	2
1.1.2 SiC as a Candidate for X-ray Mask Membrane Material.....	6
1.2 Literature Overview.....	7
1.2.1 SiC as a X-ray Mask Membrane Material.....	7
1.2.2 Earlier Studies on the Synthesis of Amorphous SiC.....	8
1.2.3 Earlier Studies on the Synthesis of Crystalline SiC.....	10
1.2.4 SiC as a Semiconductor Device Material.....	13
1.3 Significance of this Study.....	14
1.4 Chemical Vapor Deposition.....	16
1.4.1 Fundamental Aspects of CVD.....	17
1.4.2 Transport Phenomena of CVD.....	18
1.4.3 Film Growth Aspects of CVD.....	21
1.5 Low Pressure CVD Process.....	21
1.5.1 Mechanism Involved in Film Deposition.....	22
1.5.2 Factors Affecting Film Uniformity.....	22
1.6 Advantages of CVD.....	23
1.7 Limitations of CVD.....	24
2 EXPERIMENTAL PROCEDURE.....	25
2.1 Introduction.....	25
2.2 LPCVD Reactor.....	26
2.3 Pre-Deposition Procedure.....	28
2.3.1 Leak Check.....	28

**TABLE OF CONTENTS**  
**(Continued)**

<b>Chapter</b>	<b>Page</b>
2.3.2 Flow Rate Calibration.....	29
2.4 Deposition Procedure.....	31
2.4.1 Wafer Loading.....	31
2.4.2 Film Deposition.....	32
2.5 Film Characterization Techniques.....	33
2.5.1 Initial Analysis.....	33
2.5.2 Refractive Index Measurements.....	34
2.5.3 Infra-red Spectroscopic Studies.....	35
2.5.4 Stress Measurements.....	35
2.5.5 X-ray Diffraction Studies.....	37
2.5.6 Optical Transmission Studies.....	38
2.5.7 Compositional Analysis.....	39
2.5.8 Hardness and Young's Modulus Measurements.....	39
2.5.9 Electrical Characterization of SiC Thin Films.....	42
2.5.9.1 Wafer Preparation.....	42
2.5.9.2 Metallization.....	43
2.5.9.2 Electrical Parameters Measurements.....	44
2.6 Membrane Preparation.....	44
3 RESULTS AND DISCUSSION.....	46
3.1 Introduction.....	46
3.2 Results and Discussion on Characterization Studies of Amorphous SiC Films	47
3.2.1 Growth Kinetic Study.....	47
3.2.1.1 Growth Kinetics with Respect to Flow Rate.....	47
3.2.1.2 Growth Kinetics with Respect to Pressure.....	48

**TABLE OF CONTENTS**  
(Continued)

Chapter	Page
3.2.1.3 Growth Kinetics with Respect to Temperature.....	51
3.2.2 Characterization of a-SiC Films.....	55
3.2.2.1 Infra-red Spectroscopic Studies.....	55
3.2.2.2 X-ray Diffraction Studies.....	55
3.2.3 Compositional Analysis.....	57
3.2.4 Analysis of Mechanical Properties.....	59
3.2.5 Stress Analysis.....	59
3.2.6 Optical Characterization.....	62
3.2.6.1 Optical Transmission Characteristics.....	62
3.2.6.2 Optical Band Gap Estimation.....	62
3.2.7 On the Optimization of Stress and Optical Transmission.....	64
3.2.7.1 Methods to Improve Optical Transmission by Adding Ammonia	64
3.2.7.2 Methods to Optimize Stress Values for a-SiC Films Deposited at 750°C.....	67
3.2.8 Electrical Characterization Results of a-SiC Films.....	69
3.3 Results and Discussion on Characterization Studies of Crystalline SiC Films	73
3.3.1 Growth Kinetic Study.....	73
3.3.1.1 Growth Kinetics with Respect to Temperature.....	73
3.3.1.2 Growth Kinetics with Respect to Flow of Precursors.....	74
3.3.2 Characterization of Crystalline SiC Films.....	76
3.3.2.4 Infra-red Spectroscopic Studies.....	76
3.3.2.5 X-ray Diffraction Studies.....	77

**TABLE OF CONTENTS**  
**(Continued)**

<b>Chapter</b>	<b>Page</b>
3.3.3 Compositional Analysis.....	77
3.3.4 Stress Analysis.....	80
3.3.5 Surface Morphological Studies.....	81
3.3.6 Optical Characterization.....	83
3.3.6.1 Optical Transmission Characteristics.....	83
3.3.6.2 Optical Band Gap Estimation.....	83
3.3.7 Electrical Characterization.....	83
4 CONCLUSIONS.....	87
REFERENCES.....	93

## LIST OF TABLES

<b>Table</b>	<b>Page</b>
1.1 Comparison of lithographic techniques.....	4
2.1 Specification of Si wafer.....	32
2.2 Parameters for metallization of SiC thin films.....	43



## LIST OF FIGURES

Figure	Page
1.1 Schematic Representation of lithographic Process.....	4
1.2 Deposition rate as a function of substrate temperature exemplifying diffusion controlled and surface reaction controlled regimes.....	20
2.1 Schematic representation of the LPCVD reactor.....	27
2.2 Schematic diagram of a typical silicon wafer showing points where thickness was measured.....	33
2.3 Schematic representation showing the experimental setup to measure the radius of curvature of the bending of silicon substrate due to stress in the film.....	36
2.4 Schematic representation showing the setup to measure hardness of SiC film.....	40
2.5 Typical load displacement curve for SiC film.....	41
2.6 Experimental setup to measure the high frequency C-V characteristics of Si-SiC-metal structure.....	45
3.1 Variation of growth rate as a function of the square root of DTBS flow rate.....	49
3.2 Variation of growth rate as a function of the square root of pressure for a-SiC.....	49
3.3 Variation of growth rate as a function of reciprocal temperature for a-SiC.....	52
3.4 Variation of silicon concentration in the silicon carbide films using ESCA (at a depth of 150 Å) and RBS as a function of deposition temperature for constant pressure (200 mTorr) and DTBS flow rate (30 sccm) .....	54
3.5 Growth rate of the <i>i</i> th wafer normalized to that of the 2nd wafer as a function of wafer position for deposition temperatures above 800°C.....	54
3.6 FTIR spectrum of a-SiC sample deposited at 750°C showing strong Si-C vibration mode.....	56
3.7 X-diffraction spectrum of a-SiC sample deposited at 900°C, revealing <111> oriented β-SiC peak.....	56
3.8 The Auger depth profile, taken on a sample of a-SiC deposited at 650°C.....	57
3.9 ESCA spectrum for a sample of a-SiC deposited at 700°C, showing peaks corresponding to carbon as neutral and carbide species.....	58

**LIST OF FIGURES**  
(Continued)

<b>Figure</b>	<b>Page</b>
3.10 ESCA spectrum for a sample of a-SiC deposited at 850°C, showing peaks corresponding to carbon as neutral and carbide species.....	58
3.11 Plot of Young's modulus of a-SiC films as a function of deposition temperature.....	60
3.12 Plot of hardness of a-SiC films as a function of deposition temperature.....	60
3.13 Optical microscopic picture showing the crystallographically oriented micro cracks of a-SiC sample deposited on <100> Si substrate, with a magnification of 110.....	61
3.14 Optical spectrum of a 1µm thick a-SiC film deposited at 750°C.....	63
3.15 A plot to estimate the optical band gap for the sample deposited at 750°C.....	63
3.16 Composition as a function of NH <sub>3</sub> flow rate for films deposited at a temperature of 800°C, pressure of 200mTorr, and DTBS flow rate of 30 sccm.....	65
3.17 Variation of the optical transmission normalized to 1µm thick SiC films as a function of NH <sub>3</sub> flow rates for films deposited at a temperature of 800°C, pressure of 200 mTorr, and DTBS flow rate of 30 sccm.....	65
3.18 IR spectrum showing the broadening of SiC peak due to increase in N content..	66
3.19 X-ray diffraction spectrum of a-SiC sample that was deposited at 750°C and annealed at 1000°C in vacuum showing micro-crystallinity.....	68
3.20 High frequency C-V plot for Si-SiC-Al (MIS) structure. The film was deposited at 850°C, 100 mTorr. The Al dot was 500 µm in diameter.....	72
3.21 High frequency C-V plot for (1) the sample without temperature bias stress (2) after the temperature bias stress was performed.....	72
3.22 Variation of deposition rate as a function of reciprocal temperature for β-SiC...	75
3.23 Variation of deposition rate as a function of precursors flow rate for β-SiC.....	75
3.24 Variation of deposition rate as a function of precursors flow ratio for β-SiC.....	76
3.25 FTIR spectrum of a β-SiC sample deposited at 1000°C, with dichlorosilane to acetylene flow ratio of 4:1, and chamber pressure of 200 mTorr.....	78
3.26 X-ray diffraction spectrum of β-SiC sample deposited at 1000°C, with dichlorosilane to acetylene flow ratio of 4:1, and chamber pressure of 200 mTorr, showing a strong peak corresponding to <111> β-SiC orientation.....	78

## LIST OF FIGURES

(Continued)

Figure	Page
3.27 Variation of Si-C percentage composition as a function of acetylene flow rate...	79
3.28 Variation of percentage composition of Si-C as a function of deposition temperature.....	79
3.29 Variation in the stress of $\beta$ -SiC films as a function of deposition temperature...	82
3.30 Atomic Force Microscopic picture showing the surface morphology of a $\beta$ -SiC sample deposited at 1000°C, with dichlorosilane and acetylene flow rate of 20 and 5 sccm respectively, and under the chamber pressure of 500 mTorr.....	82
3.31 Optical transmission spectrum for 1 $\mu$ m thick $\beta$ -SiC sample deposited at 1000°C, with dichlorosilane and acetylene flow rates of 20 and 5 sccm respectively, and chamber pressure of 200 mTorr.....	84
3.32 A plot to estimate the optical band gap for the sample deposited under the conditions mentioned in figure 3.31.....	85
3.33 Forward current-voltage characteristics of silicon- $\beta$ SiC-metal structure showing a typical diode behavior. The film was deposited under conditions mentioned in figure 3.31.....	85
3.34 Reverse current-voltage characteristics of silicon- $\beta$ SiC-metal structure showing a typical diode behavior. The film was deposited under conditions mentioned in figure 3.31.....	86
4.1 Bandgap versus lattice constant data for the column IV, III-V, and II-VI semiconductors. (After reference 51).....	91

# CHAPTER 1

## INTRODUCTION

The purpose of this thesis was to develop a process for synthesizing amorphous and crystalline silicon carbide films on silicon wafers, and to study the properties of such films. The motivation for this study stems from the fact that many properties of silicon carbide make it an attractive candidate as a mask membrane material in x-ray lithography. The following sections briefly describe the lithographic process in general and x-ray lithography in particular. The application of silicon carbide in x-ray lithography is described. An overview of previous research work done on SiC is also presented. Then the motivation for this study and its significance is described. Finally, the chapter concludes with a discussion on the fundamental aspects of chemical vapor deposition, a process employed to synthesize SiC films.

### 1.1 Review of Lithography

Lithography is a process in Integrated Circuit (IC) fabrication, where a pattern on a membrane, representing geometric shapes of electric circuit is reproduced on a semiconductor wafer coated with a thin layer of silicon dioxide or silicon nitride and a layer of photo-sensitive resist [1]. These geometric shapes define various regions in an integrated circuit such as the implantation regions, the contact windows and bonding pad areas. In such a process, electromagnetic radiation (typically in UV-visible region) is passed through a membrane which is transparent to that radiation. The membrane holds a

pattern representing the geometric shapes of the electric circuit. The pattern is made out of material which is opaque to that radiation and thereby creating sharp shadow image on to the semiconductor wafer containing photoresist layer. The exposure of the photoresist layer to the radiation alters the chemical bonding of the resist material. By exploiting this property, either the exposed or the unexposed regions can be selectively removed by etching, leaving behind the oxide or nitride layer for subsequent processing steps. The schematic for a lithographic process is shown in figure 1.1. Since this technique uses radiation in the UV-visible region, it is called *optical lithography*. It is, at present, the most widely adapted technique for the pattern transfer.

As the IC technology advances, the demand for the fabrication of electrical devices with dimensions of less than a micron is also on the increase. However, optical lithography is not suitable for such fabrication as this method imposes severe restriction on the resolution of the pattern that is reproduced. This is due to the large wavelength of the optic radiation (2000 to 4000 Å), resulting in diffraction effects as the radiation passes through the membrane, when pattern line widths of less than a micron are used. Hence other methods such as electron beam lithography, ion beam lithography, and x-ray lithography are being developed.

### **1.1.1 Comparison of Lithographic Techniques**

A comparison of these lithographic techniques is summarized in Table 1.1. Electron beam lithography uses a highly focused electron beam to a spot size of about 0.1  $\mu\text{m}$ , and with energies of a few thousand electron volts, to register micron and sub-micron

geometries [2]. It involves highly automated and precisely controlled operations resulting in greater depth of focus than the optical lithography. Also, direct patterning on a semiconductor wafer without using a mask is possible using this method. The disadvantages of this method are limited pattern resolution due to the so called proximity effect, low throughput (approximately five wafers per hour) and high equipment cost. Proximity effect refers to the phenomenon of irradiation of neighboring atoms of resist layer due to backscattering of incident energetic electrons. The backscattering electrons will change the chemical properties of the portions of resist layers which are located at several microns away from the incident beam. This imposes a limit on the minimum spacing between pattern features.

In ion beam lithography, as the name implies, energetic ions around 60 keV are used instead of electrons. The heavier mass of ions compared to that of electrons produce less backscattering effects. Therefore proximity effects are reduced much, resulting in higher resolution of the reproduced pattern. This technique is also used in direct-writing mode without a mask. But, this technology is still in its initial stage of development.

X-Ray lithography uses a shadow printing method similar to optical lithography. Since the x-ray wavelength involved will be about 5 to 30 Å, diffraction effects are eliminated, resulting in high resolution.

Apart from that, x-Ray lithography has other advantages. X-rays can penetrate through dust particles of low atomic number [3], hence, this method is immune to contaminants present in the system. The low absorption of x-rays in the resist material results in uniform exposure and thereby vertical resist profiles can be formed.

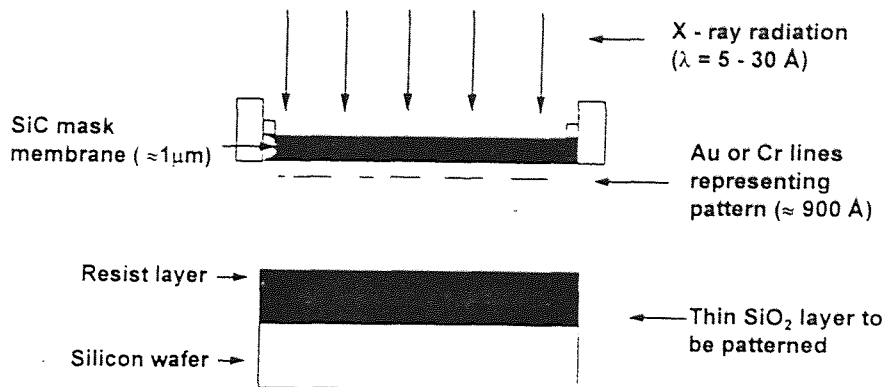


**Figure 1.1** A schematic representation of a lithographic process.

**Table 1.1** Comparison of lithographic techniques

	X-ray	Optical	e-beam	Ion beam
Source	Radiation ( $\lambda=5-30\text{\AA}$ )	Radiation ( $\lambda=2000-4000\text{\AA}$ )	Energetic electrons (few thousand eV)	Energetic ions (around 60 keV)
Resolution	$\approx 0.3 \mu\text{m}$	$\approx 1.0 \mu\text{m}$	$\approx 0.5 \mu\text{m}$	$\approx 100\text{\AA}$
Registration	$0.3 \mu\text{m}$	$0.5 \mu\text{m}$	$0.2 \mu\text{m}$	-
Limiting effects	-	diffraction effects	proximity effects	-
Throughput	high	high	low	low
Cost	low	low	high	high

Scattering effects within the resist layer are minimized in this method. Finally, x-ray lithography has higher throughput than that of electron beam or ion beam lithography. These advantages make x-ray lithography an important process technique in the future ultra-scale integrated (ULSI) circuit technology, where the critical dimension of circuit device is around 0.5  $\mu\text{m}$ .

One of the key issues in the development of x-ray lithography is the fabrication of the mask membrane. The fabrication of x-ray masks requires the use of an x-ray transparent membrane material with low atomic number on top of which is patterned a x-ray absorber consisting of a material with high atomic number, to provide good pattern definition contrast. The membrane material for an x-ray mask technology aimed at providing 0.5-0.2 micron feature dimensions must meet several requirements [1]:

- High x-ray transmission ( $> 80\%$  at 4 to 15  $\text{\AA}$ )
- Adequate optical transmission for alignment purposes ( $> 60\%$  at 6330  $\text{\AA}$ )
- High modulus of elasticity to hold the pattern ( $> 10^{11}$  Pa)
- Low tensile stress ( $< 200$  Mpa)
- Low defect density ( $< 0.1$   $\text{cm}^{-2}$ )
- Long lifetime ( $> 10^6$  exposures at 100  $\text{mW cm}^{-2}$  flux)
- Radiation hardness ( $< 10$  nm of distortions at absorbed doses  $> 10^3$   $\text{kJ cm}^{-3}$ )
- Low cost ( $< \$5,000$ )



### 1.1.2 SiC as a Candidate for X-ray Mask Membrane Material

Among the numerous choices of materials available for x-ray mask membrane, four have emerged as most promising; these are silicon, silicon nitride, boron nitride and silicon carbide. Silicon with a relatively high modulus of elasticity ( $\sim 1.5 \times 10^{11}$  Pa) has proven to be radiation-hard under synchrotron-generated x-ray exposure. However, its low optical transmission ( $\sim 20\%$ ) at  $6330 \text{ \AA}$  limits its usefulness with current optical alignment techniques. Silicon nitride has proven to be resistant to high doses of radiation and has reasonable x-ray and optical transmission. Its major drawback is in the difficulty of adjusting the film stress within the required range [4]. Boron nitride exhibits many properties that are required by a mask membrane. It has the highest optical transmission ( $> 65\%$  at  $6330 \text{ \AA}$ ), and x-ray transmission ( $>90\%$  at  $4 \text{ \AA}$ ) characteristics. It has been produced in large areas with very low defect densities ( $\sim 0.1 \text{ cm}^{-2}$ ). But boron nitride cannot withstand long or high x-ray radiation. Prolonged exposure to x-ray radiation degrades the film stress and optical properties.

Silicon carbide exhibits an optical transmission of about  $60\%$  at  $6330 \text{ \AA}$ . It is hard towards very high doses of x-ray radiation [5]. Silicon carbide also has superior mechanical stability with a high Young's Modulus ( $\sim 4 \times 10^{11}$  Pa) [6] and it is known to be the hardest material besides diamond. Its mechanical strength along with its susceptibility towards x-ray radiation makes it an excellent choice as a mask membrane material for x-ray lithography.

In view of aforementioned features of silicon carbide, many research works have been done on this material for its potential applications. The following sections will paintcut some of the research work done in this field and also will highlight the significance of this study.

## **1.2 Literature Overview**

The development of SiC as a mask membrane material for x-ray lithography and as a semiconductor material has been pursued for more than thirty years. Many research papers have been published so far on various topics such as SiC single crystal growth on silicon wafers and mechanism involved in the process, amorphous SiC growth, thin film SiC characterization, x-ray mask membrane fabrication, SiC semiconductor device fabrication and its electrical behavior. This chapter will describe some of them to enunciate the trend of research on this material.

### **1.2.1 SiC as X-ray Mask Membrane Material**

The prospects of x-ray lithography were discussed in detail by H. Luthje [3]. In this paper, different types of lithographic methods were mentioned along with their advantages and disadvantages. Then, the importance of x-ray lithography was discussed. This paper also addressed the key issues of x-ray lithography, such as x-ray sources, alignment system, x-ray resist materials and silicon carbide as a potential mask membrane material. In a paper published by A. Heuberger [7], the problems encountered with x-ray technology for sub-micron lithography were examined and approaches to

solutions were discussed. The importance of mask membrane material were stressed and the properties of certain mask membrane material such as silicon nitride, silicon carbide and silicon were compared. In another study, a a-SiC x-ray mask was fabricated for sub-micron devices and a pattern displacement test was reported by U. Mackens and others in SPIE [8]. The membrane was found to have a high Young's modulus with excellent transparency for synchrotron and optical radiation. Patterns with 0.5 micron thickness had been generated by e-beam lithography as well as mask copying by using synchrotron orbit radiation. Almost similar results were given by H. Luthje, B. Matthiessen, M. Harms and A. Bruns [6].

### **1.2.2 Earlier Studies on the Synthesis of Amorphous SiC**

Non hydrogenated SiC film for x-ray mask synthesis was reported by A. Madouri, A.M. Gosnet and J. Bourneix [9] and their properties were investigated. In that study, the stability of the film was found to be related to the strength of the chemical bond. The films were made by a rf triode sputtering system. The a-SiC HIP target was sputtered with a rf power of  $0.25 \text{ W cm}^{-2}$  under an argon pressure of 3 to 4 mTorr with the substrate temperature of  $450^{\circ}\text{C}$ . However, they could be able to achieve a membrane with an area of about  $9 \text{ mm}^2$  for a  $0.5 \text{ }\mu\text{m}$  thick film. Amorphous SiC was deposited onto fused silica by CVD using gas mixtures of  $\text{SiH}_4$ ,  $\text{CH}_4$  and  $\text{H}_2$  and its properties were reported by Y.J. Park, Y.W. Park and J.S. Chun [10]. Here, the atomic composition of hydrogen was found to be decreased as the deposition temperature was increased. Accordingly, the optical band gap was also found to be increased by increasing the deposition temperature.

Amorphous silicon carbide films synthesized by plasma enhanced CVD, r.f glow discharge methods, r.f. sputtering methods have studied extensively. Electrical and optical properties of such films grown by glow discharge of silane and ethylene gas mixtures were reported by D.A. Anderson and W.E. Spear [12]. In that study, it has been concluded that composition can be varied by volume ratio of precursors. Both optical and absorption and d.c. conductivity showed marked changes in behavior at a composition of 32% Si and 68% C. If the silicon content exceeds about 32%, the electrical transport takes place in extended states but, below this value, changes to hopping conduction. This result was attributed to the tendency of excess carbon to bond in the three-fold graphite coordination. Specimens prepared by this method were found to have an appreciably lower overall density of gap states than sputtered or pyrolytically deposited material. The role of addition of hydrogen in the formation of a-SiC from silane and ethylene mixtures was studied by Scott Meikle, Yoshiko Suzuki and Yoshinori Hatanaka [13]. In this study, the deposition rate was found to be increased as the hydrogen partial pressure fraction was increased up to 50%. The optical band gap was found to be decreased as the H<sub>2</sub> pressure fraction was increased. XPS measurements showed that the density of Si-C bond increased as the slope of the optical edge becomes steeper.

The effect of boron doping on hydrogenated a-SiC were studied by H.D. Mohring *et al.*[14]. Here, the band gap, refractive index, Penn gap and Urbach energy remain unchanged. An atmospheric pressure plasma jet generated by inductively coupled rf

discharge and containing vapors of Si compounds in argon-carrier gas was used to deposit a-SiC films [15]. Rapid deposition up to  $10 \mu\text{m min}^{-1}$  could be achieved in this method. Highly photoconductive hydrogenated a-SiC films were prepared by alternating monolayer deposition and hydrogen passivation by plasma enhanced CVD in multi zone apparatus. This was reported by A. Asano, T. Ichimura and H. Sakai [16]. In this, films with photoconductivity of  $3 \times 10^{-5} \text{ S cm}^{-1}$ , an optical band gap of 1.91 eV was prepared. In another study, a high rate deposition around  $10 \mu\text{m}$  per hour with a optical band gap of 2 to 2.1 eV and with high photosensitivity exhibiting a conductivity change more than  $10^4$  of magnitude under illumination with  $50 \mu\text{W cm}^{-2}$  in intensity was investigated using a glow discharge in  $\text{SiH}_4\text{-C}_2\text{H}_2\text{-H}_2$  mixture gas. This was reported by Y. Nakayama, S. Akita, M. Nakano and T. Kawaura [17]. It was showed that  $\text{C}_2\text{H}_2$  based gas system has high efficiency of the carbon incorporation into the films. Most of amorphous SiC film fabrications have been based on rf glow discharge or sputtering methods resulting in hydrogenated a-SiC films.

### 1.2.3 Earlier Studies on the Synthesis of Crystalline SiC

Generally, crystalline SiC films grown on Si substrate exhibit interface defects. This problem has been addressed by many people and this is generally attributed to lattice mismatch between SiC and Si (about 20%) [19] and the difference in the thermal coefficient of expansion between film and substrate [20]. Films with crystalline defects show excessive stress and cracks. Several works have been published to solve the above problem. A two step process to grow single crystal SiC on Si was reported by H.P. Liaw

and R.F. Davis [21]. Here, Si wafers with  $1^\circ$  or  $6^\circ$  off axis from the (100) plane and  $2^\circ$  and  $4^\circ$  off axis from the (111) plane were used. Initially, Carbon was deposited on and reacted with the Si substrate to form an approximately 15 nm thick chemically converted layer containing Si and C in progressively varying ratios as a function of depth. This was followed by the deposition of both Si and C to form the  $\beta$ -SiC films. Silane and ethylene gas mixtures were used in cold wall CVD reactor to deposit these films. The stress in these films was also found to be optimal in these cases. Films of p+ microcrystalline SiC:H films were deposited and studied by B. Goldstein and C.R. Dickson and others [18]. These films grown by conventional rf glow discharge showed conductivities  $2 - 2 \times 10^{-3} \Omega \text{ cm}^{-1}$  and activation energies 0.05 to 0.1 eV with carbon concentrations of 0-6 atomic %, respectively. Increasing carbon content was found to suppress the microcrystallinity.

Shigehiro Nishino *et al.* studied the growth of single crystal films by chemical vapor deposition with r.f sputtered SiC intermediate layer [19]. They found that even though the sputtered layer was polycrystalline, the subsequent layer deposited by CVD was a single crystal. The crystallinity of the deposited layer was strongly affected by the thickness of the sputtered layer, the substrate temperature during sputtering, and the temperature of chemical vapor deposition. In another study, P. Rai-Choudhury and N.P. Formigoni found that single crystal SiC can be grown on Si substrates with pyrolysis of  $\text{SiCl}_4$  and  $\text{CH}_4$  only at high deposition temperature of not less than  $1500^\circ\text{C}$  [21]. Use of acetylene and dichlorosilane as precursors in the deposition of polycrystalline film and single crystal films by LPCVD method was noted by two groups [22, 23]. H. Nagasawa

and Y. Yamaguchi [22] used an unusual technique of alternating the supply of precursors for short duration of time. However, this process also relied on growth of an intermediate buffer layer of SiC achieved by reacting acetylene with Si substrate. The same authors along with Tsutomu Shoki, Isao Amemiya, Hiroyuri Kosuga and Osamu Nagarekawa developed a LPCVD process with the same precursors to develop polycrystalline SiC films to make x-ray mask membranes suitable for x-ray lithography [23]. They did not describe the growth process in detail, but studied certain properties of the films such as mechanical strength and optical transmission.

Hetero-epitaxial SiC was synthesized and studied by M. Yamada, *et.al.* [11] in a cold wall LPCVD reactor at 1000 °C and at 3.5 Torr using a gas mixture of SiHCl<sub>3</sub>, C<sub>3</sub>H<sub>8</sub> and H<sub>2</sub>. The stress for such films was found to be  $4 \times 10^9$  dyn cm<sup>-2</sup> and Young's modulus was determined as  $4.7 \times 10^{12}$  dyn cm<sup>-2</sup>. A carbonization layer was formed before SiC was grown. This was found to be effective in improving the crystallinity. The formation of the buffer layer mitigates a lattice mismatch of 20% between SiC and Si and enhances the epitaxial growth. It resulted in decreased film stress. Optical absorption properties of crystalline SiC material were reported by two groups [24, 25]. Intrinsic optical absorption of single crystal silicon carbide has been measured in both cubic and hexagonal type modifications by Hekrert R. Philipp [24]. It was found that at longer wavelengths the cubic structure absorbs the radiation more strongly. The electron affinity of silicon carbide is estimated from photoelectric data to be about 4 eV. The absorption of light in alpha SiC of photons of energy 2.6 to 3.3 eV has been measured and reported by W.J. Choyke and Lyle Patrick [25]. Here, the measurements showed that the

interband transitions are indirect, requiring the absorption or emission of a phonon of energy of 0.09 eV. The minimum energy gap was found to be 2.86 eV at 300 K, and above this temperature the slope of the band gap - temperature curve was found to be  $-3.3 \times 10^{-4}$  eV/degree.

#### 1.2.4 SiC as a Semiconductor Device Material

As an application to solar cell fabrication, high conductive p-type microcrystalline SiC:H was prepared using electron cyclotron resonance plasma CVD. This was done by Y. Hattori, D. Kruangam, T. Toyama, H. Okamoto and Y. Hamakawa [26]. Such films with an optical band gap of 2.25 eV exhibited a dark conductivity as high as  $10 \text{ S cm}^{-1}$ . Utilizing this material as a wide-gap heterojunction contact in amorphous silicon solar cell, a conversion efficiency of 12% had been obtained with a large open circuit voltage. Heterojunction of a-SiC and c-Si were studied by K. Sasaki, M.M. Rahman and S. Furukawa [27]. I-V characteristics of a p-type a-SiC/n-type c-Si diode, in which an a-SiC layer has been deposited by L-coupled plasma CVD method, were reported in that study. The n-value of diode was found to be 1.1 for planar diode structure and localized state density at the interface was also found to be small. Similarly, a solar battery made of a-SiC/c-Si structure showed good result as observed by M. M. Rahman and S. Furukawa [28].

One of the earliest work published on the study of SiC-Si heterojunction diodes was done by Don M. Jackson, Jr. and Robert W. Howard [29]. In that work, they synthesized SiC films by vapor-phase decomposition and hydrogen reduction of silicon tetrachloride



and propane. The mesa diodes formed by n-type SiC and p-type Si showed appropriate current-voltage characteristics. These diodes showed a sensitivity to white light in that, the incident light increased the forward and the reverse saturation currents. They also reported that a junction rectification occurs in the SiC-Si structure, for 1 $\mu$ m thick film.  $\alpha$ -SiC high voltage (400V) Schottky barrier diodes were fabricated and their electrical characteristics were reported by Bhatnagar.M [30]. Here, such  $\alpha$ -SiC Schottky barrier diodes showed an on-state current density of 100 A cm<sup>-2</sup> for a temperature range of 25 to 200 °C. The reverse I-V characteristics showed a sharp breakdown voltage of 400 V at 25 °C.

In conclusion, many papers were published on the fabrication and characterization of silicon carbide films in both amorphous and crystalline forms. The trend of research on this field is to understand the silicon carbide growth mechanism on silicon substrates, to reduce the defects produced on the silicon-silicon carbide interface, and to upgrade the membrane fabrication process.

### 1.3 Significance of this Study

It can be noted from the earlier section that amorphous SiC films are generally fabricated by r.f glow discharge, r.f. plasma CVD or sputtering methods. Such films are not free from impurities. The glow discharge methods and plasma CVD methods which involve ions from hydrocarbon always yield inferior films with hydrogen as impurities. Although, hydrogenated SiC finds many applications [9,10,11,16], non-hydrogenated films are preferred for mask membrane, because the presence of hydrogen degrades the x-

ray hardness of the film. In the case of crystalline SiC films, the stress developed in the film during the growth can be reduced by employing above mentioned process due to the low deposition temperature. This is because one of the reasons for the stress built up in the film is due to a difference in the coefficient of thermal expansion between the film and substrate. But, again due to impurity incorporation, these films exhibit high defects in the crystal structure and therefore show poor electrical performance.

Low pressure chemical vapor deposition is an alternate choice for synthesizing films with superior qualities such as uniform thickness and high purity. It has additional advantages like conformal step coverage, high throughput and low cost. Such advantages have not remain unnoticed. But, current CVD processes used in the synthesis of SiC films have traditionally relied on the use of silane as the source for silicon and large choice of hydrocarbons as the source for carbon. However, as widely acknowledged, silane is pyrophoric and explosive, and as such is a serious safety hazard in a laboratory or manufacturing environment. Very few papers have been published on this key issue and therefore further investigation is warranted.

This study investigated a unique LPCVD process for synthesis of both amorphous and crystalline films using novel safe precursors. Ditertiarybutylsilane (DTBS) with a chemical formula of  $(C_4H_9)_2SiH_2$  is a safe alternate precursor to silane that has flash point of 15 °C. This study addressed the use of that organosilane as a *single* precursor for synthesizing amorphous SiC films. Dichlorosilane ( $SiH_2Cl_2$ ), which is safer than silane, was used along with acetylene ( $C_2H_2$ ) for the synthesise of crystalline films. In this study, the film growth kinetics were examined first and then the interrelationships

between process variables, compositions, and select properties of the resulting deposits were also examined. Then the study contemplated on growing defect free films to make free standing membranes on silicon wafers. Furthermore, electrical characterizations of such films were performed for the potential applications of them in fabricating electrical devices.

In view of aforementioned goals of study, the following sections will discuss the fundamental principles involved in chemical vapor deposition and also concludes with advantages and disadvantages of CVD process in comparison with other conventional methods of film deposition.

#### **1.4 Chemical Vapor Deposition**

Chemical Vapor Deposition (CVD) is one of the most important methods of film formation used in the fabrication of very large scale integrated (VLSI) silicon circuits, as well as of microelectronic solid state devices in general. In this process, chemicals in the gas or vapor phase are reacted at the surface of the substrate where they form a solid product. A large variety of materials, practically all those needed in microelectronic device technology, can be created by CVD. These materials comprise insulators and dielectrics, elemental and compound semiconductors, electrical conductors, superconductors and magnetics. In addition to its unique versatility, this materials synthesis and vapor phase growth method can operate efficiently at relatively low temperatures. For example, refractory oxide glasses and metals can be deposited at temperatures of only 300° to 500°C. This feature is very important in advanced VLSI

devices with short channel lengths and shallow junctions, where lateral and vertical diffusion of the dopants must be minimized. This also helps in minimizing process-induced crystallographic damage, wafer warpage and contamination by diffusion of impurities.

#### **1.4.1 Fundamental Aspects of CVD**

Chemical vapor deposition is defined as a process whereby constituents of the gas or vapor phase react chemically near or on the substrate surface to form a solid product. This product can be in the form of a thin film, a thick coating, or if allowed to grow, a massive bulk. It can have a single-crystalline, poly-crystalline, or amorphous structure. Chemical and physical conditions during the deposition reaction can strongly affect the composition and structure of the product. This deposition technology has become one of the most means of creating thin films and coatings in solid state microelectronics where some of the most sophisticated purity and composition requirements must be met.

Chemical reaction type basic to CVD include pyrolysis, oxidation, reduction, hydrolysis, nitride and carbide formation, synthesis reactions and chemical transport. A sequence of several reaction types may be involved to create a particular end product. The chemical reactions may take place not only on the substrate surface (heterogeneous reaction), but also in the gas phase (homogeneous reaction). Heterogeneous reactions are much more desirable, as such reactions selectively occur only on the heated surfaces, and produce good quality films. Homogeneous reactions, on the other hand are undesirable, as they form gas phase clusters of the depositing material, which will result in poor

adherence, low density or defects in the film. Thus one important characteristic of CVD application is the degree to which heterogeneous reactions are favored over homogeneous reactions. This film could be a thin film or a thick coating and should be less volatile to remain on the substrate.

#### **1.4.2 Transport Phenomena of CVD**

CVD of the film is almost always a heterogeneous reaction. The sequence of the steps in the usual heterogeneous processes can be described as follows:

1. Arrival of the reactants
  - a. bulk transport of reactants into the chamber,
  - b. gaseous diffusion of reactants to the substrate surface,
  - c. adsorption of reactants onto the substrate surface.
2. Surface chemistry
  - a. surface diffusion of reactants,
  - b. surface reaction.
3. Removal of by-products
  - a. desorption of by-products from the substrate surface,
  - b. gaseous diffusion of by-products away from the substrate surface,
  - c. bulk transport of by-products out of the reaction chamber.

The steps are sequential and the slowest process is the rate determining step.

The sequential steps of deposition process can be grouped into (i) mass transport-limited regime and (ii) surface-reaction-limited regime. If the deposition process is limited by the mass transfer, the transport process occurred by the gas-phase diffusion is proportional to the diffusivity of the gas and the concentration gradient. The mass transport process which limits the growth rate is only weakly dependent on temperature. On the other hand, it is very important that the same concentration of reactants be present in the bulk gas regions adjacent to all locations of a wafer, as the arrival rate is directly proportional to the concentration in the bulk gas. Thus, to ensure films of uniform thickness, reactors which are operated in the mass-transport-limited regime must be designed so that all locations of wafer surfaces and all wafers in a run are supplied with an equal flux of reactant species.

If the deposition process is limited by the surface reaction, the growth rate,  $R$ , of the film deposited can be expressed as  $R = R_0 \cdot \exp(-E_a/RT)$ , where  $R_0$  is the frequency factor,  $E_a$  is the activation energy - usually 25-100 kcal/mole for surface process,  $R$  is the gas constant, and  $T$ , the absolute temperature. In the operating regime, the deposition rate is a strong function of the temperature and an excellent temperature control is required to achieve the film thickness uniformity that is necessary for controllable integrated circuit fabrication.

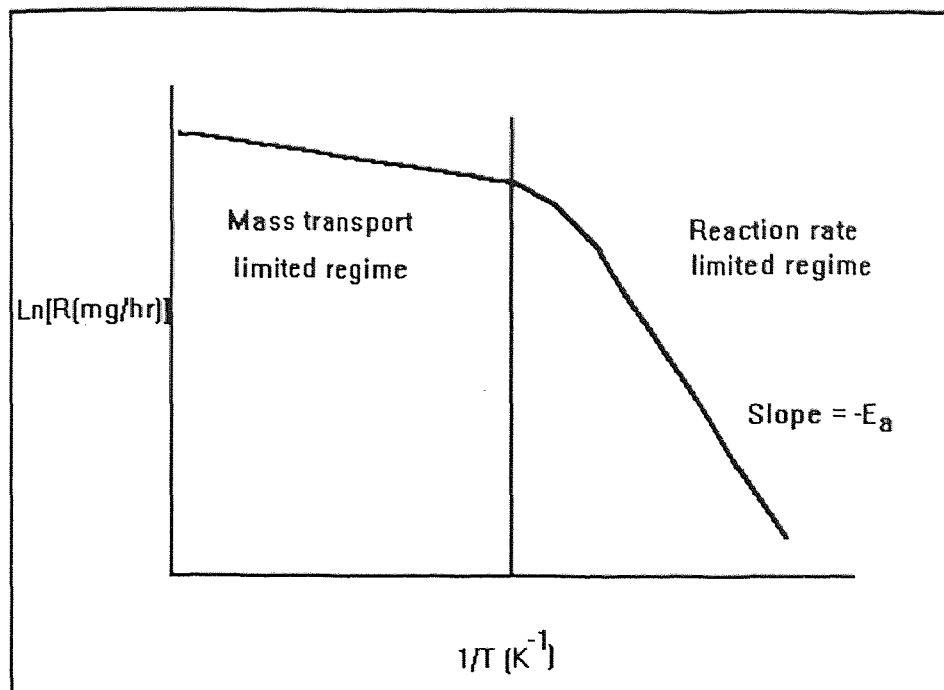


**Figure 1.1** Deposition rate as a function of substrate temperature exemplifying diffusion controlled and surface-reaction controlled regimes

On the other hand, under such conditions the rate at which reactant species arrive at the surface is not as important. Thus, it is not as critical that the reactor be designed to supply an equal flux of reactants to all locations of the wafer surface. It will be seen that in horizontal low pressure CVD reactors, wafers can be stacked vertically and at very close spacing because such systems operate in a surface-reaction-rate limited regime. In deposition processes that are mass-transport limited, however, the temperature control is not nearly as critical. As shown in Figure 1.1, a relatively steep temperature range, and a milder dependence in the upper range, indicating that the nature of the rate-controlling step changes with temperature.

### 1.4.3 Film Growth Aspects of CVD

In general, lower temperature and higher gas phase concentration favor formation of polycrystalline deposits. Under these conditions, the arrival rate at the surface is high, but the surface mobility of adsorbed atoms is low. Many nuclei of different orientation are formed, which upon coalescence result in a film consisting of many differently oriented grains. Further decrease in temperature and increase in supersaturation result in even more nuclei, and consequently in finer-grained films, eventually leading to the formation of amorphous films when crystallization is completely prevented. Amorphous films include oxides, nitrides, carbides and glasses are of great technical importance for microelectronics applications.

Deposition variables such as temperature, pressure, input concentrations, gas flow rates, reactor geometry and reactor opening principle determine the deposition rate and the properties of the film deposit.

## 1.5 Low Pressure CVD Process

The most important and widely used CVD processes are atmospheric pressure CVD (APCVD), low pressure CVD (LPCVD) and plasma enhanced CVD (PECVD). Only LPCVD is discussed in detail below as this process is employed in this study.

Most low pressure CVD processes are conducted by resistance heating and less frequently infrared radiation heating techniques to attain isothermal conditions so that the substrate and the reactor walls are of similar temperature. The deposition rate and uniformity of the films created by all CVD processes are governed by two basic



parameters (i) the rate of mass transfer of reactant gases to the substrate surface and (ii) the rate of surface reaction of the reactant gases at the substrate surface. Lowering the pressure to below atmospheric pressure enhances the mass transfer rate relative to the surface reaction rate thus making it possible to deposit films uniformly in a highly economical close spaced positioning of the substrate wafers in the standup position.

### **1.5.1 Mechanism Involved in Film Deposition**

The mass transfer of the gases involve their diffusion across a slowly moving boundary layer adjacent to the substrate surface. The thinner this boundary layer and the higher the gas diffusion rate, the greater is the mass transport that results. Surface reaction rates, on the other hand, depend mainly upon reactant concentration and deposition temperature. High deposition rates are attainable with LPCVD despite the fact that the operating total pressure is usually two to four orders of magnitude lower than atmospheric CVD. This is due to the fact that the large mole fraction of reactive gases in LPCVD, and no or little diluent gas is required. Wafer spacing has a marked effect on the deposition rate of all types of films, the deposition rate increasing linearly with increasing spacing since the quantity of available reactant per wafer increases.

### **1.5.2 Factors Affecting Film Uniformity**

Some of the main factors affecting the film thickness uniformity in LPCVD are the temperature profile in the reactor, the pressure level in the reactor and the reactant gas flow rates. To obtain a flat thickness profile across each substrate wafer throughout the reactor requires a judicious adjustments of these parameters. In tubular reactors, increase

in temperature or pressure, increases the deposition rate upstream, thereby using up more reactant gases and leaving less to react at the downstream end; the opposite effect takes place on lowering the temperature and pressure. Similar effects occur with variations of the reactant gas flow rates at constant gas partial pressure, or with changes in the size and number of the wafers processed per deposition run. The uniformity of thickness and step coverage of these films are very good. These films have fewer defects, such as particulate contaminants and pinholes, because of their inherently cleaner hot wall operations and the vertical wafer positioning that minimize the formation and codeposition of homogeneously gas phase nucleated particulates.

### **1.6 Advantages of CVD**

Thin films are used in a host of applications in VLSI fabrication, and can be synthesized by a variety of techniques. Regardless of the method by which they are formed, however, the process must be economical, and the resultant films must exhibit uniform thickness, high purity and density, controllable composition and stoichiometries, high degree of structural perfection, excellent adhesion and good step coverage. CVD processes are often selected over competing deposition techniques because they offer the following advantages:

1. A variety of stoichiometric and non stoichiometric compositions can be deposited by accurate control of process parameters.
2. High purity films can be deposited that are free from radiation damage without further processing.

3. Results are reproducible.
4. Uniform thickness' can be achieved by low pressures.
5. Conformal step coverage can be obtained.
6. Selective deposition can be obtained with proper design of the reactor.
7. The process is very economical because of its high throughput and low maintenance costs.

### **1.7 Limitations of CVD**

Fundamental limitations of CVD are the chemical reaction feasibility and the reaction kinetics that govern the CVD processes. Technological limitations of CVD include the unwanted and possibly deleterious but necessary by-products of reaction that must be eliminated, and the ever present particle generation induced by homogeneous gas phase nucleation that must be minimized.

## CHAPTER 2

### EXPERIMENTAL PROCEDURE

#### 2.1 Introduction

Silicon carbide thin films with varying composition and properties were synthesized in a LPCVD reactor by adjusting various deposition parameters including temperature, pressure, gas composition and time of deposition. The experiments yielded a variety of films which were carefully subjected to physical and chemical analyses. These characterization procedures were aimed at standardizing the processing conditions to produce films that are suitable for making x-ray mask membrane. Fourier transform infrared (FTIR) analyses were done on the synthesized films to examine the vibrational modes of the deposited material. Stress in the films was measured and calculated from the principle of radius of curvature difference of the substrate. Refractive index and thickness of the films were measured by ellipsometry and interferometry respectively. The optical transmission of the films were measured using a UV-visible spectrophotometer. The elemental composition analyses were done by Rutherford Backscattering (RBS), Auger electron spectroscopy (AES) and X-ray photoelectron spectroscopy (XPS). X-diffraction analysis were performed in order to verify the amorphous or crystalline nature of the deposits. Mechanical properties such as Young's Modulus and hardness of these films were measured using Nano Instruments. Surface roughness studies, in the case of poly crystalline films were done by atomic force microscopy. Electrical characterizations such as high frequency capacitance-voltage and current-voltage relationships for substrate-film-metal structure were performed. From

these measurements parameters like dielectric constant, trapped charge density, breakdown voltage, and idiality factor were estimated. The following sections describe the experimental setup and brief theoretical aspects of characterization procedures.

## 2.2 LPCVD Reactor

The low pressure chemical vapor deposition reactor is schematically shown in figure 2.1. The horizontal reaction chamber consisted of a fused quartz tube of 142cm in length and 11.5 cm in diameter which was encapsulated with a three-zone Lindberg heating furnace. The heating furnace used Lindbar silicon carbon heating elements which could raise the temperature of the reaction chamber up to 1200 °C. The entire tube was insulated from the environment by a ceramic enclosure. A varying temperature profile could be set within the three zones, even though this facility was rarely used. Temperature control and stability was achieved by the associated electronic feedback circuits, which included Platinel II thermocouples, that sensed the temperature of the reaction zone. The temperature inside the furnace was confirmed against the setting by using a calibrated K type thermocouple and were controlled within  $\pm 5^\circ$  with respect to the set temperature. The pressure inside the chamber was monitored at the input end of the furnace by an MKS baratron gauge with a range of 10 torr.

The other end of the reaction chamber was connected to a vacuum station comprised of a booster pump and a mechanical backing pump. Booster pump was used to enhance the flow of gases and thereby the pumping speed. Mechanical backing pump did the real pumping and this combination provided a vacuum of as low as 5 milli torr.

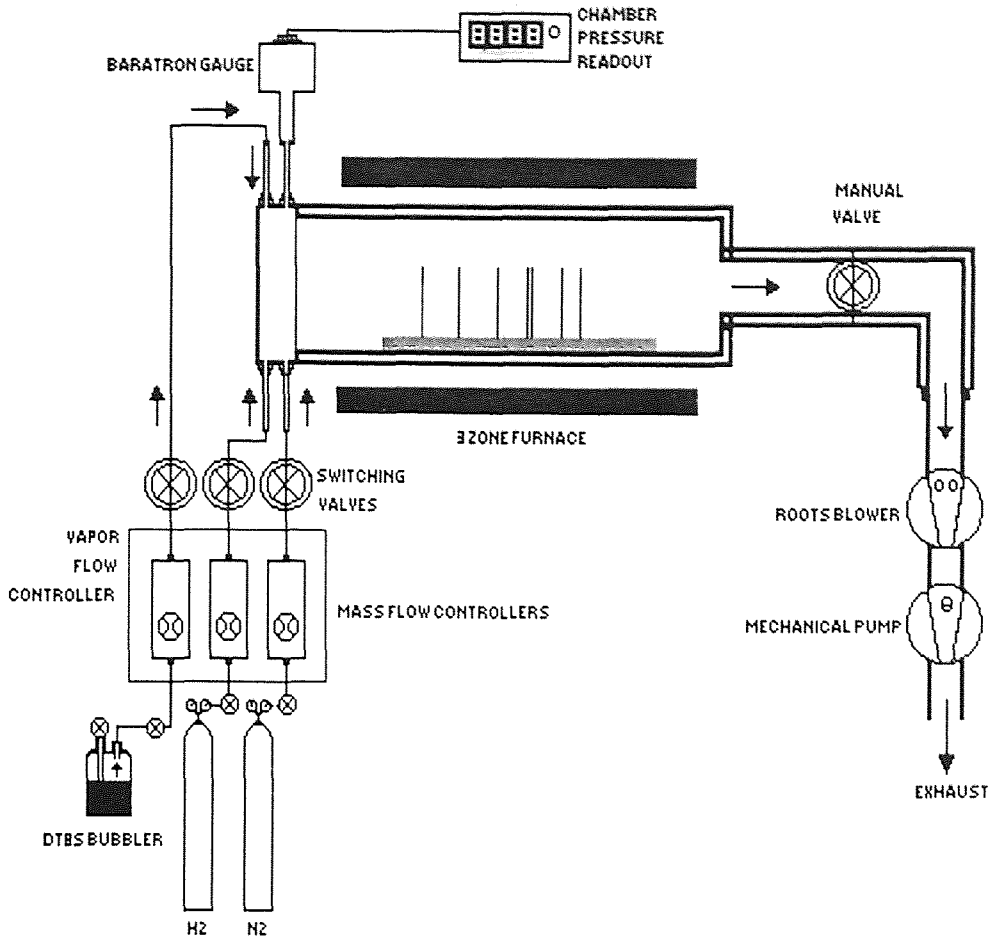


**Figure 2.1** Schematic representation of the LPCVD reactor

Booster pump was a Ruvac single stage roots pump operated at 220 V supply and that the backing pump was a Trivac dual stage rotary vane pump. Nitrogen ballast gas was used in the pump to dilute any hazardous outgoing gas. Apart from this, an oil filter system was used to filter micron sized particles from the pump oil, which would help in increasing the lifetime of the pump. The reaction chamber was sealed on both ends by end caps and metallic lids. During heating process, thermal expansion of O-rings may

cause leakage of outside air in to the system. To avoid this problem, end caps designed for this reactor have a provision for cold water circulation (not shown in the figure) to prevent overheating of the O-rings. A manual valve at the output end was used to control the removal rate of gases and thereby maintaining a steady pressure inside the chamber. Precursors were delivered inside the chamber, in a controlled manner using mass flow controllers. In the case of DTBS, an MKS 200 sccm vapor-phase flow controller Model 1150B-162M was used to measure and control the flow rate of DTBS. The calibration of these flow controllers is described in later section. A spare nitrogen mass flow controller was installed to incorporate any necessary additional reactant gas into the chamber or for back filling. This spare controller could be calibrated for gases other than nitrogen.

A carrier gas for DTBS was not required since it has a low vapor pressure (200 Torr @ 25°C). Other reactants were metered by means of Applied Materials model AFC 550 automatic N<sub>2</sub> mass flow controllers which were calibrated to regulate respective gases. All delivery lines were stainless steel with VCR type connections.

## **2.3 Pre-Deposition Procedure**

### **2.3.1 Leak Check**

Air leak into the chamber may cause due to improper delivery line connections and improper chamber end cap connection. Such leakage will affect the quality of deposits and result in useless experiments. Therefore, routine leak checks were conducted keeping all valves and mass flow controllers fully open. After evacuating the chamber, the manual valve was closed and from the pressure rise in the reactor the leak rate was

calculated. Typical leak rates were of the order of 4 mTorr/min. This was mostly due to outgassing from the deposits on the chamber wall resulted from the previous depositions.

### 2.3.2 Flow Rate Calibration

Generally flow rate of the precursor is expressed in units of sccm, i.e., standard cubic centimeter per minute. This is the volume that would be occupied by the precursor, which is measured at standard temperature and pressure, as result of flow for one minute. In order to verify the rate of flow, the precursor was delivered into the CVD reaction chamber at a known initial pressure and at room temperature, using the standard flow controller which was set to control at desired flow. The manual output valve was then closed and the rise in chamber pressure over a fixed time interval was measured. Assuming that the temperature inside the reaction chamber was at  $T_r$  (i.e., room temperature) and precursor to be an ideal gas under these conditions, Ideal Gas Law gives,

$$PV = nRT \quad (2.1)$$

Since chamber volume,  $V$ , is fixed, and was determined by the geometrical measurements,

$$\frac{P}{n} = \frac{R * T_r}{V} = \text{const} \quad (2.2)$$



$$\frac{\partial n}{\partial t} = \frac{V}{R \cdot T_r} * \frac{\partial P}{\partial t} \quad (2.3)$$

where, t is the time.

At standard condition of temperature (273 K) and pressure (760 Torr) therefore,

$$V_s = \frac{nRT}{P} = nR * \frac{273}{760} \quad (2.4)$$

and,

$$\frac{\partial V_s}{\partial t} = R * \frac{273}{760} * \frac{\partial n}{\partial t} \quad (2.5)$$

Substituting equation (2.3) into (2.5), gives flow rate at room temperature of  $T_r$ ,

$$F.R. = \frac{\partial V_s}{\partial t} = \frac{V}{760} * \frac{273}{T_r} * \frac{\partial P}{\partial t} \quad (2.6)$$

or,

$$\frac{760}{V} = \frac{\Delta P / \Delta t}{F.R.} * \frac{273}{T_r} \quad (2.7)$$

Where, V is the volume of the reaction chamber (which was measured as 16,700 cm<sup>3</sup>),  $T_r$  is the room temperature and  $\Delta P / \Delta t$  is the rate of increase in pressure. Equation 2.7 was used to calibrate the flow rate of the reactants. Special mass flow controllers for

some of the reactants used, such as acetylene, were not commercially available, and therefore a correction of  $N_2$  mass flow controllers which were employed to meter these gases, was necessary. The flow conversion factor was obtained from the manual provided by the suppliers of mass flow controllers, and that was verified by taking the ratio of the actual flow rate of the reactant gas (which was measured by the above procedure) to the actual flow rate of nitrogen.

## 2.4 Deposition Procedure

### 2.4.1 Wafer Loading

Films were synthesized on virgin silicon and quartz substrates. The specification of silicon wafers are depicted in table 2.1. Fused quartz substrate had the same diameter of that of silicon. These substrates were first labeled and weighed, using an electronic weighing balance up to an accuracy of 0.01 mg. Then, they were mounted vertically on a fused silica boat with 12 single wafer slots and 10 double wafer slots. Single and double wafer slots alternated along the length of the boat with a distance of 1.25 cm between them. Dummy wafers were placed at the first and the last position in each experiment. For convenient handling of boat, the first dummy wafer was mounted on the second single wafer slot at 6 cm from the front end of the boat. The virgin wafers were placed on subsequent slots. Some wafers need to be deposited on one side only, in order to measure the stress of the film. This was accomplished by placing two wafers together, back to back, on a double wafer slot. The quartz boat was then placed with its front at 65 cm

downstream, ensuring that they were placed in the middle zone of the furnace. The front end of the chamber was then closed and the chamber was pumped down.

#### 2.4.2 Film Deposition

The reaction chamber and the reactant delivery lines were evacuated for about 30 minutes. The reaction chamber was then gradually heated to the deposition temperature and stabilized for fifteen minutes to ensure thermal equilibrium. Water circulation and fans were used to cool the end cap O-rings. Once thermal equilibrium was reached, the reactants were allowed to flow for stipulated time.

After the deposition, the furnace was left for cooling at its normal rate. The chamber was opened next day, by breaking the vacuum. This was done by delivering a fixed flow of nitrogen in to the chamber, when the output valve was completely closed. This would bring the chamber to the atmospheric pressure and thereby enabling the front lid to open.

**Table 2.1** Specifications of the Si wafer

Source	Silicon Sense Inc.
Diameter	100 mm
Orientation	<100>
Thickness	525 ± 25 μm
Type/Dopant	p/Boron n/Phosphorus
Resistivity	5 - 15 Ω-cm
Grade	Test

## 2.5 Film Characterization Techniques

### 2.5.1 Initial Analysis

Once the wafers were taken out, they were weighed again. The difference in weights before and after the reaction would give the mass of the film deposited. The mass divided by the time of deposition would give the *deposition rate*.

Film thickness was measured by Nanospec Interferometer which bases its estimates on the monochromatic light interface fringes formed within a zone limited by the sample surface and a semi-transparent mirror. The thickness of the film deposited on one side was measured at five different points on the wafer i.e. 1 cm off both edges of both the equatorial and the longitudinal axis, and at the center, as shown in figure 2.2. Uniformity in radial distribution of the deposits was then estimated from the relationship:  $(T_{\max} - T_{\min}) / (T_{\max} + T_{\min}) * 100$  where, T is the average film thickness.

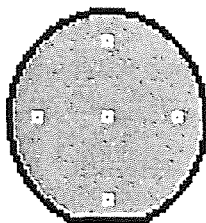


**Figure 2.2** Schematic diagram of a typical silicon wafer showing points where thickness was measured

An optical microscope, Reichert Wein (BTL 122815), was used to detect cracks, gas phase nucleation clusters, and other defects in the films.

### 2.5.2 Refractive Index Measurements

Refractive index of the was determined using ellipsometry. The measurement technique is mainly concerned with the measurement of changes and the state of polarization of light upon reflection with the surface. It employs monochromatic, plane polarized light with its plane of polarization  $45^\circ$  to the plane of incidence. When the elliptically polarized light is reflected from an absorbing substrate its state of polarization is changed.

The ellipticity of the reflected beam is determined by the relative phase difference  $\delta$  and azimuth  $\psi$ . An in-built computer program numerically solves the equations generated by these  $\delta$  and  $\psi$  and the refractive index and the thickness of the film is obtained. The index of refraction is an important parameter which gives indication of stoichiometry of the film. This parameter is also used in measuring thickness using interferometry. The index of refraction measurements for the samples that were synthesized, were collected at NASA Lewis Research Center on a home-built rotating analyzer ellipsometer using a 75 W Xe arc lamp, a computer-controlled double gradient monochromator, and calcite polarizers. Measurements were taken in the range of 500-720 nm in 20 nm steps at three angles of incidence ( $72^\circ$ ,  $73^\circ$ ,  $74^\circ$ ).

### **2.5.3 Infra-red Spectroscopic Studies**

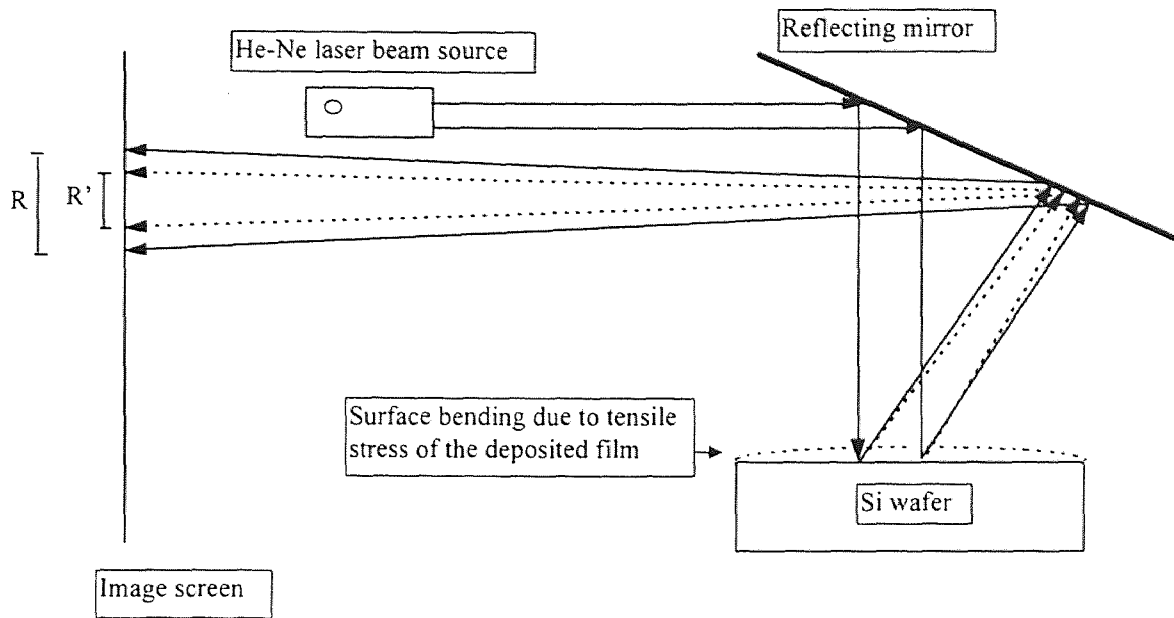
Infra red spectroscopy is a powerful method by which one can detect the presence of particular type of molecular vibration. Materials will absorb certain frequencies in the infra-red region (wavelengths of 2 to 25 microns) because of the excitation of vibrational energy transitions in molecular species. In the same way the electronic transitions in atoms can absorb radiation of specific frequencies, the vibration of a molecule (stretching or bending) will have a resonance value, and it will be excited by any radiation of this frequency. When IR radiation of a particular frequency impinges a sample containing molecular species, it may or it may not be absorbed. If all frequencies are passed through, some will be absorbed to varying degrees depending on the molecular species involved. The intensity of the return radiation therefore depends upon the vibrational mode of the molecules. The presence of a particular molecular vibration can be detected by an absorption or transmission peak in the spectrum.

Infrared spectroscopic analysis was done on a routine basis using a Perkin Elmer 1600 series FTIR spectrophotometer and Perkin Elmer 580 spectrophotometer to determine the bonding characteristics of the deposits.

### **2.5.4 Stress Measurements**

Stress develops in the film due to difference in the thermal coefficient of expansion of the film and the substrate, lattice mismatch between a crystalline film and the substrate, and also due to defects developed in the bulk during the growth process, which is termed as

intrinsic stress. The stress in the film will cause the substrate to slightly bend after the deposition resulting in some radius of curvature.



$R - R'$  is the radius of curvature of bending

**Figure 2.3** Schematic representation showing the experimental setup to measure the radius of curvature of the bending of silicon substrate due to stress in the film.

Stress of the film can be calculated using Stony's formula

$$\sigma_s = ED^2/6(1-\nu)Rt \quad (2.8)$$

where  $E$  and  $\nu$  are Young's modulus and Poisson ratio of the substrate.  $D$ ,  $t$  are the substrate and film thickness' respectively,  $R$  is the radius of curvature of the composite.

By convention  $R$  is negative for a convex wafer surface (compressive film stress) and positive for a concave wafer surface (tensile film stress).

Film stress was determined with a home-built system that measured changes in the radius of curvature of a wafer resulting from deposition on a single side. Such depositions were achieved by placing two wafers back to back. The experimental setup to measure the radius of curvature of the substrate bending is shown in the figure 2.3. The distance between two points generated by light from two fixed and parallel He-Ne lasers was determined after reflection from the surface of a wafer before and after deposition. An angled mirror was used to project the reflection of the two points onto a wall where their separation could be more accurately measured.

In the present set of experiments, for the wafers used, Young's modulus of the substrate was taken as  $1.85 \times 10^{11}$  Pa with a Poisson ratio of 0.3. Substrate average thickness was 525  $\mu\text{m}$ . Considering the geometry of the instrument used, the equation (2.8) reduces to

$$\sigma_s(\text{MPa}) = 12.3R'/t (\mu\text{m}) \quad (2.9)$$

where  $R'$  is the difference of the deflection of the projected laser spots after and before deposition.

### 2.5.5 X-ray Diffraction Studies

X-ray diffraction patterns were studied to verify the crystalline or amorphous nature of the deposited films using IBM PC based Rigaku diffractometer with a Cu target and operating at 45 kV and 40 mA. Typical beam size of the radiation was 150  $\text{\AA}$ .



### 2.5.6 Optical Transmission Studies

The optical transmission of the films were measured using a Varian DMS 300 UV/visible spectrophotometer over a range of wavelength from 200nm to 900nm. This was carried out with samples deposited on quartz substrate. The optical transmission of SiC films were of particular interest at a wavelength of 6320 Å, since x-ray mask alignment equipments rely on light rays around this wavelength. From the optical transmission spectrum, it is possible to estimate the optical band gap [31]. The optical band gap is determined from the calculated values of absorption coefficient,  $\alpha$ . The intensity of the transmitted wave,  $I$ , through a film of thickness  $t$ , is related to the intensity of incident wave  $I_0$  by Beer-Lambert law

$$I = I_0 e^{-\alpha t} \quad (2.10)$$

If the average thickness of the film is known, then absorption coefficient for each wavelength can be calculated. The absorption coefficient of semiconducting films in the high-absorption region ( $\alpha > 10^4 \text{ cm}^{-1}$ ), assuming parabolic band edges and energy-independent matrix elements for interband transitions, is given according to Tauc [32] by the following equation:

$$\alpha h\nu = K_1 \frac{(h\nu - E_{g(\text{opt})})^2}{h\nu} \quad (2.11)$$

where  $h\nu$ ,  $E_{g(\text{opt})}$  and  $K_1$  denote the photon energy, optical energy gap, and an energy-independent constant, respectively. Formally, the optical band gap  $E_{g(\text{opt})}$  is obtained as the intercept of the plot of  $(\alpha * h\nu)^{1/2}$  against  $h\nu$ .

### 2.5.7 Compositional Analysis

The elemental composition and chemical states were studied by X-ray photoelectron spectroscopy (XPS) and Auger electron spectroscopy (AES) using a Perkin-Elmer 570 ESCA/SAM. Unmonochromotized Al K $\alpha$  x-rays (1486.6 eV, 25W) were the X-ray photoelectron spectroscopy (XPS) excitation source; a 5kV, 1 $\mu$ A electron beam was rastered over a square 250  $\mu$ m on a side during Auger analysis. The base pressure of the system during analysis was  $2 \times 10^{-9}$  Torr. Auger depth profiles were generated using a 4 kV, 3  $\mu$ A Ar ion beam rastered over a 5 X 8 mm area. The core level binding energies were referenced to the Au 4f<sub>7/2</sub> line at 83.9 eV. A low energy electron gun was also used for charging neutralization. Atomic compositions were calculated from XPS peak areas using the Perkin Elmer software cross-sectional values which had been previously verified using standard SiC materials.

The Rutherford backscattering spectroscopy (RBS) measurements were taken using a High Voltage Engineering AK accelerator with He<sup>+</sup> ions at an energy of 1.8 MeV to corroborate the ESCA data. All compositional results were reported with  $\pm 3\%$  error.

The ESCA analyses were performed by Dr. Herman J. Boeglin at Olin Hunt Inc., and RBS analyses were performed by Dr. Robert Pfefer at Fort Monmouth.

### 2.5.8 Hardness and Young's Modulus Measurements

The hardness and Young's modulus of the SiC films were determined using a Nano Instruments indenter. The system consisted of a diamond tip, with the same area-to-depth ratio as the traditional Vickers pyramid, mounted on a loading column that was

suspended on thin leaf springs as shown in figure 2.4. At the top of the loading column was a coil and magnet assembly that provided a controlled loading force with a resolution of about  $0.5 \mu\text{N}$ . The position of the indenter was determined by a capacitance displacement gauge which allows one to detect displacement changes of  $0.2\text{-}0.3 \text{ nm}$ . In this work, the maximum drift rate prior to testing was  $0.1 \text{ nm/s}$ , the loading rate was  $200 \mu\text{N/s}$  to a maximum load of  $4.5 \text{ mN}$ , the hold time was  $1 \text{ min}$ , and the ambient temperature was kept constant within  $1^\circ$  at  $21^\circ \text{C}$ . In all cases a minimum of 16 indents were performed on each sample.

As reported for a variety of materials, [33,34] a typical load displacement curve for a SiC deposit is shown in figure 2.5. The initial increase in that

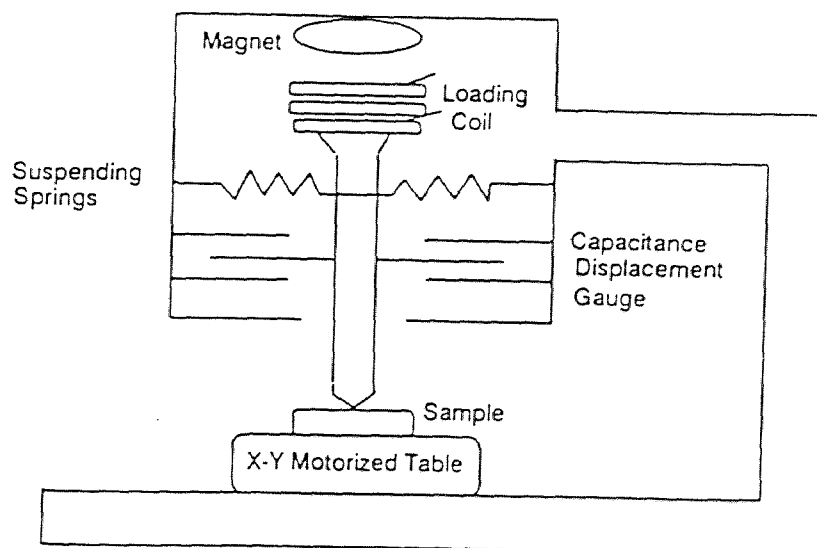


**Figure 2.4** Schematic representation showing the setup to measure hardness of SiC film.

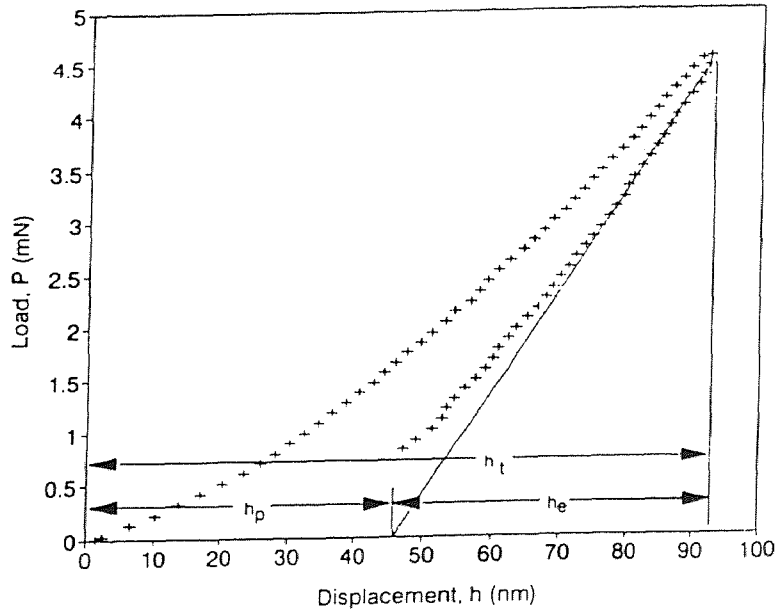


**Figure 2.5** Typical load displacement for a SiC film.

curve represents the observed displacement due to an increased loading at a constant rate of  $200 \mu\text{N/s}$  to a maximum of  $4.5 \text{ mN}$ . The second segment of the curve represents the unloading at the same constant rate down to 20% of maximum load. From that latter segment, the deformation contact depth  $h_p$  and elastic recovery depth  $h_e$  can be measured. A linear least squares fit of the upper segment extrapolated down to 0 yields the value of  $h_p$ . The difference between the maximum displacement and  $h_p$  yields the value of  $h_e$ . The hardness is obtained at the maximum displacement using the formula

$$H = P / A \quad (2.12)$$

where  $P$  is the applied load and  $A$  is the contact area calculated from the known geometry of the indenter

$$A = 24.56 h_p^2 + 225.94 h_p^{3/2} + 519.61 h_p \quad (2.13)$$

Assuming that the area in contact remains constant during initial unloading and adopting Sneddon's solution for the elastic deformation of an isotropic elastic material, the elastic modulus is obtained from the contact stiffness  $S$ , the slope of the unloading curve, given by

$$S = dP / dh = 2 E_r \sqrt{A / \pi} \quad (2.14)$$

where  $h$  is the displacement of the indenter, and  $E_r$  is the composite modulus for the indenter/sample combination

$$E_r = \frac{1}{[(1-\nu_f^2) / E_f] + [(1-\nu_i^2) / E_i]} \quad (2.15)$$

where  $E_f$  and  $E_i$  are Young's moduli for film and indenter, respectively, and  $\nu_f$  and  $\nu_i$  are Poisson's ratios for the film and the indenter, respectively. Since  $\nu$  appears as a quadratic term and therefore represents only a small correction,  $\nu_f$  was taken as 0.3, while the values for the diamond indenter  $E_i$  and  $\nu_i$  were taken to be 1010 GPa and 0.213, respectively.

## 2.5.9 Electrical Characterization of SiC Thin Films

**2.5.9.1 Wafer Preparation:** Two sets of wafers were employed to study interface behavior and other electrical parameters. One set of wafers were used as obtained. The other set of wafers were undergone standard RCA cleaning followed by furnace pre-

clean. Such furnace pre-cleaned wafers along with the as obtained wafers were loaded immediately into the CVD furnace for film deposition. Standard RCA cleaning was done by dipping wafers in a chemical bath containing 5:1  $H_2SO_4:H_2O_2$  at  $110^\circ C$  for 10 minutes. The wafers were rinsed in hot de-ionised (DI) water at  $80^\circ C$  for 10 minutes, and they were rinsed again in cold DI water for 5 minutes, and spin dried. In order to remove the native oxide, wafers were dipped in solution 100:1  $H_2O:HF$  for 1 minute. Subsequently, the wafers were rinsed in cold DI water for 10 minutes and spin dried. Films were deposited under optimum conditions, such that they exhibit nominal stress values.

**2.5.9.1 Metallization:** To study electrical characteristics of the synthesized films, the films were coated with pure Al dots to form a substrate-film-metal structure. This was done in an evaporator, and the important parameters of deposition is given in Table 2.2. A mask was used to obtain Al dots of diameter  $300\mu m$  and  $500\mu m$  on the silicon carbide film, while a uniform coating of Al is deposited on the back surface (Si surface of the stress monitor).

**Table 2.2** Parameters for metallization of SiC thin films

Base pressure	$10^{-6}$ Torr
Heating source	Tungsten filament (resistance heating)
Evaporating source	Al wire
Purity of evaporating source	99.9999% (Al)
Rate of deposition	$50 \text{ \AA}/\text{min}$ .
Ultimate thickness of deposit	$900 \text{ \AA}$
Substrate temperature	room temperature
Distance between the filament and the substrate	200 mm
Size of the dots	$300 \mu m$ and $600 \mu m$ diameter

**2.5.9.2 Electrical Parameters Measurements:** High frequency capacitance - voltage (C-V) measurement was done for the amorphous films on p-type Si substrates. All samples went through a forming gas annealing at 450°C for 30 minutes after evaporation of Al dots through a shadow mask. The back side SiC was removed by plasma etching (if necessary) and Al was deposited for back contact as explained in the previous section. HF C-V measurements were done using HP 4145B semiconductor parameter analyser in conjunction with Boonton 72VD capacitance meter. The experimental setup is shown in figure 2.5. The dielectric constant of the SiC films were measured at different positions along the axis of the wafer. Bias-temperature stress measurements were also made to find out if there are trapped charges in the insulator. This was done by applying a positive and negative polarity of  $\sim 1\text{MV/cm}$  for 30 minutes at 165°C and repeating the HF C-V measurements. From the shift in the plot, the interface trapped charges were estimated. To find out the nature of the charges, bias-temperature aging studies were done on the samples. The flat-band voltages was determined from the HF C-V plot. The current voltage characteristics for Si-SiC-metal structure were conducted using HP 4145B wherein a standard diode circuitry was employed.

## 2.6 Membrane preparation

The process of producing free standing silicon carbide membranes involved etching the silicon carbide from a central circular region on the back side of the wafer using an Applied Materials Plasma II AMP 3300 plasma etch reactor at a typically RF power of 500 W, frequency of 100 kHz, and a base pressure of 2 mTorr. The etch gas consisted of

30 sccm  $O_2$  and 10 sccm 92 %  $CF_4$  / 8 %  $O_2$  mixture. Under these conditions the etch rate was close to 50 Å/min. Subsequent etching through the exposed silicon substrate was achieved using a 50% KOH in water mixture at a temperature of  $\sim 80^\circ C$  which took  $\sim 8$  h to clear the 500  $\mu m$  substrate.

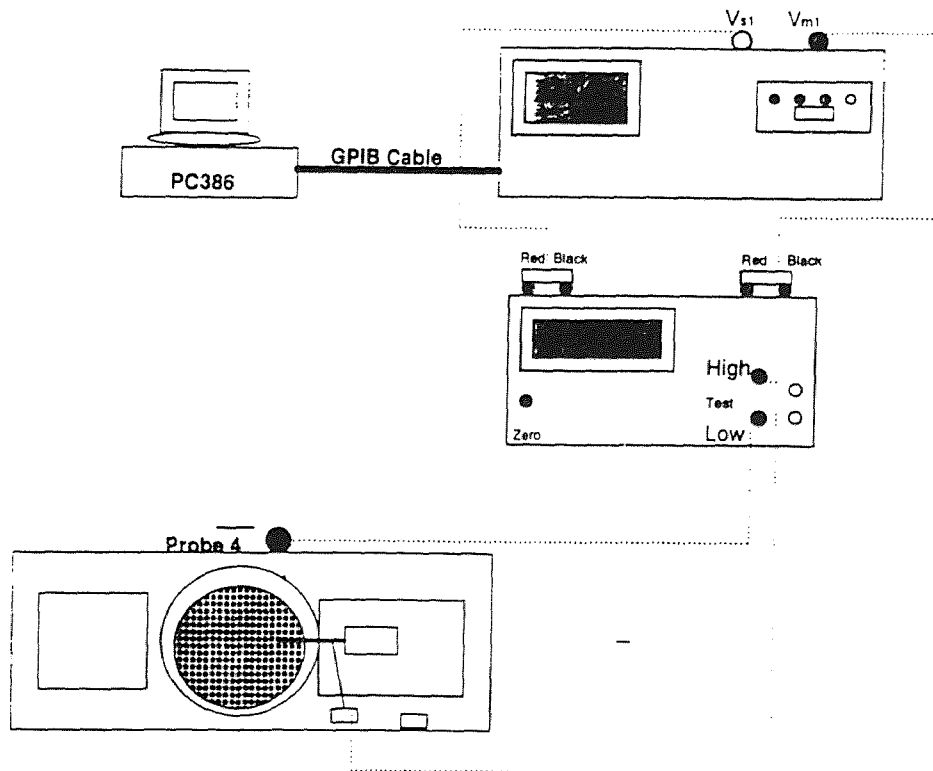


**Figure 2.5** Experimental setup to measure the high frequency C-V characteristics of Si-SiC-metal structure.



## CHAPTER 3

### RESULTS AND DISCUSSION

#### 3.1 Introduction

The results of various characterization studies that were performed on the samples of amorphous and crystalline SiC films are described in the following sub-sections of this chapter. These characterizations were aimed at standardizing the synthesizing process, so that the resulting films are suitable for making x-ray lithographic masks. As explained earlier, the initial study was aimed at synthesizing amorphous SiC films which can render smooth surface and thereby minimizing the x-ray scattering effects. In the following sections, the growth kinetics of amorphous SiC films with respect to various LPCVD parameters are discussed. The effect of such parameters on the composition, mechanical and optical properties of the films are deduced. Electrical characterization were performed to investigate the insulating or conducting behavior of these films. Certain electrical parameters such as dielectric constant, trapped charge density, and dielectric breakdown voltage were estimated from these characterizations. The electrical characterization was aimed at exploring the potential applications of SiC films that were synthesised by this method in fabricating electrical devices. Then, the reason for pursuing the synthesis of crystalline films and their characterization results are explained. Finally, the chapter concludes by summarizing the LPCVD parameters that produced films with optimum qualities required for fabricating x-ray masks.

## 3.2 Results and Discussion on Characterization Studies of Amorphous SiC Films

LPCVD silicon carbide films have traditionally been deposited at high temperatures ( $>1000^{\circ}\text{C}$ ) using two precursors to provide the stoichiometric composition. [6,35]. In this study, DTBS is used as single precursor to produce amorphous silicon carbide films at lower temperatures. This method results in fewer process variables and thus a simpler interpretation of the kinetics.

### 3.2.1 Growth Kinetics Study

The deposition rates were determined as a function of processing parameters using DTBS flow rates in the range of 5 to 60 sccm, pressures in the range of 0.05 to 0.3 Torr, and temperatures in the range of 600 to 850  $^{\circ}\text{C}$ . The range of deposition temperature was decided from the decomposition data given by the manufacturer of DTBS, Olin Hunt Inc. The deposition pressure range and the flow range of the precursor, were limited by the monitoring or controlling devices of these parameters.

**3.2.1.1 Growth Kinetics with Respect to Flow Rate:** Figure 3.1 illustrates the variation in deposition rate as a function of the square root of DTBS flow rate at constant conditions of temperature ( $650^{\circ}\text{C}$ ) and pressure (0.2 Torr). The observed linear dependence can be explained by recognizing that the rate of laminar flow in the annular region can affect the partial pressure of DTBS in the interwafer region. The small variation in film thickness measured across the wafers ( $<5\%$ ) is indicative of uniform composition in the gas phase and therefore a high diffusion rate. As the DTBS flow rate

is increased in the annular region, the pumping rate in this region must increase accordingly in order to maintain the desired constant pressure of DTBS in the interwafer region until a maximum concentration ( $\rho_{\text{DTBS}}/RT$ ) is approached. Thus, the dependency of deposition rate on flow rate is expected to exhibit the same dependency as that observed for pressure as seen below. For the aforementioned processing conditions, the composition of the deposits, as determined by ESCA, appeared to be independent of flow rate in the range of 5-60 sccm and to be close to the stoichiometric value of SiC.

**3.2.1.2 Growth Kinetics with Respect to Pressure:** In Figure 3.2, the deposition rate is plotted as function of the square root of pressure for constant conditions of temperature (650°C) and flow rate (30 sccm). For values less than 300 mTorr, a linear dependency is observed. Such behavior is in contrast to that reported for the synthesis of silicon from silane [36] and the synthesis of SiC from diethylsilane [37] both of which follow a Langmuir-Hinshelwood reaction mechanism where the initial dependency of growth rate on pressure is linear and given by [38].

$$\text{Rate} = (k \exp(-E_a/RT)) Kp/(1+Kp) \quad (3.1)$$

where  $k$  is the reaction rate constant,  $E_a$  is the activation energy,  $R$  is the gas law constant,  $T$  is temperature,  $p$  is the partial pressure of the reacting gas, and  $K$  is the adsorption equilibrium constant. However, if it is assumed that two adjacent adsorption sites are necessary due to the bulkiness of the t-butyl group, the above equation becomes

$$\text{Rate} = (k \exp(-E_a/RT))(Kp_{\text{DTBS}})^{1/2}/(1+(Kp_{\text{DTBS}})^{1/2}) \quad (3.2)$$

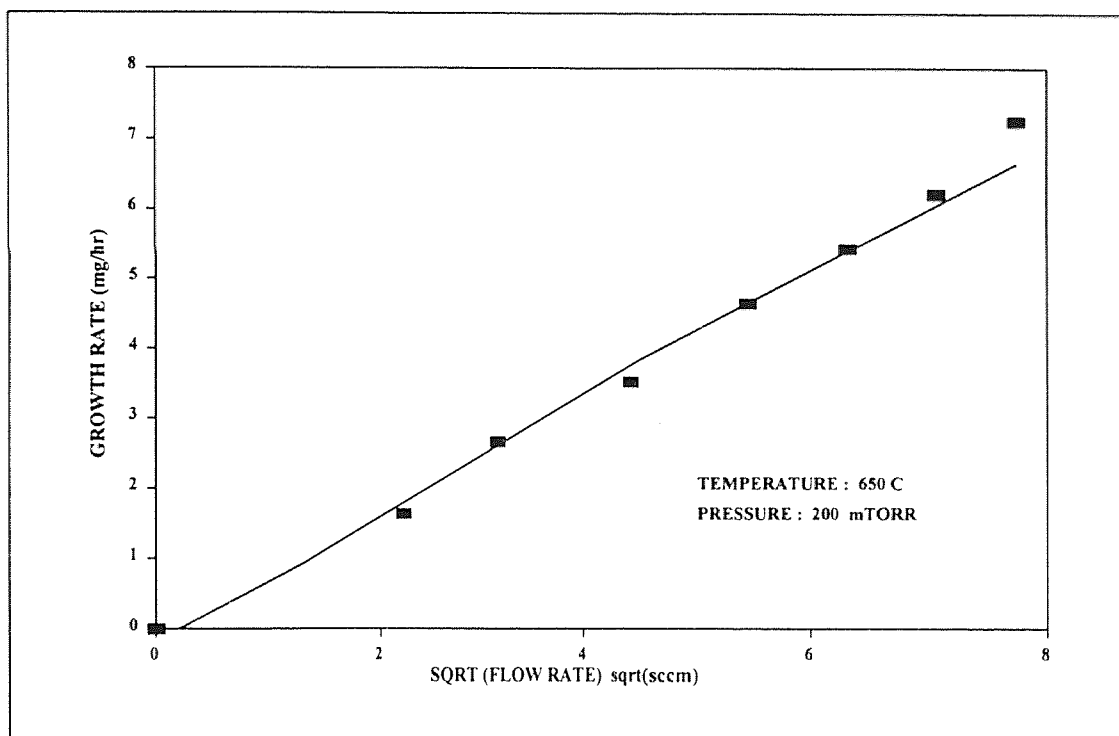


Figure 3.1 Variation of growth rate as a function of the square root of DTBS flow rate.

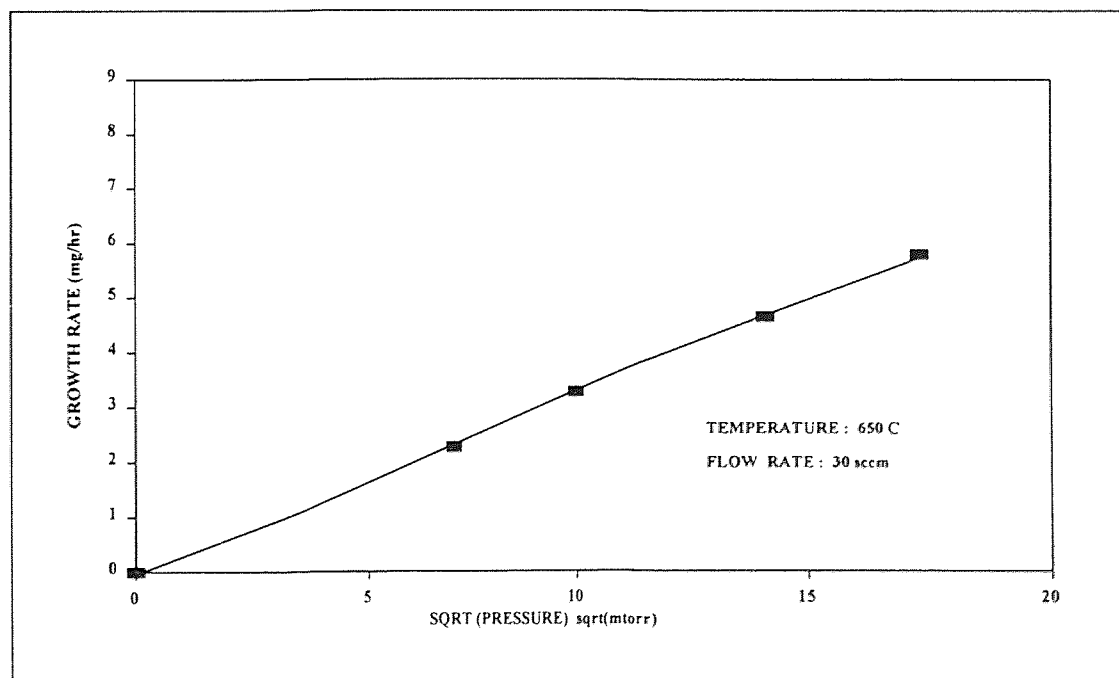


Figure 3.2 Variation of growth rate as a function of the square root of pressure.

When  $K_{p_{DTBS}}$  is small compared to 1, the observed square root dependency on pressure occurs.

An alternate explanation for the square root dependency is to assume that the adsorption specie is the organosilylene which necessitates a gas-phase dissociation of the organosilane as follows



where the pressure of the  $(C_4H_9)_2Si$  is related to the pressure of  $(C_4H_9)_2SiH_2$  through the equilibrium constant

$$K'' = K' \exp(-\Delta H/RT) = [(C_4H_9)_2Si][H_2]/[(C_4H_9)_2SiH_2] \quad (3.4)$$

The pressure of DTBS in the Langmuir-Hinshelwood reaction mechanism is thus replaced by  $(K''p_{DTBS})^{1/2}$  since  $[(C_4H_9)_2Si] = [H_2]$  yielding

$$\text{Rate} = [k \exp(-E_a/RT)] K (K''p_{DTBS})^{1/2} / [1 + K (K''p_{DTBS})^{1/2}] \quad (3.5)$$

Upon collecting the temperature contributions, the above rate equation becomes

$$\text{Rate} = [k \exp(-E_a + \Delta H/2)/RT] K (K''p_{DTBS})^{1/2} / [1 + K (K''p_{DTBS})^{1/2}] \quad (3.6)$$

which will be used to estimate the change in enthalpy for this dissociation reaction. Similar to the flow rate study, the composition of the deposits showed little variation with pressure over the investigated range and was determined to be close to SiC.

**3.2.1.3 Growth Kinetics with Respect to Temperature:** Generally, the rate of most reactions increases as the temperature is raised. It can be stated approximately that the rate doubles for every 10°K increase in temperature. But the temperature dependence of rate has been found to fit the expression proposed by Arrhenius:

$$\text{Growth rate} = A \exp ( -E_a / RT ) \quad (3.7)$$

where,  $A$  is the pre-exponential factor (nearly independent of temperature) and  $E_a$  is Activation Energy, which has to be supplied for the reaction to occur. Activation energy depends upon the chemicals that take part in the reaction.  $R$  is the gas constant and is equal to 1.98717 cal/Kmol and  $T$  is the absolute temperature of the reaction. Taking natural logarithm on both sides of the above equation, and plotting a graph on logarithmic growth rate versus reciprocal of temperature, leads to a straight line with negative slope, This type of curve is called Arrhenius plot. The negative slope of the curve gives the ratio between Activation Energy and Gas constant. By determining the slope of the curve, the activation energy for the reaction can be calculated.

The temperature-dependent behavior of the deposition rate is shown in figure 3.3. For a constant flow rate of 30 sccm and pressure of 0.2 Torr, the deposition rate is seen to follow an Arrhenius behavior in the range of 600-675°C with an activation energy of 24 kcal mol<sup>-1</sup> ( 1.04eV/atom). This behavior is consistent with the existence of a single-rate limiting step controlling the deposition process. The observed activation energy is substantially lower than the value of 40 kcal mol<sup>-1</sup> which was common to that reported in the synthesis of silicon from SiH<sub>4</sub>[39] silicon from chlorosilane precursors [40] and silicon carbide from DES [37]. The difference in the values of the activation energy can be used to estimate the value of  $\Delta H$  from equation 6 which turns to be about  $\sim 32$  kcal mol<sup>-1</sup> for the dissociation of DTBS.

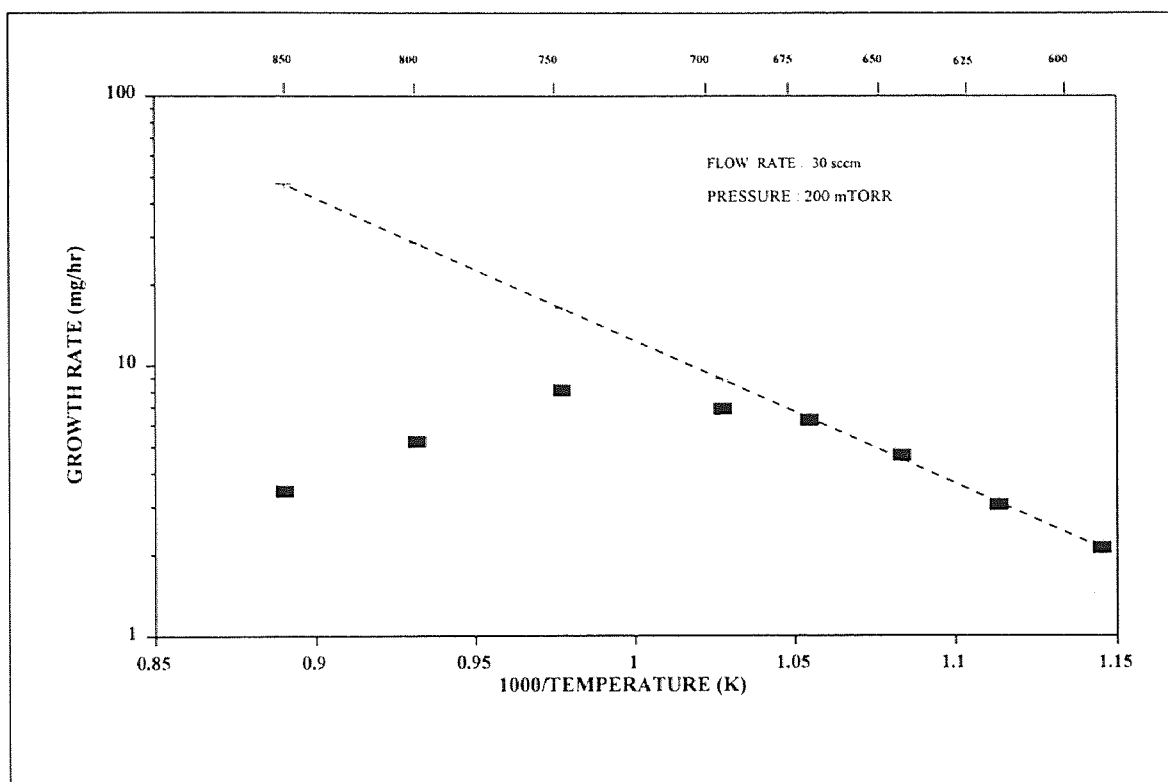


**Figure 3.3** Variation of growth rate as a function of reciprocal temperature for a-SiC.

At temperatures above 675°C, the deposition rate was observed to decrease reflecting a combination of factors including the transition into the mass-transfer limited regime and the adsorption of decomposition products which act as retardants to the growth process. In the range between 625 to 750°C, the composition of the deposits changed progressively from slightly silicon rich to slightly carbon rich as shown in figure 3.4. Above 750°C, there was a rapid increase in the carbon content from the near stoichiometric value to about 75% C at 850°C. It is worth noting that the RBS results yielded compositional values for Si that were systematically higher than those obtained from ESCA over the investigated temperature range. This is believed to be due to an overestimate of the stopping power value for carbon at 1.8 meV in the rump simulation program used to fit the RBS data. The primary decomposition pathway for DTBS is believed to involve silylene formation either by extrusion of H<sub>2</sub> or C<sub>4</sub>H<sub>10</sub> [41]. For similar dialkylsilanes, the homolytic cleavage of Si-C bonds were noted to be negligible below 725°C but to be important at higher temperatures. The availability of this additional carbon source enhances adsorption on the surface, thus causing the observed increase in the carbon content with higher temperatures.

In figure 3.5, a plot of deposition rate as a function of wafer position reveals an increase in the depletion as the temperature is increased between 600 and 800°C. This is consistent with an increased rate of consumption of DTBS as the temperature is raised. At constant temperature, depletion effects as a function of pressure or DTBS flow rate were much smaller and could not be correlated to changes in either parameter.



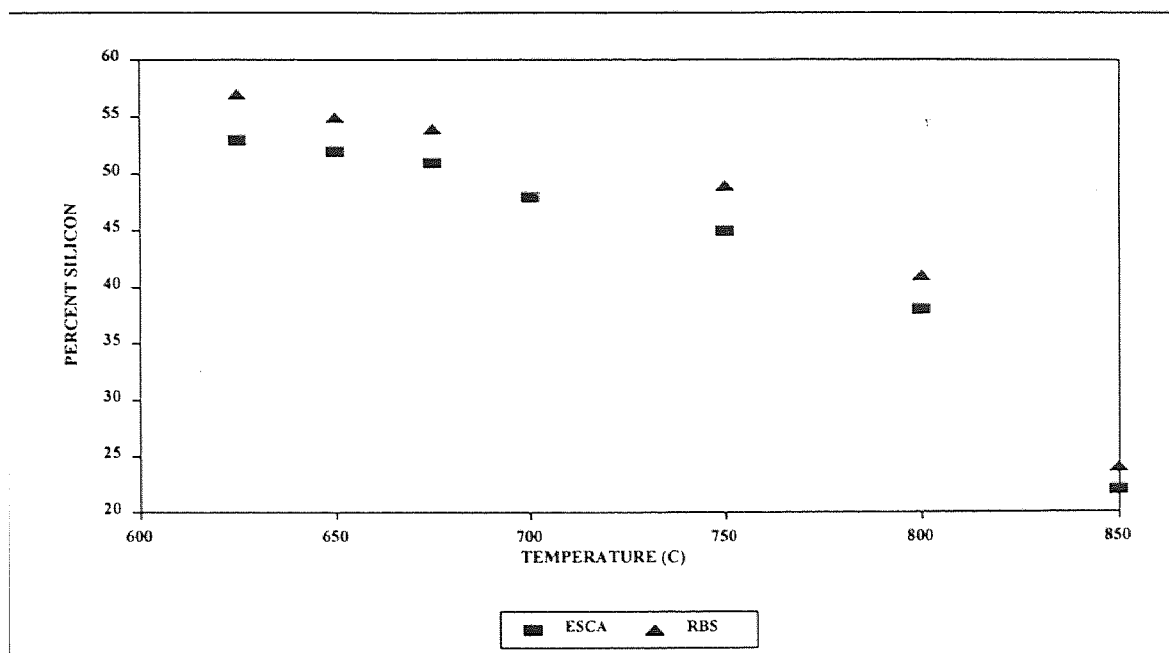


**Figure 3.4** Variation of silicon concentration in the silicon carbide films using ESCA (at a depth of 150 Å) and RBS as a function of deposition temperature for constant pressure (200 mTorr) and DTBS flow rate (30 sccm).

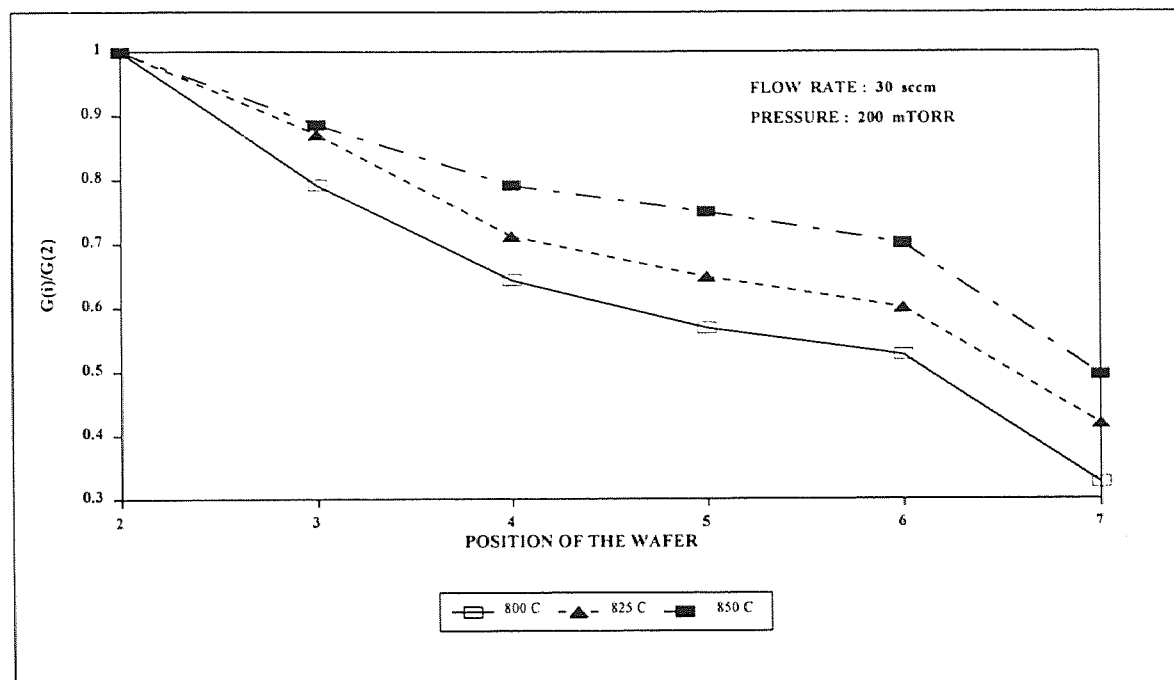


**Figure 3.5** Growth rate of the  $i$ th wafer normalized to that of the 2nd wafer as a function of wafer position for deposition temperatures above 800°C.

At deposition temperatures above 800°C, there was a reversal in trend as the depletion effects decreased with higher temperatures as seen in figure 3.5. This is believed to be due to an increase in the decomposition of DTBS into hydrocarbon species which occupy surface sites thus liberating the silicon species to occupy other sites further down the reactor chamber.

### **3.2.2. Characterization of a-SiC Films**

**3.2.2.1 Infra-red Spectroscopic Studies:** Figure 3.6 shows a typical IR spectrum of a-SiC sample deposited at 750°C. The presence of strong peak centered around 790  $\text{cm}^{-1}$  shows the presence of Si-C vibration mode. All a-SiC samples deposited over the above mentioned temperature range showed this vibrational mode. It is interesting to note that, these spectrum do not show any peak around 2300  $\text{cm}^{-1}$ , corresponding to C-H vibration, or any peak around 2100  $\text{cm}^{-1}$ , corresponding to Si-H vibration, indicating the absence of hydrogen in the bulk. Conventional SiC synthesizing methods which rely on other hydrocarbons always show the presence of hydrogen in the film as an impurity. The presence of hydrogen in the film is a disadvantage, since such impurity will result in the phase transformation of SiC, when they are exposed to strong x-ray doses in the x-ray lithographic process. The absence of hydrogen in the film indicates the superiority of this process.

**3.2.2.2 X-ray Diffraction Studies:** The x-ray diffraction patterns indicated that the films were indeed amorphous at the deposition temperature of 850°C, and below. At the

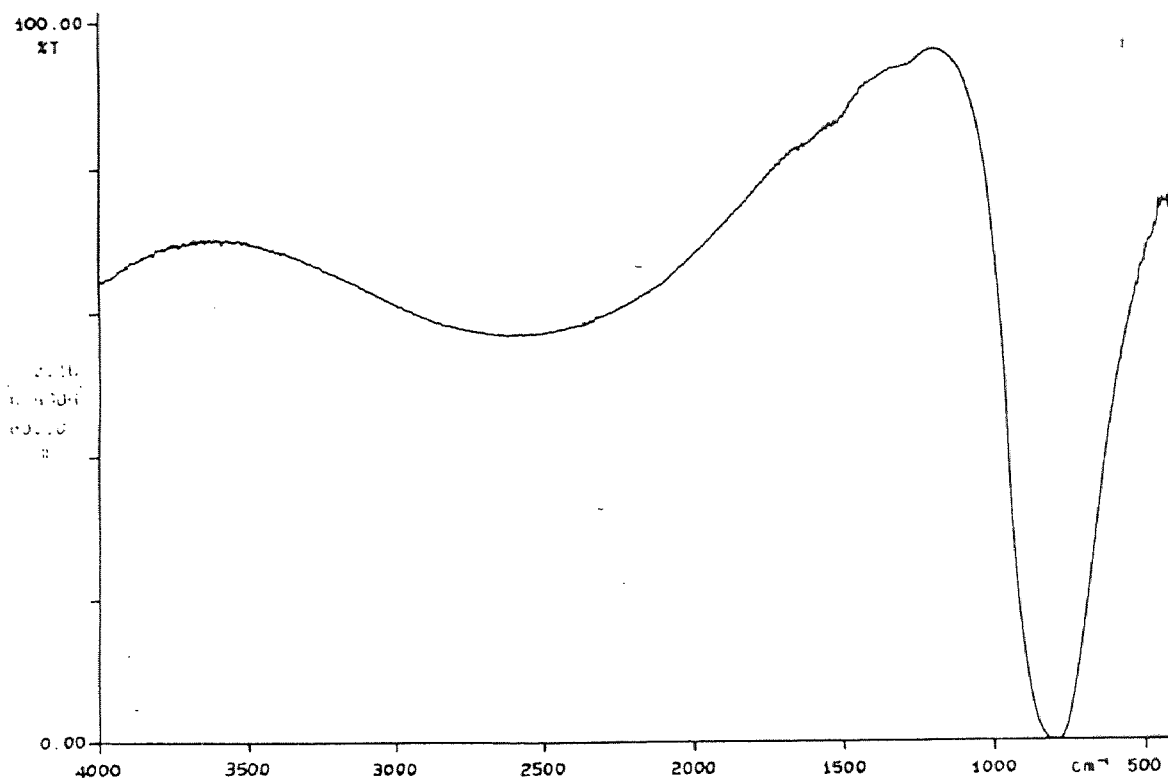


Figure 3.6 FTIR spectrum of a-SiC sample deposited at 750°C showing strong Si-C vibration mode.

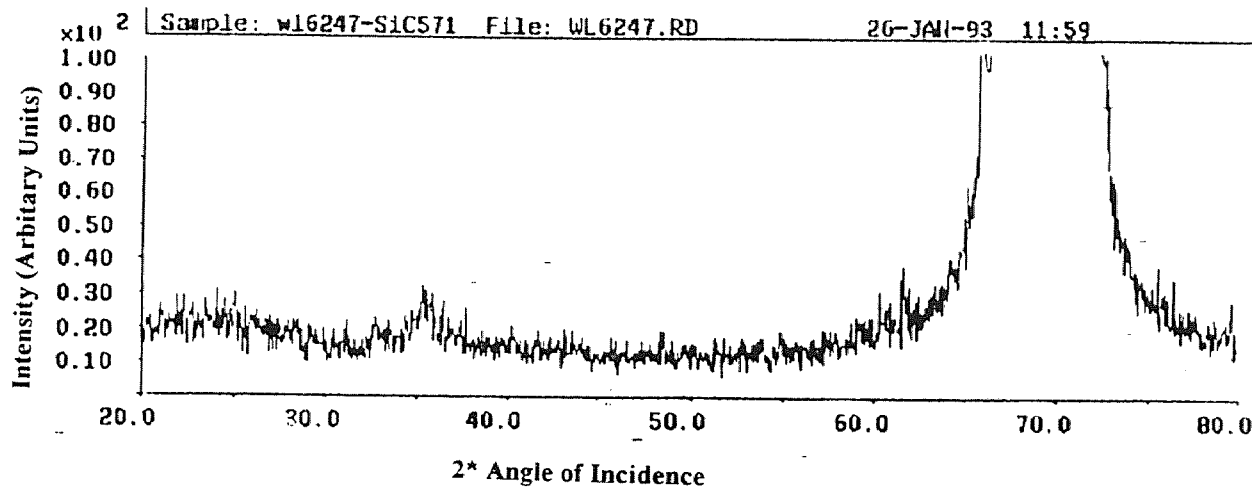
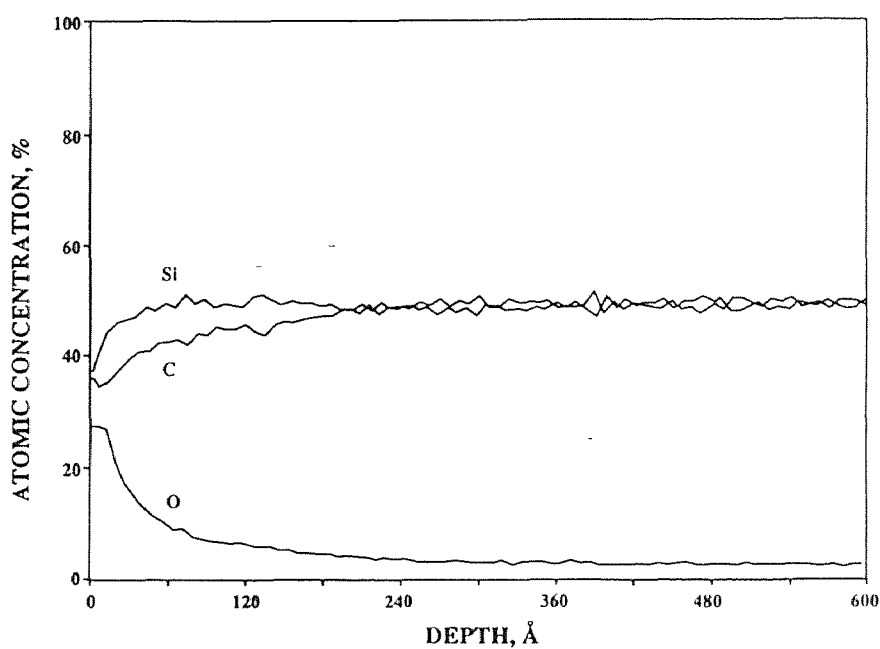


Figure 3.7 X-diffraction spectrum of a-SiC sample deposited at 900°C, revealing <111> oriented β-SiC peak.

deposition temperature of 900°C, the pattern presented in figure 3.7 reveals, in addition to the expected (400) Si substrate peak, the emergence of a peak at 35.3° which is attributed to  $\beta$ -SiC.

### 3.2.3 Compositional Analysis

The Auger depth profile, (figure 3.8) taken on a sample deposited at 650°C indicates that the composition is uniform through the bulk of the deposit. Although oxygen was detected on the surface of the film, there was a negligible amount observed within the film. The ESCA analysis revealed two types of carbon species, one with a binding energy around 283.2 eV characteristic carbon in carbides,[11, 12], and the other at a binding energy of 284.5 eV characteristics of carbon in a more neutral specie such as graphite. At 700°C most of carbon (~90%) was observed to be present as, while at 850°C most of the carbon (~70%) was present as a neutral specie (figures 3.9 and 3.10).



**Figure 3.8** The Auger depth profile, taken on a sample of a-SiC deposited at 650°C

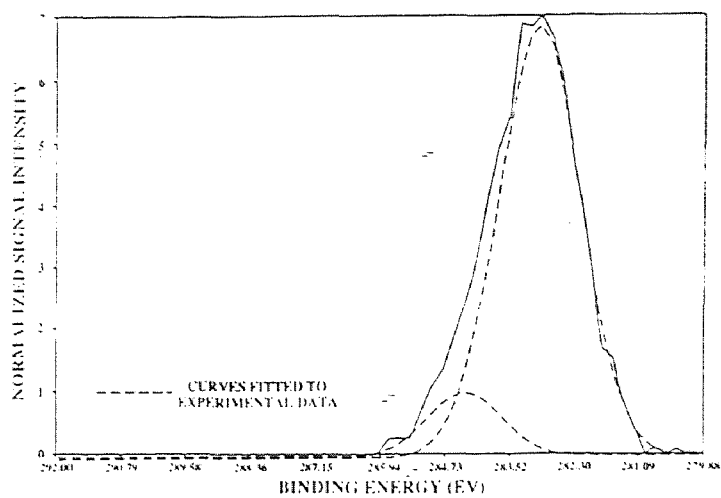


Figure 3.9 ESCA spectrum for a sample of a-SiC deposited at 700°C, showing peaks corresponding to carbon as neutral and carbide species.

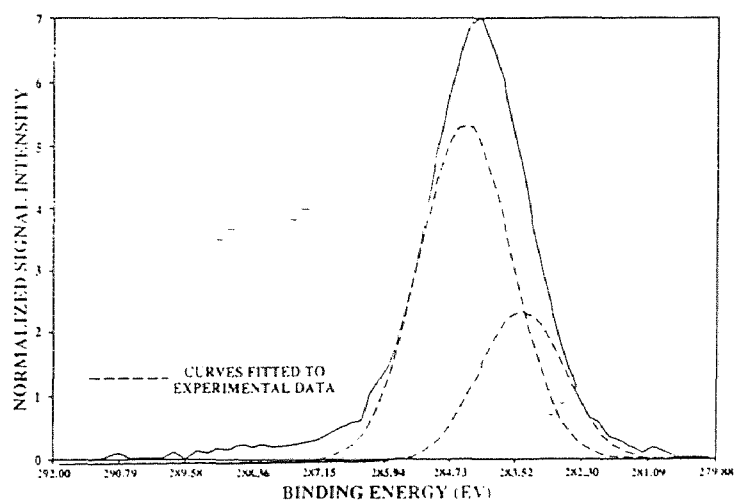


Figure 3.10 ESCA spectrum for a sample of a-SiC deposited at 850°C, showing peaks corresponding to carbon as neutral and carbide species.

### 3.2.4 Analysis of Mechanical Properties

Figure 3.11 and Figure 3.12 represent plots of Young's modulus and hardness as a function of deposition temperature. In both cases, there appears to be an increase in these values as the deposition temperature is raised to 750°C. This increase parallels the increase in the carbon content in the deposits until the stoichiometric SiC composition is reached. At 750°C, the values for hardness and Young's modulus were close to 20 and 200 GPa, respectively. These values are with a factor of 5 of the diamond used for the indenting process and attest well to the strength of these amorphous films. Above 750°C, the decrease in the values for both hardness and Young's modulus reflect the deviation from stoichiometry and the increased presence of carbon in a neutral charged state.

### 3.2.5 Stress Analysis

In the compositional regime where the films were silicon-rich, the deposits were observed in all cases to be tensile on the silicon substrates as evidenced by the presence of the crystallographically oriented cracks shown in figure 3.13. These cracks are believed to arise from the epitaxial precipitation of the excess silicon along a preferred direction of the underlying substrate. For films 7000Å in thickness deposited at 800°C under constant conditions (15 sccm DTBS, 200 mTorr), the stress values were near 100 MPa. Above 800°C, the stress decreased rapidly achieving values near zero at 810°C and becoming compressive with values exceeding 250 MPa at 825°C. These changes in stress parallel the compositional changes and can be readily correlated to the carbon content of the films. At the constant deposition temperature of 825°C, a change in the reaction chamber

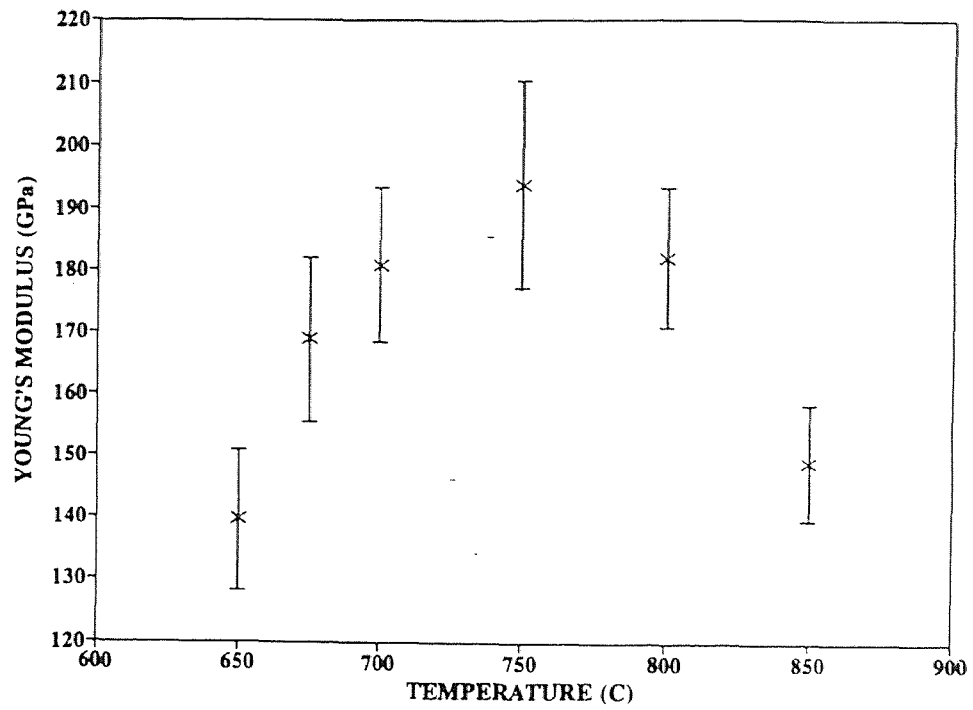


Figure 3.11 Plot of Young's modulus of a-SiC films as a function of deposition temperature.

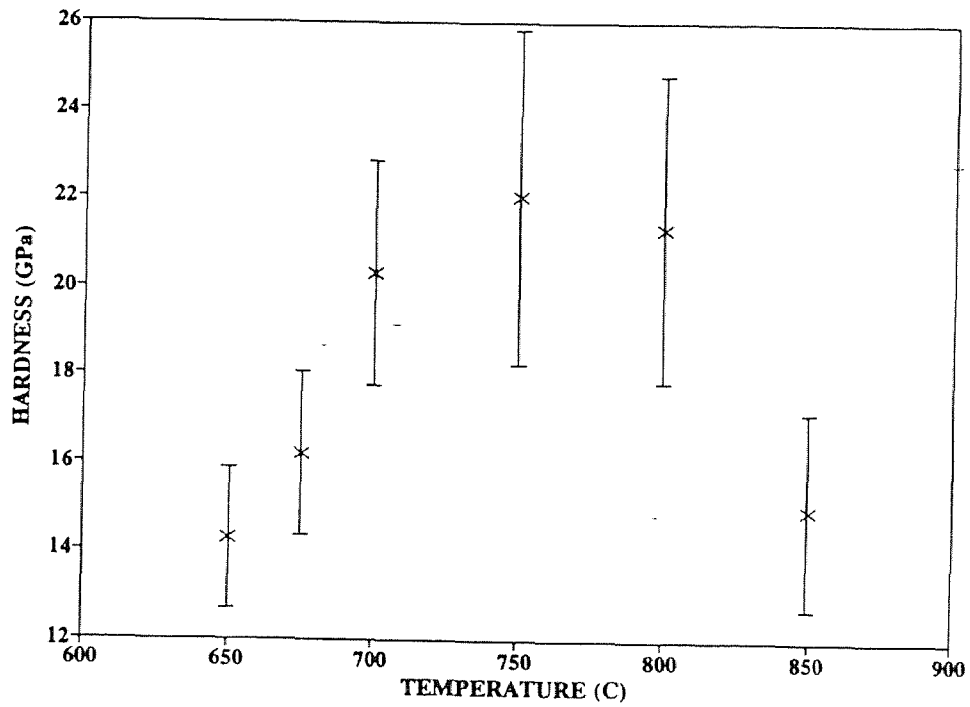
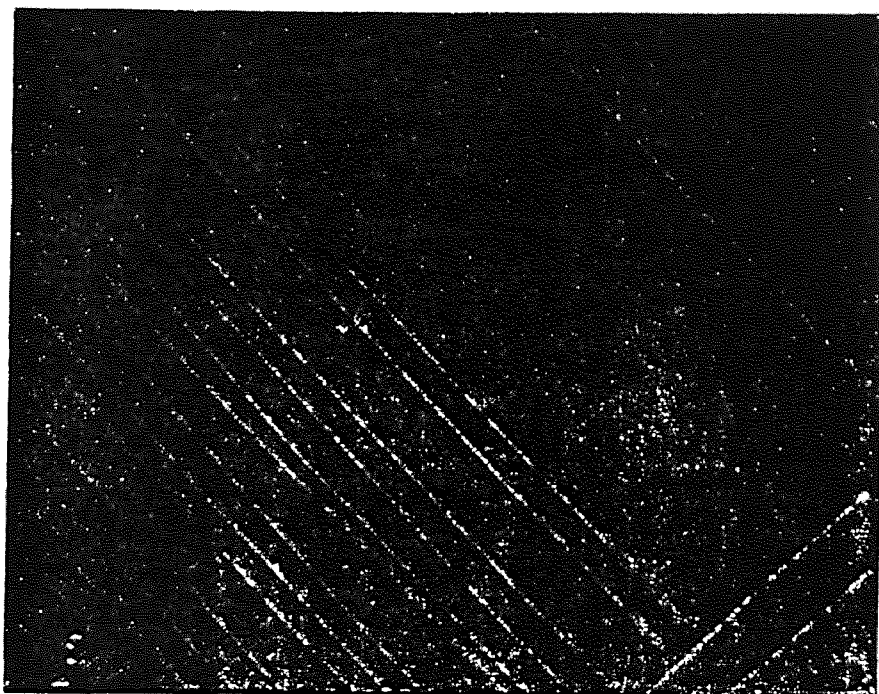


Figure 3.12 Plot of hardness of a-SiC films as a function of deposition temperature.

pressure from 200 down to 100 mTorr was observed to alter the composition of the deposits from  $\text{Si}_{0.25}\text{C}_{0.75}$  to  $\text{Si}_{0.42}\text{C}_{0.58}$  due to an increased hydrocarbon removal at the higher pumping rate. This reduction in carbon content resulted in higher film stress values.

At a deposition temperature of  $850^{\circ}\text{C}$ , with DTBS flow rates in the range of 5-15 sccm, and pressures in the range of 50 to 100 mTorr, free-standing tensile membranes 4 cm in diameter were produced.



**Figure 3.13** Optical microscopic picture showing the crystallographically oriented microcracks of a-SiC deposited on  $\langle 100 \rangle$  Si substrate, with a magnification of 110.



### 3.2.6 Optical Characterization

**3.2.6.1 Optical Transmission Characteristics:** Figure 3.14 shows typical optical transmission spectrum for a micron thick film deposited on a quartz substrate under stoichiometric conditions. The optical transmission was studied between the wavelength of 400 and 850 nm. The percentage transmission around red wavelength of 6320Å is of particular interest, since optical alignment instruments in x-ray lithographic process use optics around this wavelength. A minimum value of optical transmission of around 50% around 6320Å is required for a micron thick film in order for carrying out the alignment process. Even though films deposited under stoichiometric conditions showed a transmission of around 50% for a micron thick film, these films exhibited high stress values and developed cracks during etching. The membranes that could be produced were high in carbon content and exhibited undesirable low optical transmission characteristics (<20% for films of one micron in thickness).

**3.2.6.2 Optical Band Gap Estimation:** An useful parameter, optical band gap, can be estimated from a optical transmission spectrum as explained in chapter 3. Figure 3.15 shows a plot of square root of  $(\alpha h\nu)^{1/2}$  versus  $(h\nu)$ . The intercept of the tangent to the portion of the curve showing sharp absorption edge, is the value of optical band gap, which came out to be 1.77 eV for the case a-SiC film.

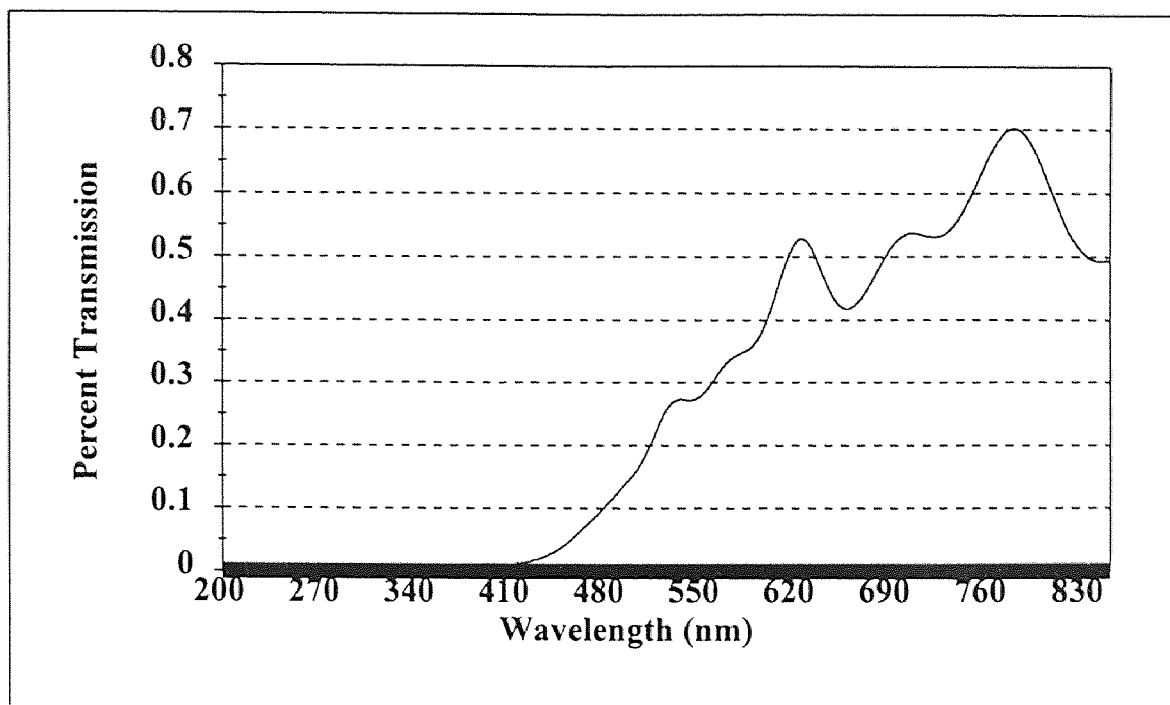


Figure 3.14 Optical spectrum of a one micron thick a-SiC film deposited at 750°C.

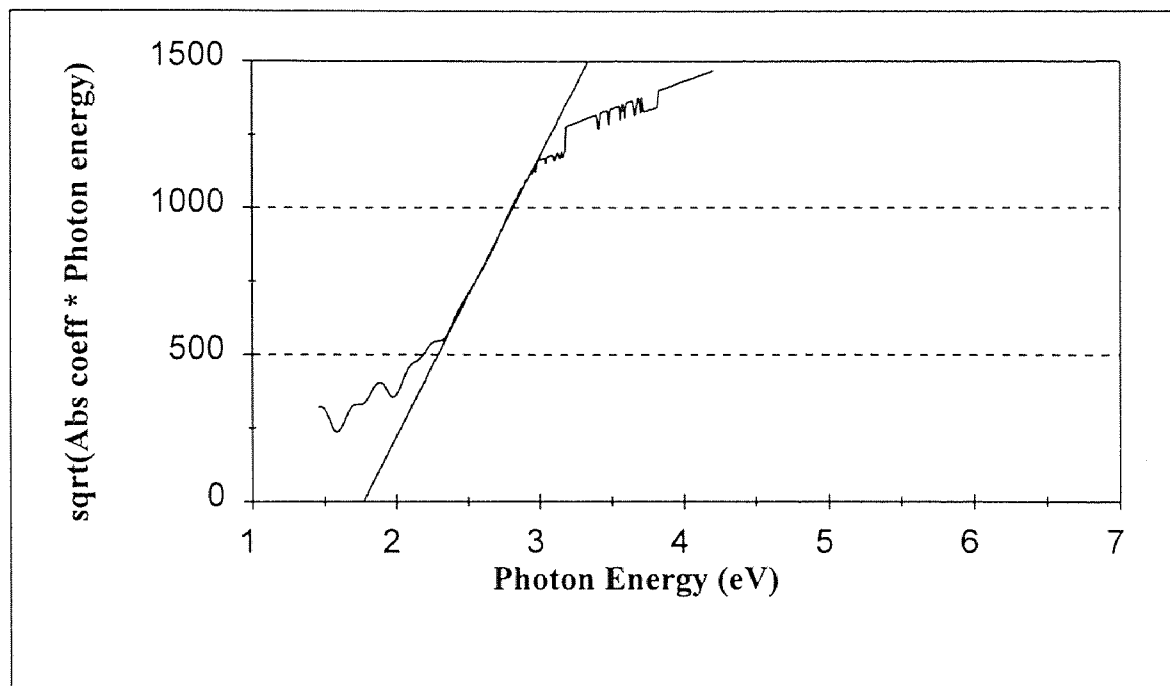
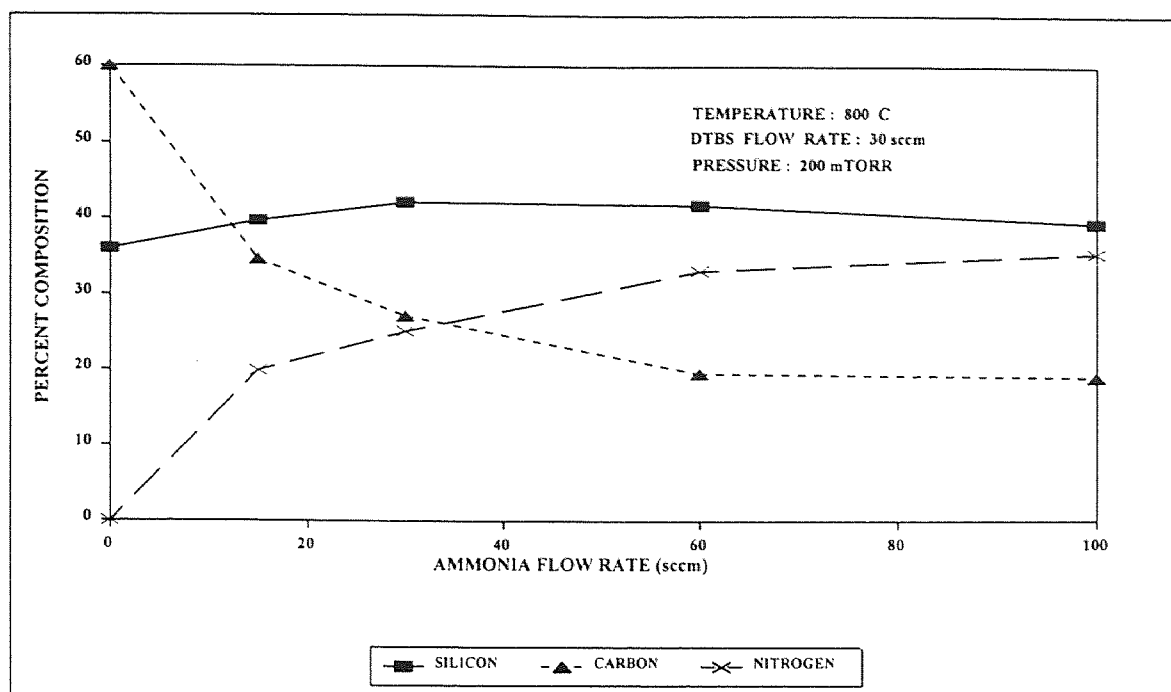


Figure 3.15 A plot to estimate the optical band gap for the sample deposited at 750°C.

### 3.2.7 On the Optimization of Stress and Optical Transmission

As explained in the earlier section, films with desired level of optical transmission showed excessive tensile stress, whereas films with optimal stress values (around 100 MPa) showed poor optical transmission. Several attempts were made to optimize either stress values at lower deposition temperature of around 700°C, or to improve optical transmission for films deposited at higher temperature of around 850°C, with which membranes could be produced. In the following sub-sections, such studies and their results are explained.

**3.2.7.1 Methods to Improve Optical Transmission by Adding Ammonia:** The effect of adding NH<sub>3</sub> to DTBS in order to alter the mechanical and optical characteristics of the films was investigated. Although no significant change in growth rate was noted as a function of NH<sub>3</sub> flow rate for constant conditions of temperature (800°C), DTBS flow rate (30 sccm), and pressure (0.2 Torr), the C and N content of the deposits varied while the Si content remained fairly constant. It is apparent from figure 3.16 that the C content decreases rapidly while the N content correspondingly increases until they become nearly equal at equal DTBS and NH<sub>3</sub> flow rates (30 sccm). A smaller compositional change is seen to occur when the NH<sub>3</sub> flow rate (60 sccm) increases to twice that of DTBS. At higher flow rate ratios, the composition of the deposits remained fairly fixed with a N concentration close to 40% and a residual C content of nearly 20%.



**Figure 3.16** Composition as a function of  $\text{NH}_3$  flow rate for films deposited at a temperature of  $800^\circ\text{C}$ , pressure of 200 mTorr, and DTBS flow rate of 30 sccm.

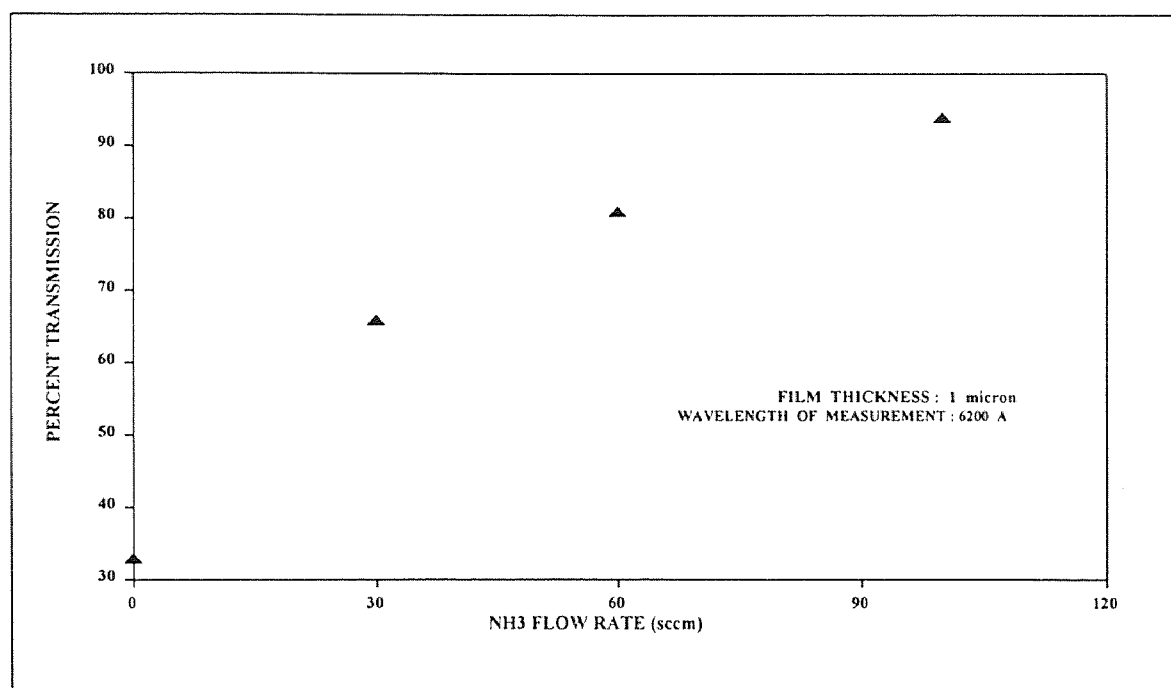


**Figure 3.17** Variation of the optical transmission normalized to  $1\mu\text{m}$  thick SiC films as a function of  $\text{NH}_3$  flow rates for films deposited at a temperature of  $800^\circ\text{C}$ , pressure of 200 mTorr, and DTBS flow rate of 30 sccm.

These  $\text{SiC}_x\text{N}_y$  deposits exhibited significant improvement in the optical transmission as shown in figure 3.17, but also caused the film stress to increase beyond acceptable levels for membrane formation as evidenced by the presence of cracks. The incremental addition of  $\text{NH}_3$  to DTBS caused the IR peak of the resulting deposits to broaden and shift to higher reciprocal wave numbers to reflect the presence of the Si-N vibrational mode centered at  $830\text{ cm}^{-1}$  as shown in figure 3.18.

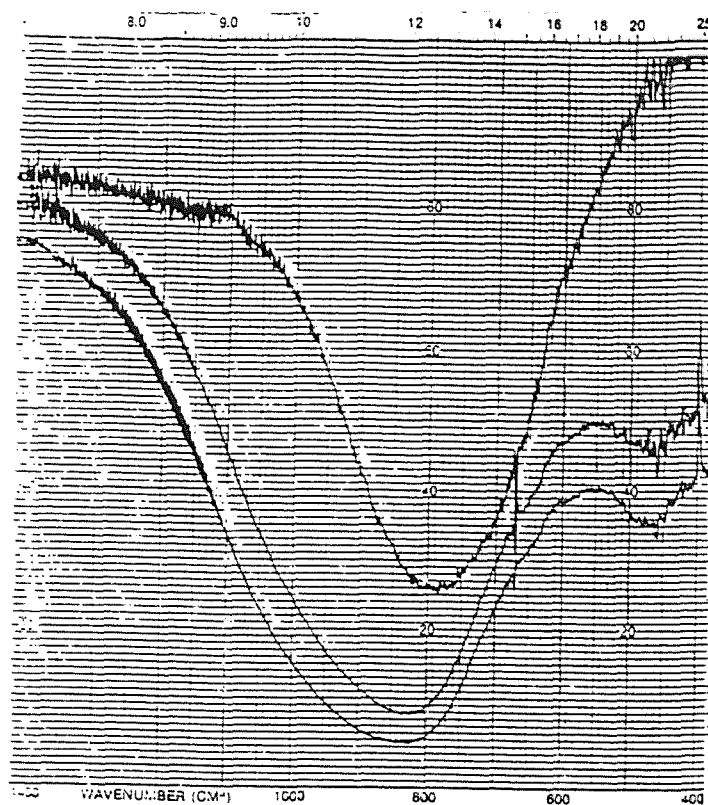


**Figure 3.18** IR spectrum showing the broadening of SiC peak due to increase in N content.

### 3.2.7.2 Methods to Optimize Stress Values for a-SiC Films Deposited at 750°C:

Since attempts to improve optical transmission by adding ammonia failed, following methods were tried to control the stress of the deposited stoichiometric films, since the optical transmission was maximum for such films.

- (1) SiC films were deposited on wafers already coated with BN films of around 1500 Å. The idea is to compensate for the mismatch of the thermal coefficient of expansion between Si wafers and SiC films. BN has a negative value of thermal coefficient of expansion with respect to Si, thus always resulting in compressive stress that could compensate for tensile stress of SiC.
- (2) SiC films were deposited on wafers already coated with SiO<sub>2</sub> films of around 4000 Å. Here, the aim was to eliminate any effect that could result in increase in intrinsic stress due to defects that were formed between Si-SiC interface.
- (3) SiC films were deposited at 750°C along with 15 sccm of Borane complex and 200 sccm of NH<sub>3</sub>. This attempt was to incorporate boron and nitrogen in the SiC films to relieve the stress due to the bigger size of such atoms.
- (4) Acetylene was added to DTBS at a deposition temperature of 650°C to increase the carbon composition that could result in stoichiometric SiC and at the same time thermal contribution to the stress could be minimized.
- (5) SiC films were deposited at 750°C on Si wafers that were baked at 1000°C for 10 minutes in 200 sccm H<sub>2</sub> environment. Here, the aim was to remove the native oxide on Si wafers in-situ [50] so that this could result in lower interface defects.

All these attempts did not reduce the stress to the required level of 100 to 200 MPa. Therefore attempts to make membranes out of these films also failed.

(6) In an another method samples deposited at  $750^{\circ}\text{C}$  was annealed for one hour at  $1000^{\circ}\text{C}$ . In this case, annealing was expected to releave intrinsic bulk stress. However, the annealing caused the sample crack heavily in crystallographic direction. Subsequent x-ray diffraction study confirmed that, the sample was crystallized due to annealing. The x-ray diffraction spectrum for the annealed sample is shown in the figure 3.19.

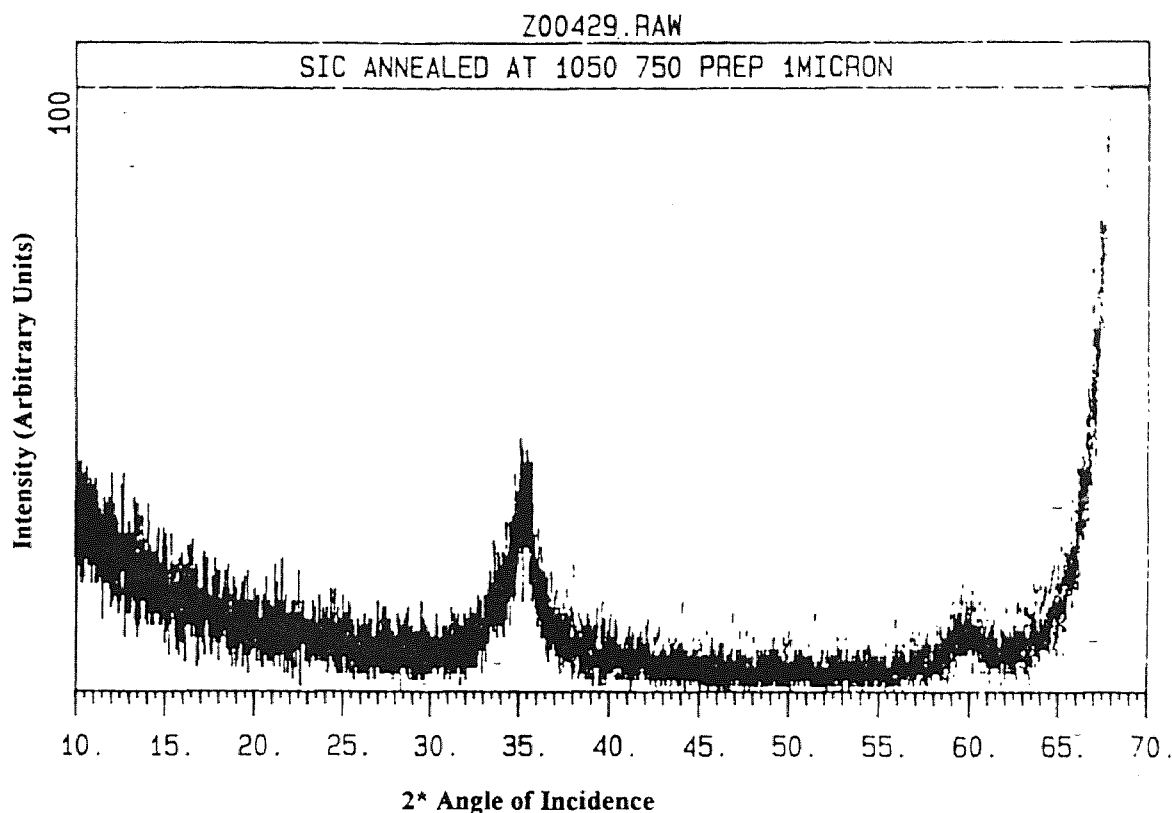


**Figure 3.19** X-ray diffraction spectrum of a-SiC sample that was deposited at  $750^{\circ}\text{C}$  and annealed at  $1000^{\circ}\text{C}$  in vacuum showing micro-crystallinity.

(7) Two layers of SiC were deposited on Si wafers. The first layer was deposited at 900°C which always resulted in high compressive stress and the second layer was deposited at 750°C on top of it. Several experiments were done by depositing varying thickness of underneath layer. The aim was to reduce the overall bulk stress. It was interesting to note that the overall bulk stress was reduced as the thickness of the bottom layer was increased. From this it was concluded that SiC films deposited at 750°C have high intrinsic stress and that the interface growth defects or mismatch in the coefficient of thermal expansion did not contribute that much to the stress value. It is believed that low density of amorphous film is the main reason for such intrinsic stress.

### 3.2.8 Electrical Characterization Results of a-SiC Films

Figure 3.20 shows a high frequency C-V plot for a a-SiC film deposited at 850°C, 100 mTorr. The study was made on the sample deposited under optimized condition so as to produce membrane. The plot shows that the film exhibits insulating property. The dielectric constant for this sample was calculated from the value of accumulation capacitance.

The dielectric constant  $\epsilon$  was measured using the formula

$$\epsilon_{\text{SiC}} = C_{\text{SiC}}d/A \quad (3.8)$$

where  $\epsilon_{\text{SiC}}$  permittivity of silicon carbide which is equal to  $\epsilon_0 * \epsilon_r$ ,  $\epsilon_0$  is permittivity of free space and  $\epsilon_r$  is the **dielectric constant** of the film,

$C_{\text{SiC}}$  is the accumulation capacitance,



A is the circular area of substrate-film-metal structure with 500 $\mu$ m in diameter,

d is the thickness of the film, which is measured as 4109  $\pm$  210  $\text{\AA}$ .

Value of  $\epsilon_r$  thus evaluated came out to be in the range of 9.4 to 10.7 when measured across the wafer. Flat band voltage was estimated from the plot, corresponding to the flat band capacitance ( $C_{FB}$ ).  $C_{FB}$  was calculated from the expression [47]:

$$C_{FB}(\text{per unit area}) = \frac{\epsilon_{SiC}}{d + (\epsilon_{SiC} / \epsilon_{Si}) \sqrt{(kT \epsilon_{Si} / p_{po} q^2)}} \quad (3.9)$$

where  $\epsilon_{SiC}$  and  $\epsilon_{Si}$  are the permittivity of the film and substrate respectively.  
d is the thickness of the film.  
k Boltzman constant.  
T temperature in  $^{\circ}$ K.  
 $p_{po}$  substrate doping density which is taken as  $10^{16} \text{ cm}^{-3}$ .  
q charge of electron.

Total flat band capacitance for 500  $\mu$ m came out to be 39.6 pF and estimated  $V_{FB}$  came out to be -3.4 V, indicating presence of substantial amount of fixed charges.

In order to obtain the information about trapped charges in the film, temperature bias stressing experiment was performed as explained in the previous chapter. C-V plot obtained after the stressing experiment is shown in figure 3.21. Curve (1) is for sample without temperature bias stressing. Curve (2) is for sample with temperature bias stressing and for both positive and negative bias polarity. The curve did not shift for negative bias. As noted by Nicollian and Brews [47], this shows that the first moment of oxide trapped charged is reduced. Gate bias polarity has no effect. The retracing of the C-V curve after both positive and negative bias stressing clearly indicated the dominating trapped charges in the bulk of the film. The trapped charge density was

estimated from the product of shift in the flat band voltage and the accumulation capacitance per unit area.

Shift in the flat band voltage ( $\Delta V_{FB}$ ) due to temperature-bias stressing (165°C, 30 min)

$$\Delta V_{FB} = 0.6V$$

Therefore, the trapped charges =  $(\Delta V_{FB}) * (\epsilon_{SiC} / d) = 1.391 C$

Trapped charge density =  $0.869 \times 10^7 \text{ cm}^{-2}$ .

In an attempt to estimate the interface behavior, quasi static C-V measurement was performed using HP 4140B. However, no meaningful C-V curve could not be obtained due to the highly leakage current through the bulk. Hence, no interface properties could be investigated under the presence circumstances. The dielectric breakdown voltage was found to be more than 250 MV/m. However, exact value could not be estimated due to the thickness of the film.

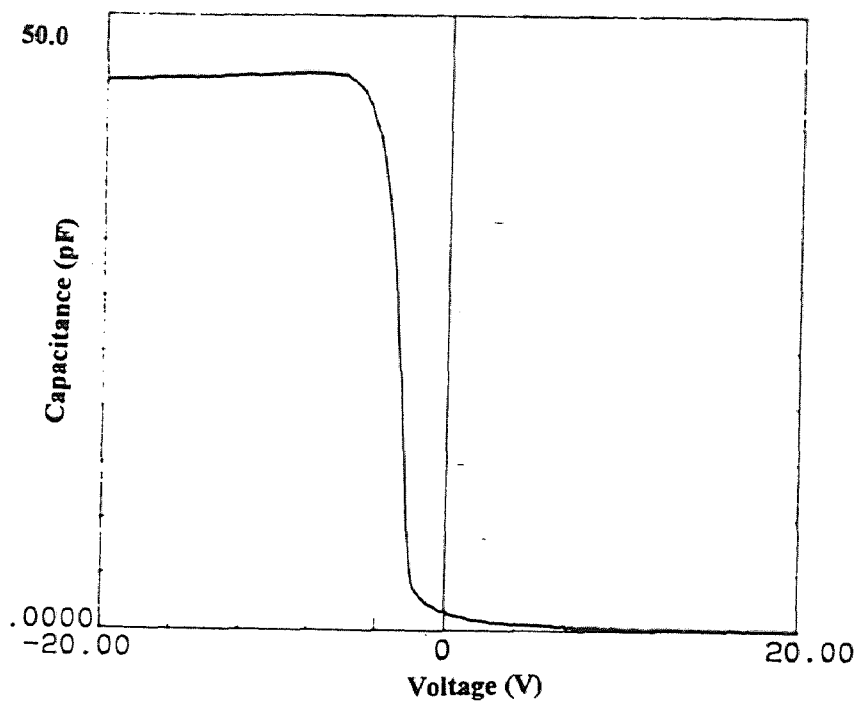


**Figure 3.20** High frequency C-V plot for Si-SiC-Al (MIS) structure. The SiC film was deposited at  $850^{\circ}\text{C}$ , 100 mTorr. The Al dot was  $500\ \mu\text{m}$  in diameter.

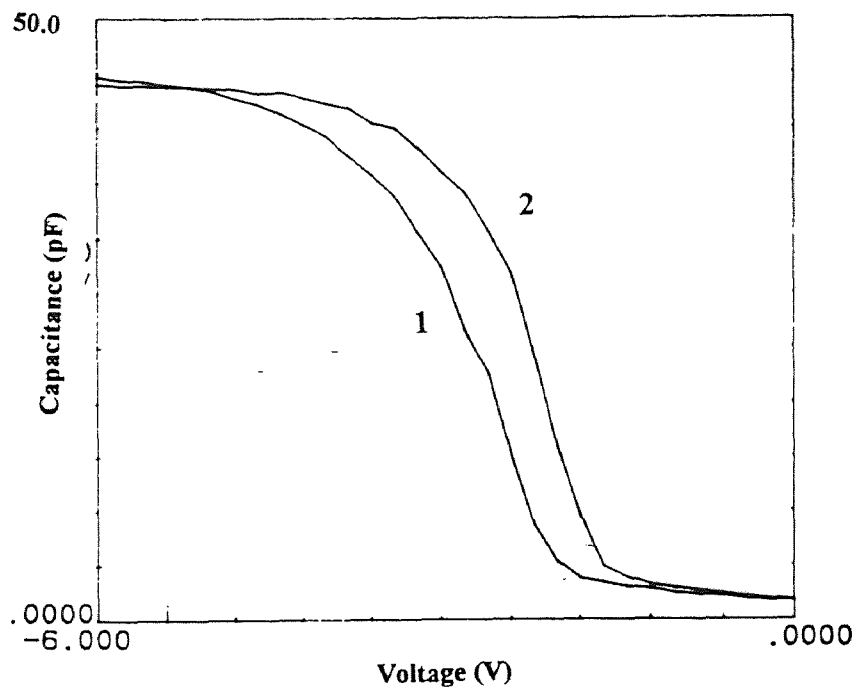


**Figure 3.21** High frequency C-V plot for the MIS structure for (1) the sample without temperature bias stress (2) after the temperature bias stress was performed.

### 3.3 Results and Discussion on Characterization Studies of Crystalline SiC Films

As described in the earlier sub-sections, there exists a tradeoff in controlling the stress and the optical transmission of amorphous SiC films synthesised. Therefore, a study towards the synthesis of crystalline SiC was pursued. Crystalline SiC films were grown on Si <100> substrates using dichlorosilane and acetylene as precursors. The following sub-sections will describe the growth kinetics and characterization results for these films.

#### 3.3.1 Growth Kinetic Study

The deposition rates were determined as a function of processing parameters using precursors flow rates of 10 to 50 sccm, pressures in the range of 0.1 to 0.75 Torr, and temperatures in the range of 950 to 1050°C. The growth kinetics with respect to temperature was analysed first by choosing the flow rate of precursors arbitrarily to 50 sccm. The temperature range was decided by decomposition rate of dichlorosilane and the upper limit of the LPCVD furnace. Selecting the optimum deposition temperature, the growth kinetics with respect to precursor flow rates and precursor flow ratio were analysed.

**3.3.1.1 Growth Kinetics with Respect to Temperature:** Figure 3.22 shows the variation in deposition rate as a function of deposition temperature for constant precursors flow rate of 50 sccm each, and for a constant chamber pressure of 0.2 Torr. The deposition rate followed an Arrhenius behavior between 950 to 1025°C, with an activation energy of 58 kcal/mole (~2.517 eV/atom). This activation energy is higher

than that of the observed activation energy for the synthesis of amorphous SiC films, but close to the reported values by others [8] for the synthesis of crystalline SiC. Above 1025°C, the deposition rate was found to decrease due to mass-transfer limitation. At the deposition temperature of 950°C, the film exhibited the presence of excess silicon. The stress of the film under this deposition condition was found to be slightly compressive. At all other deposition temperatures, the film showed excess carbon ranging from 51 to 55%. The stress of films under these conditions could not be determined accurately due to heavy deposition of material, resulting in cracks.

**3.3.1.2 Growth Kinetic Study with Respect to Flow of Precursors:** The growth rate study with respect to total flow, ranging from 10 sccm to 50 sccm for both precursors, with flow ratio equal to one, was done at a deposition temperature of 1000°C, and with chamber pressure of 200 mTorr. The variation of deposition rate with respect to the flow rates is shown in the figure 3.23. The observed linear dependency for flow rates above 10 sccm explains the Langmuir-Hinshelwood reaction mechanism, if the flow rate is expected to exhibit the same dependency as that for pressure, as explained elsewhere. The carbon composition was in the range of 50 to 68% for these flow rates. These carbon rich films showed poor optical transmission and at the same time high stress values, in the range of 400 - 500 MPa.

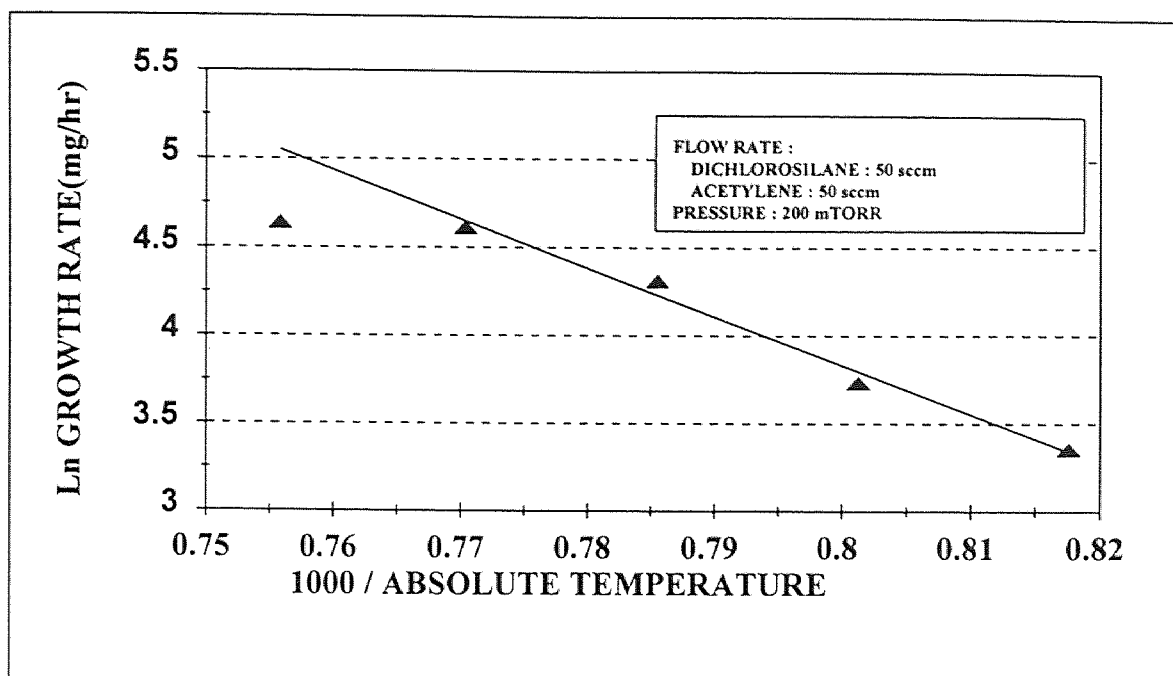


Figure 3.22 Variation of deposition rate as a function of reciprocal temperature for  $\beta$ -SiC.

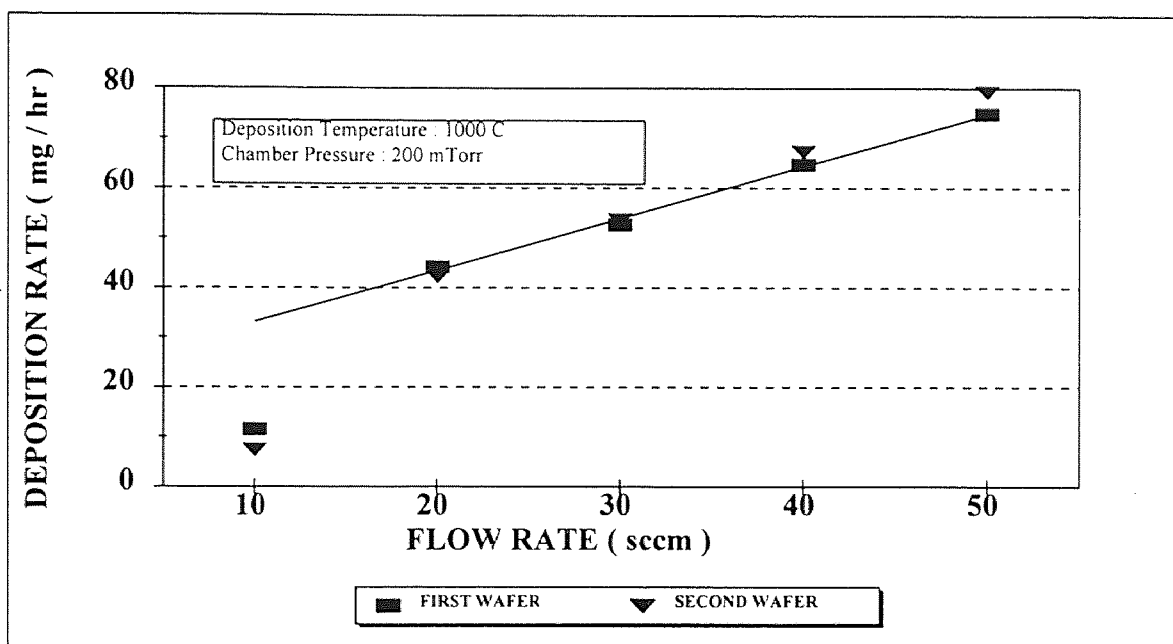
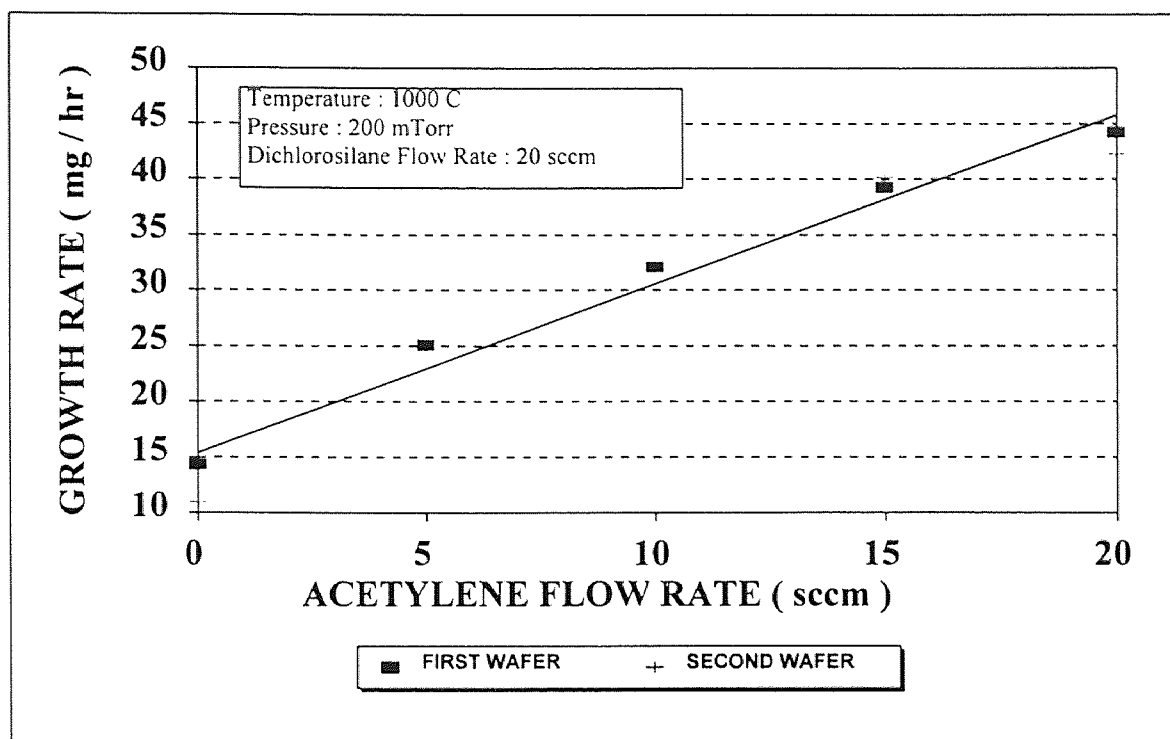


Figure 3.23 Variation of deposition rate as function of precursors flow rate for  $\beta$ -SiC, at a deposition temperature of  $1000^{\circ}\text{C}$ , chamber pressure of 200 mTorr and precursors flow ratio 1:1.

In the flow ratio study, which was performed with a constant flow of 20 sccm of dichlorosilane (which was chosen for optimum total depositon, so that, stress could be measured properly), and under the above mentioned deposition temperature and pressure, the deposition rate followed a linear dependency on acetylene flow rate. This is shown in figure 3.24.



**Figure 3.24** Variation of deposition rate as a function of precursors flow ratio for  $\beta$ -SiC.

### 3.3.2 Characterization Crystalline SiC Films

**3.3.2.4 Infra-red Spectroscopic Studies:** Figure 3.25 shows a typical IR spectrum of SiC sample deposited at 1000°C, with dichlorosilane and acetylene flow of 20 and 5 sccm respectively, under a chamber pressure of 500 mTorr. Such spectrum showed a peak

around  $790\text{ cm}^{-1}$ , like that of one for amorphous SiC films, confirming the presence of Si-C vibration mode. Here also, the absence of hydrogen in the bulk was confirmed by noting the fact that no observable peak centered around  $2100$  or  $2300\text{ cm}^{-1}$  was present.

**3.3.2.5 X-ray Diffraction Studies:** All x-ray diffraction studies performed on these samples showed a strong peak at  $35.3^\circ$  showing the presence of  $\langle 111 \rangle$  oriented  $\beta$ -SiC films. Figure 3.26 shows such a typical spectrum deposited at  $1000^\circ\text{C}$ , with equal precursors flow rate.

### 3.3.3 Composition Analysis

The ESCA analysis were performed on all samples deposited under conditions explained in previous sections. When flow ratio of precursor was equal to one, all samples showed excess carbon content between 51 to 55%, for deposition temperatures of  $975$  to  $1050^\circ\text{C}$ . The carbon composition was sharply dependent on the flow ratio of precursors as shown in figure 3.27. The stoichiometric composition could be achieved for a dichlorosilane to acetylene flow ratio of 4:1. Once the flow ratio was kept constant at 4:1, the deposition temperature has no effect in the composition, as shown in figure 3.28. For 20 sccm of dichlorosilane, and for deposition temperature of  $1000^\circ\text{C}$ , with a chamber pressure of 200 mTorr, film composition was found to be near stoichiometry, for the flow of 5 sccm of acetylene.



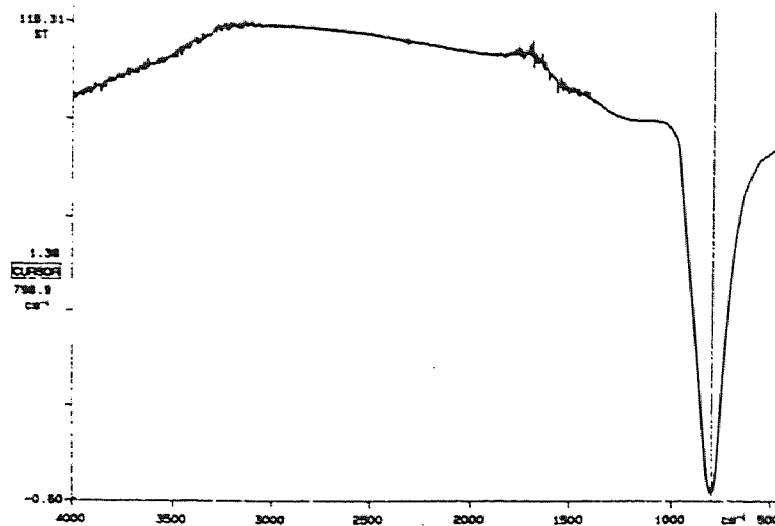


Figure 3.25 FTIR spectrum of a  $\beta$ -SiC sample deposited at  $1000^{\circ}\text{C}$ , with dichlorosilane to acetylene flow ratio of 4:1, and chamber pressure of 200 mTorr.

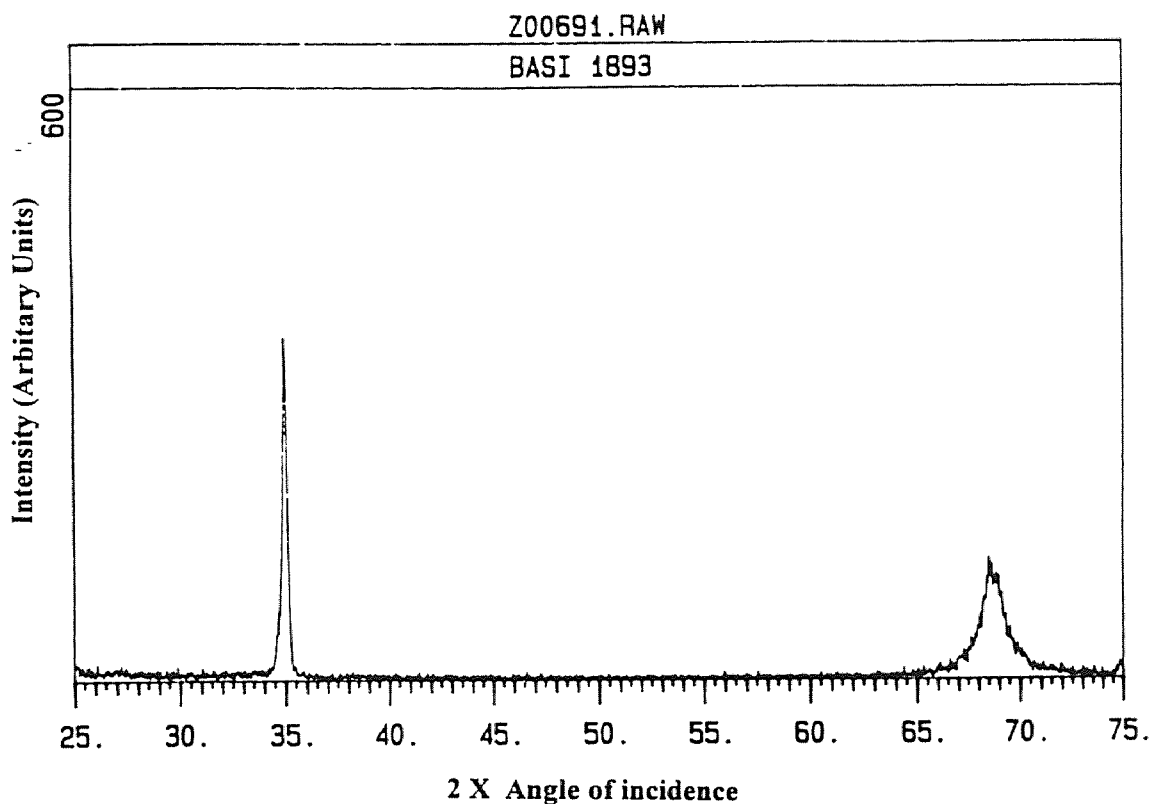


Figure 3.26 X-diffraction spectrum of a  $\beta$ -SiC sample deposited at  $1000^{\circ}\text{C}$ , with dichlorosilane to acetylene flow ratio of 4:1, and chamber pressure of 200 mTorr, showing a strong peak corresponding to  $\langle 111 \rangle$   $\beta$ -SiC orientation.

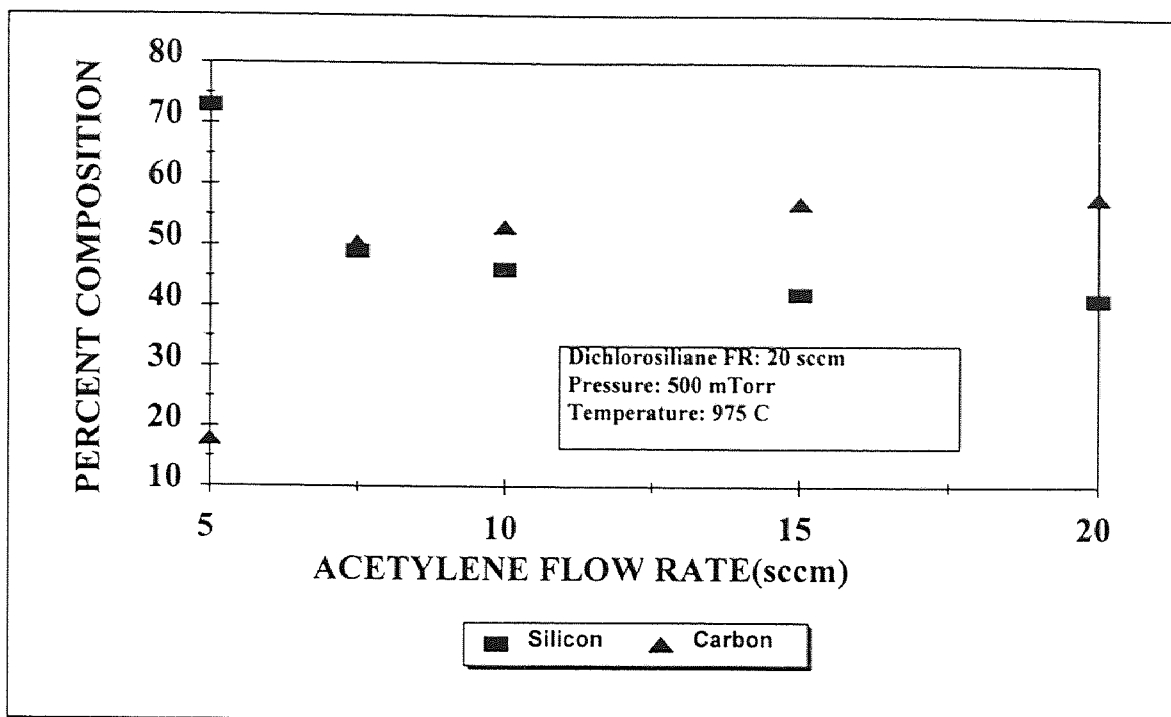


Figure 3.27 Variation of Si-C percentage composition as a function of acetylene flow rate.

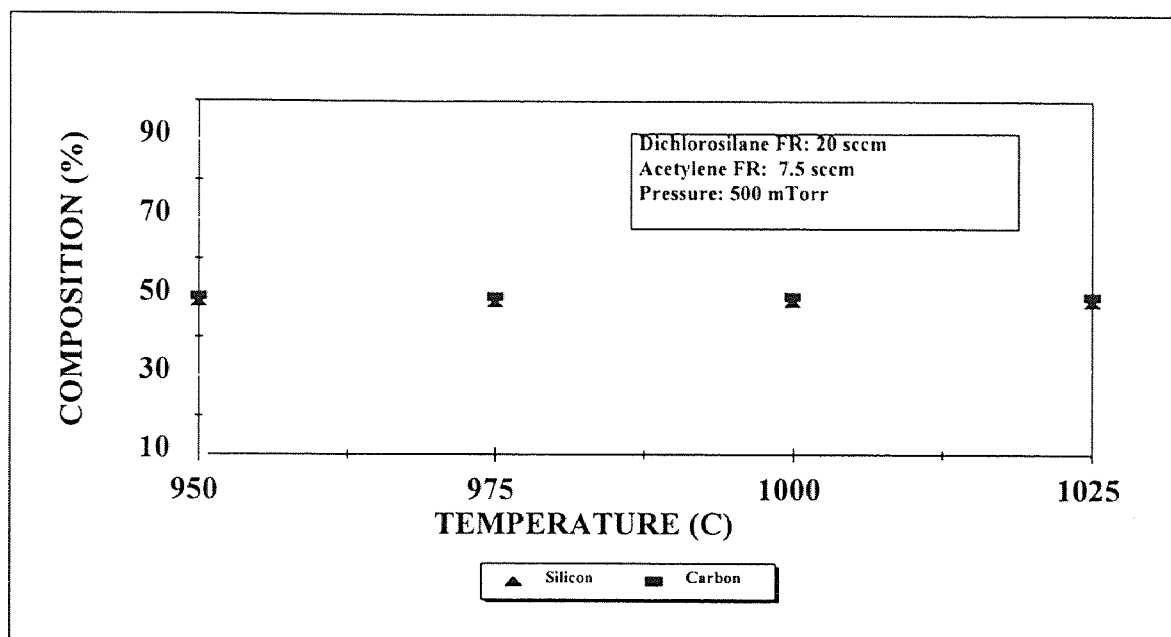


Figure 3.28 Variation of percentage composition of Si-C as function of deposition temperature.

### 3.3.4 Stress Analysis

It was found that the stress of films deposited with equal precursor flow rates were all high in the range of 500 to 700 MPa irrespective of deposition temperature. The lowest stress value was exhibited by stoichiometric film, deposited at 1000°C, with dichlorosilane and acetylene flow of 20 and 5 sccm each, and with chamber pressure of 200 mTorr. However, that stress value was around 400 MPa which is still a high value to make membrane.

The experiments performed by varying the pressure, with chamber temperature of 1000°C, 20 sccm of dichlorosilane and 5 sccm of acetylene revealed that increasing the chamber pressure resulted in decreased stress values, without change in film composition. Under the chamber pressure of 500 mTorr, films with stress values of around 250 MPa could be achieved. With this stress values, membrane could be produced.

Even though, membranes could be made under the above mentioned conditions, the reproducibility of film stress was difficult due to the fact that the stoichiometry of the film is sensitive to the acetylene low flow rate of around 5 sccm.

It was aimed to reduce the stress of the film further for other applications. In this view, an entire kinetic study was performed by varying the deposition temperature from 950 to 1050°C, with chamber pressure of 500 mTorr, keeping the dichlorosilane and acetylene flow at 20 and 7.5 sccm respectively. It was interesting to note that the composition of the films were remain unchanged for different deposition temperatures ranging from 950 to 1025°C, keeping other conditions same, but at the same time, stress

values showed a decreasing trend with increasing deposition temperature. Figure 3.29 shows the variation in stress with respect to the deposition temperature. For the deposition temperature of 1000°C, the stress values were minimal of around 200 MPa. Further increase in temperature caused severe depletion effects and thereby restricting the advantage of depositing at higher temperatures.

Thus optimum deposition conditions to produce SiC membranes were determined. It is emphasized at this point, that the stoichiometric composition is critically depend on acetylene flow which is between 5 and 7.5 sccm.

### **3.3.5 Surface Morphological Studies**

Surface morphology was analysed by atomic force microscopy for a sample deposited under stoichiometric conditions showed an average surface roughness of 6nm. This is shown in the figure 3.30.

Generally, crystalline SiC films show large surface roughness of about 50 nm. Surface smoothness is a key issue from x-ray mask membrane point of view, since rough surface will scatter x-ray radiation. However, this synthesizing process produced films with above mentioned average roughness which is acceptable in x-ray lithography. This also indicates the superiority of the process.

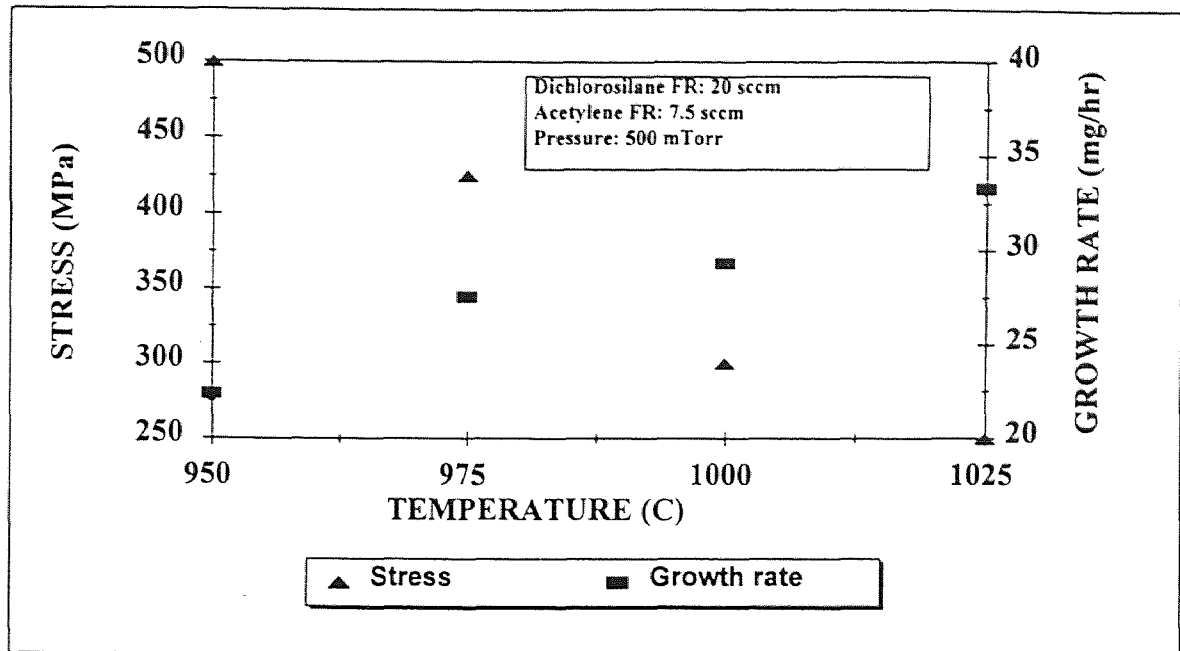


Figure 3.29 Variation in the stress of  $\beta$ -SiC films as a function of deposition temperature.

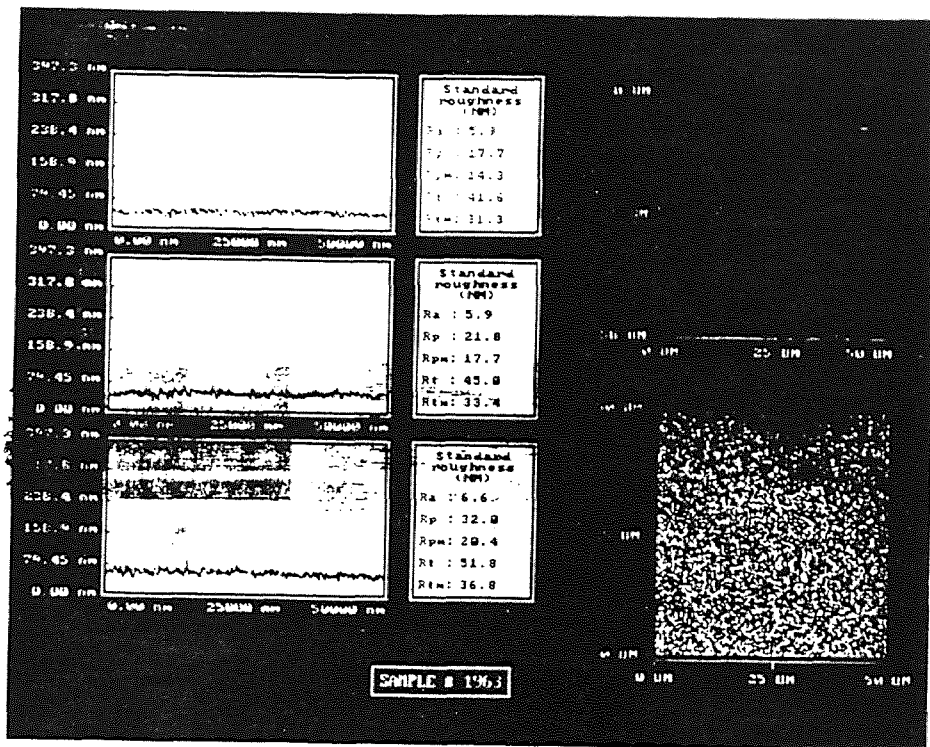


Figure 3.30 Atomic Force Microscopic picture showing the surface morphology of a  $\beta$ -SiC sample deposited at  $1000^{\circ}\text{C}$ , with dichlorosilane and acetylene flow rate of 20 and 5 sccm respectively, and under the chamber pressure of 500 mTorr.

### 3.3.6 Optical Characterization

**3.3.6.1 Optical Transmission Characteristics:** Figure 3.31 shows typical optical transmission spectrum for a 1.2  $\mu\text{m}$  thick sample with stoichiometric Si-C composition. It is evident from the figure that such samples showed desired optical transmission of at least 50% around 6320  $\text{\AA}$  of wavelength. Films with excessive carbon content of more than 50%, showed poor optical transmission. Membranes with 4 cm in diameter could be produced consistently with desired optical transmission.

**3.3.6.2 Optical Band Gap Estimation:** A plot used to estimate the optical band gap is shown in figure 3.32. This plot is for the sample for which optical transmission was depicted in the previous figure. The estimated optical band gap came out to be 1.92 eV which is close to the accepted literature value of 2.01 eV at room temperature.

### 3.3.7 Electrical Characterization

Stoichiometric crystalline SiC samples were found to behave like semiconductor. This was evident from the I-V analysis performed on a substrate-SiC-metal structure. Both, forward and reverse current-voltage characteristics were measured at temperatures from 20 to 220  $^{\circ}\text{C}$  in steps of 50  $^{\circ}\text{C}$ . Such I-V curves are shown in figure 3.33 and 3.34. The systematic change in the I-V characteristics at different temperatures clearly indicate the diode behavior. This observation could be correlated to the earlier studies performed on such samples [46] indicating an intrinsic n-type conductivity for crystalline SiC ( $\sim 10^{16} \text{ cm}^{-3}$ ) which was grown on p-type substrate. Ideality factor was estimated from forward I-

V curve and came out to be 4.03 at 20°C, and as 4.17 at 120°C, in the diffusion current dominating regime. This structure also exhibited high leakage current density in the order of 0.7 A cm<sup>-2</sup>. This is attributed to the interface defects that are developed due lattice mismatch between the film and the substrate.

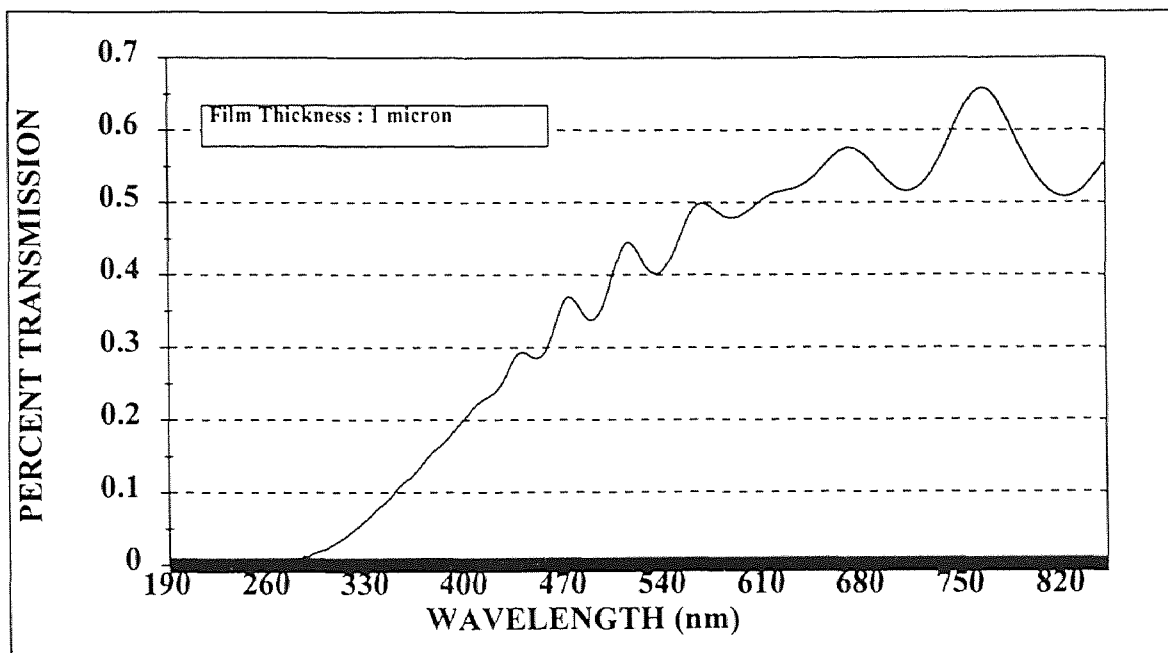


**Figure 3.31** Optical transmission spectrum for 1 μm thick β-SiC sample deposited at 1000°C, with dichlorosilane and acetylene flow rates of 20 and 5 sccm respectively, and under chamber pressure of 200 mTorr.

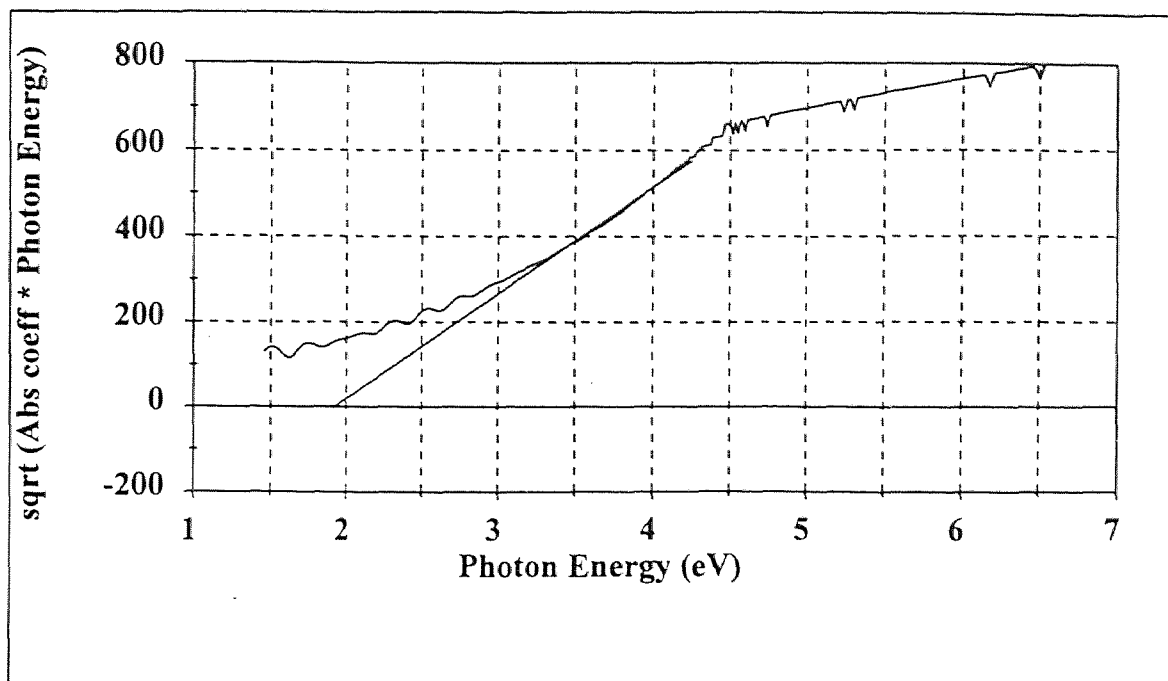


**Figure 3.32** A plot to estimate the optical band gap for the sample deposited under the conditions mentioned in figure 3.30.

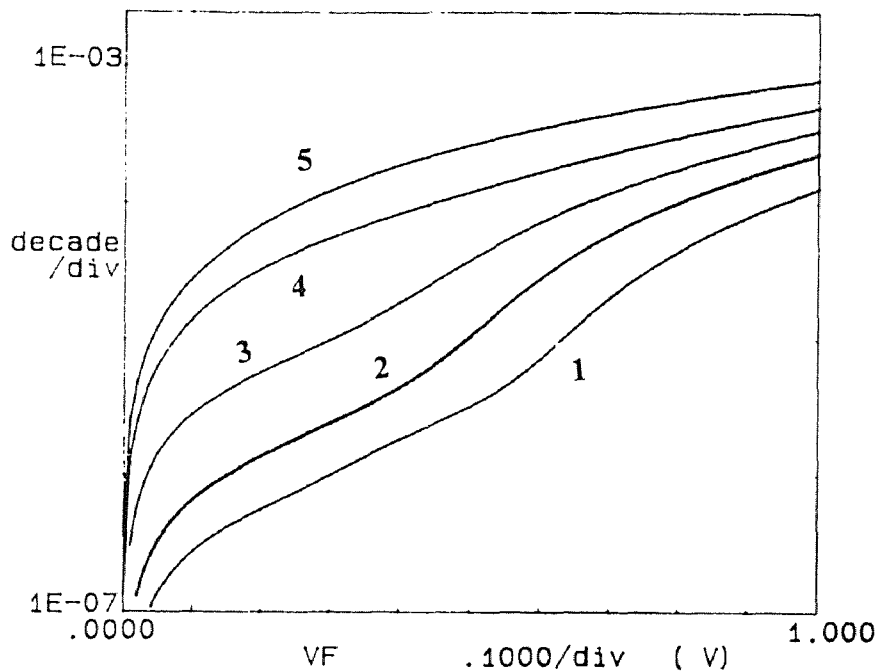


**Figure 3.33** Forward current-voltage characteristic of silicon- $\beta$  SiC-metal structure at various temperatures ranging from 20 °C (1) to 220°C (5) in step of 5 °C. The film was deposited under conditions mentioned in figure 3.31.



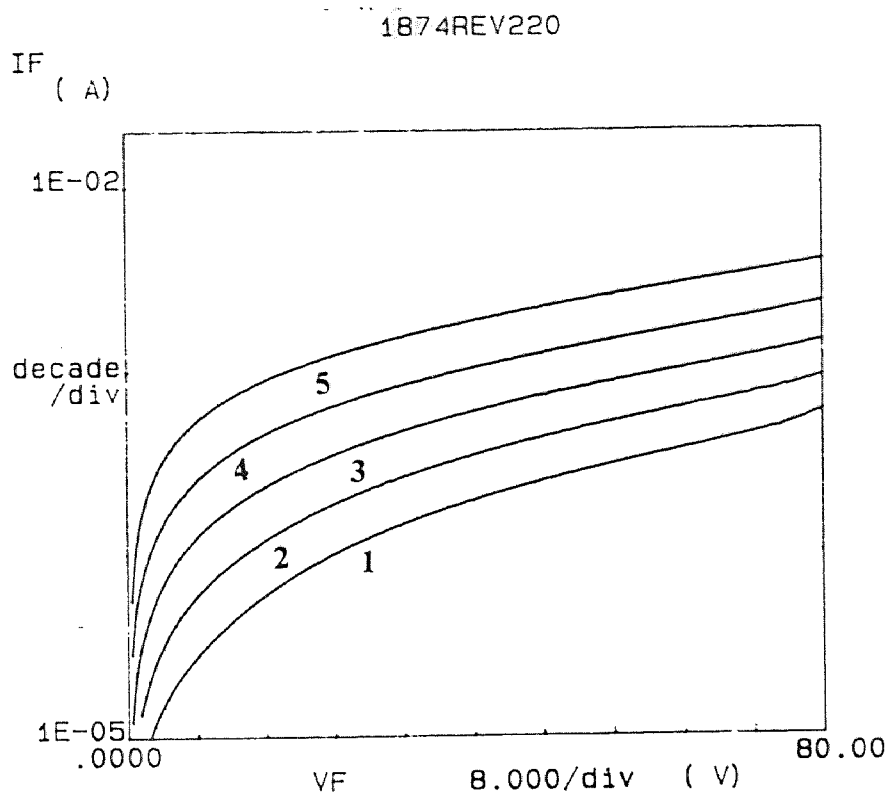


**Figure 3.34** Reverse current-voltage characteristic of silicon- $\beta$  SiC-metal structure at various temperatures ranging from 20°C (1) to 220°C (5) in step of 50°C. The film was deposited under conditions mentioned in figure 3.31.

## CHAPTER 4

### CONCLUSIONS

This project demonstrated the development of a unique low pressure chemical vapor deposition process for fabricating amorphous and crystalline silicon carbide films using safe chemicals. The initial goal of this project, which was aimed at developing a process for synthesizing amorphous SiC films that can be used to produce high quality mask membranes in x-ray lithography, was achieved. A single precursor, ditertiarybutylsilane was used to synthesize amorphous films in the temperature range of 600 to 850°C. This precursor is non pyrophoric, as against conventional precursors like silane that are used to synthesize silicon carbide films. The precursor is also a source for both silicon and carbon. The synthesizing processes rendered films with high degree of thickness uniformity (within  $\pm 5\%$  along the surface of the wafer), and with good adhesion with the substrate.

The infrared spectroscopic studies of the deposited samples confirmed the presence of a Si-C vibrational mode around  $790\text{ cm}^{-1}$  in all cases. In addition, absence of hydrogen in the films was also confirmed, which indicates the superiority of these deposits over films synthesized by conventional plasma assisted CVD or glow discharge methods. The x-ray diffraction measurements that were conducted to verify the amorphous nature of the deposit showed that films deposited below 850°C were amorphous in all cases. The results of the elemental composition analysis performed on these samples showed that the silicon and the carbon content could be controlled by the deposition temperature and that

in the deposition temperature range of 625 to 750°C the composition of the deposits changed progressively from slightly silicon rich ( $55 \pm 3\%$ ) to slightly carbon rich ( $51 \pm 3\%$ ). Above 750°C, there was a rapid increase in the carbon content from the near stoichiometric value to about 75%-C at 850°C. The Auger depth profile taken on these samples indicated that the composition was uniform through the bulk of the deposit. Also, it was found that, above 800°C, lowering the chamber pressure resulted in decreased carbon content of the deposits. The stoichiometric control (which is generally critical in the synthesis of amorphous films) was well established for this process.

High frequency C-V characterization conducted on a-SiC samples showed that the films exhibit insulating properties. The dielectric constant for these films was measured to be  $10.1 \pm 0.5$ . Such films also showed a breakdown voltage of  $2.5 \times 10^6$  V cm<sup>-1</sup>. Aforementioned quantities were in close agreement with values reported by others [2, 48]. From the temperature bias stress studies, the trapped charge density was estimated to be  $0.869 \times 10^7$  cm<sup>-2</sup>, which is at least twice an order of magnitude less than that for SiO<sub>2</sub> films synthesized by CVD methods.

Stress analysis performed on the stoichiometric amorphous films showed high tensile stress of  $700 \pm 50$  MPa. It was found that to obtain free standing membranes film stress values of about 100 MPa were required. This was a major challenge since increasing the carbon content in the film while reducing the film stress also lowered the optical transmission. Experiments were conducted that led to a set of optimum processing parameters for minimizing optical absorption (to ~20% transmission), due to excess carbon content, while maintaining the necessary stress level of 100 MPa. To further

minimize stress and optical absorption, microcrystalline / polycrystalline SiC films were prepared and investigated. An improvement in transmission to a value of 50% (at only  $200 \pm 50$  Mpa) was obtained at the expense of surface smoothness.

Polycrystalline SiC films were grown on Si (100) substrates using dichlorosilane and acetylene as precursors at 950 to 1050°C. The carbon content in the film was found to increase with deposition temperature, keeping the flow ratio of precursors equal to one. The carbon composition was also found to be sharply dependent on acetylene flow, for constant deposition temperature and pressure. Stoichiometric films were achieved for a dichlorosilane to acetylene flow ratio of 4:1. For that flow ratio, the stress of the deposited film was found to decrease as the deposition temperature was increased from 950 to 1050°C. The IR spectroscopic studies conducted on all the samples confirmed the presence of a strong peak due to Si-C coupling and the absence of Si-H bond vibrations. X-ray diffraction confirmed the growth of  $\beta$ -SiC with  $\langle 111 \rangle$  orientation in all the cases. Atomic force microscopic studies conducted on a stoichiometric sample deposited at 1000°C revealed an average roughness of about 6 nm for 1  $\mu$ m thick film with 50% transmission, which is acceptable for lithographic processing for 0.1  $\mu$ m resolution.

Forward and reverse current-voltage relationships were studied for a substrate-film-metal structure at different temperatures ranging from 20 to 220°C in step of 50°C. Measurements revealed that the structures had diode characteristics with ideality factors ranging from 4.03 at 20°C to 4.17 at 120°C. The devices had high leakage current densities of about 0.7 A cm<sup>-2</sup> at 20°C. Such high leakage current densities may be tolerable in high power devices. The fact that the device avalanche breakdown voltages

were more than 80 V indicates that these films could be employed as high voltage / high power devices.

The fabrication parameters could be further studied and optimized to develop SiC thin film structures for low power electrical devices. Suggested investigations that might be pursued to achieve low power high quality device structures are listed below:

(1) A study could be pursued to reduce the leakage current through the device. Such high leakage current is attributed to interface defect densities that are formed due to the lattice mismatch of SiC (4.3 Å) and Si (5.43 Å) and stacking faults that are formed during the film growth, thus resulting in trapping centers at the interface. The 20% lattice mismatch has to be brought down to at least 14% [49] in order to reduce the leakage current appreciably. This might be achieved in several ways. One method is to grow a carbonized layer of Si with a deposited SiC film on top of it. This could be accomplished by first *in-situ* cleaning of the native oxide layer of the substrate at 1000°C, in H<sub>2</sub> ambient for 10 min, and then forming a pitted carbonized layer with acetylene for 5 min [50], followed by the growth of a stoichiometric SiC film on top of it by the method developed in this study. The lattice mismatch could also be varied by directly depositing Si<sub>x</sub>C<sub>1-x</sub> layers first and progressively changing  $x$  with thickness until the stoichiometric value is reached. This could be easily achieved by changing the acetylene flow values as done in the process developed in this research. Another approach that could be tried would be to use Si substrates with substrate surface orientations either 1° to 6° off-axis from the (100) plane or 2° to 4° off-axis from (111) plane, as reported by H.P Liaw et al. [21].

Another approach that is worth investigating is to employ substrates other than Si. From figure 4.1, which shows the lattice constants and bandgaps of column IV, III-V, and II-VI semiconductors [51], it can be inferred that materials like ZnS, AlP, GaP, and associated ternary compounds might be alternate substrate choices. Such materials might be grown on low cost Si (which has ~0% lattice mismatch with the above mentioned compounds). By grading their composition, the lattice constant for the top layers could be made to match SiC. It is interesting to note that the lattice constant of sapphire ( $\text{Al}_2\text{O}_3$ ) is within 20% of SiC [49].

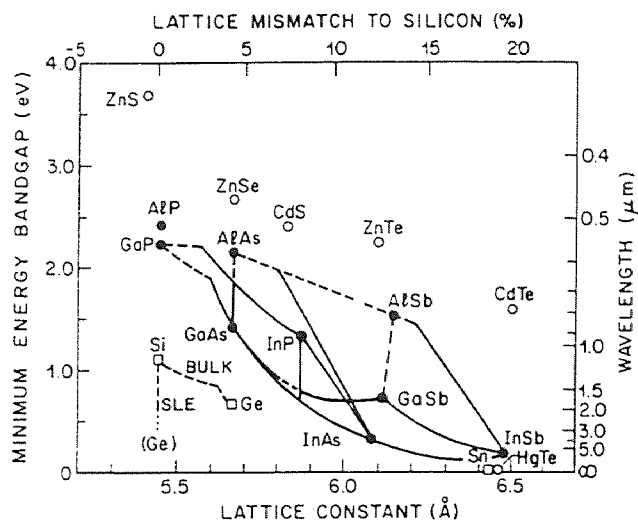


**Figure 4.1** Bandgap versus lattice constant data for the column IV, III-V, and II-VI semiconductors. (After reference 51).

(2) Diode structures based on doped p and n-type SiC films should have lower leakage currents than the SiC/Si heterojunction structures, since SiC has larger band gap (2.2 eV) [48] than that of Si (1.1 eV). *In-situ* p and n-type doping could readily be achieved by

incorporating additional precursors such as  $\text{PH}_3$  for phosphorus and  $\text{B}_2\text{H}_6$ , and  $\text{B}(\text{CH}_3)_3$  for boron doping. Doping by ion implantation might also be possible, with crystal lattice damage removed by annealing.

(3) The ideality factor might be lowered by doping the deposited SiC films, i.e., introducing phosphorus at the film/substrate interface. The effect of doping levels on interface stress and surface state density could be studied.

(4) The voltage-current relationship of diode structures made with doped a-SiC layers deposited on Si substrates could be studied. Such doped a-SiC film junctions could be used in the fabrication of high temperature bipolar transistors [52].

(5) Similarly doped a-SiC films on a-Si layers could be studied. a-Si/a-SiC superlattice structures could possibly be high quality solar cells [53]. a-Si layers can be readily grown at temperatures around  $850^\circ\text{C}$  using dichlorosilane alone. Doped a-SiC layers could be grown using DTBS and additional precursors.

In conclusion, this research has shown that the required fabrication processes for the growth of SiC thin film layers allow for a variety of amorphous and polycrystalline thin film structures to be constructed. Thus it should be possible to fabricate many different types of novel electrical and optoelectronic devices utilizing the properties of the wide bandgap material silicon carbide.

## REFERENCES

1. R.A. Levy, *Microelectronic Materials and Processes*, Proceedings of the NATO Advanced Study Institute, Series E: Applied Science, Vol. **164** (1989).
2. S.M. Sze, *Semiconductor Devices*, Bell Telephone Laboratories Inc., New Jersey (1985).
3. Fay, A. Cornette and J.P. Niveliers, *IEEE*, **15.7** IEDM 82-411-13 (1982).
4. Grow, R.A. Levy, X. Fan, M. Bhaskaran, *Materials Letters*, **23** (1995) 187-193.
5. Luthje, *Phillips Tech. Review*, **41**, 15-169 (1983-84).
6. Luethje, B. Matthiessen, M. Harms, and A. Burns, *Proc. SPIE*, **15** (1987).
7. Heuberger, *Solid State Technology*, Vol. **29**, 93-101, February (1986).
8. Mackens, H. Lutheje, U. Mescheder, F. Mund, S. Pongratz, *SPIE*, Vol.**923** E-beam, Ion-beam Tec.: Submicrometer Lithographies VII (1988) 9-15.
9. Madouri, A.M. Gosnet and J. Bournex, *Microelectronic Engineering*, North Holland, **6** (1987) 241-245.
10. Jin Park, Y. Wook Park, and John S. Chun, *Thin Solid Films*, **166** (1988) 367-74.
11. Yamada, K. Kondo, M.N. Nakaishi, J. Kudo, and K. Sugishima, *J.Electrochem. Soc.*, Vol.**137**, No.7, July (1990).
12. Anderson, and W.E. Spear, *Philosophical Magazine*, Vol **35**, (1976).
13. S.Meikle, Y. Suzuki, Y. Hatanaka, *J. Appl. Phys.* **67**(2), 15, Jan (1990) 1048-50.
14. Mohring, M.B. Schubert, G. Schumm, G.H. Bauer, *J. Non-crystalline Solids* **97** and **98** (1987) 1447-1450.
15. Goldfrab and J. Woodroffe, *Plasma Chemistry and Plasma Processing*, Vol.**9**, No.1, (1989) 195s-206s.
16. Asano, T. Ichimura, and H. Sakai, *J. Appl. Phys.*, **65**(6), 15 Mar (1989) 2439-44.
17. Nakayama, S. Akita, M.Nakano, T.Kawamura, *J. Non-crystalline Solids* **97** and **98** (1987) 1447-1450.



18. Goldstein and C.R. Dickson, I.H. Campbell and P.M. Fauchet, *Appl. Phys. Lett.* **53**(26), 26 Dec (1988) 2672-74.
19. Shigehiro Nishino, Yoshikazu Hazuki, Hiroyuki Matsunami, and Tetsuro Tanaka, *J. Electrochem. Soc.*, Vol.**127**, No.12, Dec (1980) 2674-80.
20. Liaw and R.F. Davis, *J. Electrochem. Soc.*, Vol.**131**, No.12, Dec (1984) 3014-18.
21. Rai-Choudhury and N.P. Formigoni, *J. Electrochem. Soc.*, Vol.**116**, No.10, Oct (1969) 1440-1443.
22. Nagasawa and Y. Yamaguchi, *Thin Solid Films*, **225** (1993) 230-234.
23. Yoh-ichi Yamaguchi, Norimichi Annaka, Tsutomu Shoki, Isao Amemiya, Hiroyuki Nagasawa, Hiroyuki Kosuga, and Osamu Nagarekawa, *Mat. Res. Soc. Symp. Proc.*, Vol.**306**, (1993), 197-210.
24. Hekret R. Philipp, *Physical Review*, Vol.**111**, No.2, Jul (1958), 440-441.
25. Choyke and Lyle Patrick, *Physical Review*, Vol.**105**, No.6, Mar (1957), 1721-23.
26. Hattori, D. Kruangam, T. Toyama, H. Okamoto, and Y. Hamakawa, *Appl. Surface Science*, 33-34 (1988) 1276-84.
27. Sasaki, M.M. Rahman and S. Furukawa, *Technical Report of Inst. of Electronics and Communication Engineers of Japan*, **ED85-8**, pp. 15-20 (1985).
28. Rahman and S. Furukawa, *1st Int. PVSEC Tech. Dig.*, pp.171-174 (1984).
29. Don M. Jackson, Jr. and Robert W. Howard, *Transactions of the Metallurgical Society of AIME*, Vol.**233**, Mar (1965), 468-473.
30. Bhatnagar. M, *IEEE Elec. Dev. Lett.*, V **13**, n 10, Oct (1992).
31. Ramirez-Malo, E. Marquez, C. Corrales, P. Villares and R. Jimenez-Garay, *Material Science and Engineering*, B25(1994)53-59.
32. Tauc, *J. Non-Cryst. Solids*, 8-10 (1972)569.
33. Doerner and W.D. Nix, *J. Mater. Res.*, **1**, 601 (1986).
34. Oliver and G.M. Pharr, *ibid.*, **7**, 1564 (1992).
35. Ohshita and A. Ishitani, *J. Appl. Phys.*, **66**, 4535 (1989).

36. Van den Crekel and L.J. M. Bollen, *J. Crystal Growth*, **54**, 310 (1981).
37. Grow, R.A. Levy, Y.T. Shi, and R.L. Pfeffer, *J. Electrochem. Soc.*, **140**, 851 (1993).
38. Laidler, *Chemical Kinetics*, p.226, McGraw Hill Inc., New York (1965).
39. Classen, J. Bloem, W.G.J.N. Valenburg, and C.H.J. van den Brekel, *J. Crystal Growth*, **51**, 267 (1982).
40. Eversteyn, *Phillips Res. Rep.*, **29**, 45 (1974).
41. O'Neal and M.A. Ring, *Organometal.*, **7**, 1017 (1988).
42. Muehlhoff, W.J. Choyke, M.J. Bozak, and J.T. Yates, *J. Appl. Phys. Lett.*, **60**, 2842 (1986).
43. Bozso, L. Muehlhoff, M. Trenary, W.J. Choyke, and J.T. Yates, *J. Vac. Sci. Technol.*, **2**, 1271 (1984).
44. J. Grow, R.A. Levy, and M. Bhaskaran, *J. Electrochem. Soc.*, Vol.**140**, No.10, Oct 1993.
45. Edgar, *J. Mater. Res.*, Vol.7, No.1, 240-251, Jan 1992.
46. S.J. Pearton, J.W. Lee, J. Grow, M. Bhaskaran, F. Ren, *Applied Physics Letters* **68** (21), 2987-2989, May 1996.
47. E.H. Nicollian, J.R. Brews, *MOS Physics and Technology*, John Wiley Publications, New York (1982).
48. Max N. Yoder, *IEEE Transactions on Electron Devices*, Vol. **43**, No.10, Oct 1996.
49. Chopra, Kasturi, *Thin Film Phenomena*, McGraw Hill, New York (1969).
50. B. Desu, G. Chiu, C.Y. Tsai, W.T. Reynolds Jr., *J. Mater. Res.*, Vol.**10**, No.5, May 1995.
51. S.M. Sze, *High Speed Semiconductor Devices*, Wiley-Interscience Publication, New York (1990).
52. K. Sasaki, T. Fukazawa, and S. Furukawa, Amorphous and Crystalline Silicon Carbide, *Springer Proceedings in Physics*, Vol.**34**, 150-155, (1989).
53. Y.Kuwano and S. Tsuda, *ibid.*, Vol.**34**, 167-177, (1989).